SYNTHESIS, STRUCTURE AND CHARACTERIZATION OF POLYNUCLEAR RARE EARTH ALKOXIDE CLUSTERS

A Dissertation

by

SCOTTY LEE DEMPSEY

Submitted to the Office of Graduate and Professional Studies of
Texas A&M University
in partial fulfillment of the requirements for the degree of

DOCTOR OF PHILOSOPHY

Chair of Committee	Timothy R. Hughbanks
Committee Members	Abraham Clearfield
	Hong-Cai Zhou
	Joseph H. Ross Jr.
Head of Department	David H. Russel

May 2014

Major Subject: Chemistry

ABSTRACT

The versatile polyol/polyamine supporting ligand TDCI (1,3,5-tris(dimethylamino)-1,3,5-trideoxy-*cis*-inositol was synthesized, and several lanthanide complex clusters of this ligand were produced. The coordination chemistry and characterization of these triangular lanthanide alkoxide clusters was explored. Molecular products include $Ln_3(H_{-3}TDCI)_2(L)$ (Ln = Y, Eu, Gd, Tb, Dy, Ho, Er; L = MeOH, H_2O, dipivaloylmethanide, acetylacetonate, dibenzoylmethanide, tetraacetylethane, hexafluoroacetylacetonate). The dysprosium and gadolinium analogues of these clusters were used as secondary building units and were incorporated as preformed entities into coordination polymers linked by squarate $(C_4O_4)^{2-}$ and benzenedicarboxylate.

The dysprosium clusters $Dy_3(H_{-3}TDCI)_2(MeOH)_6$ and $Dy_3(H_{-3}TDCI)_2(dpm)_6$ (dpm = dipivaloylmethanide) as well as the coordation polymer $Dy_3(H_{-3}TDCI)_2(C_4O_4)_{3/2}$ were shown to exhibit slow relaxation of magnetization characteristic of single-molecule magnet behavior. The europium and terbium analogues were characterized by spectrofluorimetry.

Hexanuclear oxo-centered Dy and Gd clusters were synthesized: the OH-face capped $Gd_6(\mu_6\text{-}O)(\mu_3\text{-}OH)_6(\mu_3\text{-}O)_2(PhB(OEt)_2)_2(dpm)_6(HOEt)_2$ and $Gd_6(\mu_6\text{-}O)(\mu_3\text{-}OH)_8(dpm)_8$ as well as the edg-bridged $[Dy_6(\mu_6\text{-}O)(\mu_2\text{-}OCH_2CF_3)_{12}(OCH_2CF_3)_6][Na(thf)_6]_2$. All compounds were characterized by single-crystal X-Ray diffraction.

ACKNOWLEDGMENT

I would like to thank my advisor, Dr. Tim Hughbanks, for his invaluable insight and guidance throughout my graduate career. Our many debates will always be remembered. I also thank the members of my group, including Jose Delgado, Brady Dykema, Francisco Escobedo, Jenny Chen, Lindsay Roy and especially Luke Sweet. I am appreciative of Jose's patience with my impeccable organization and lab cleanliness. I thank Brady for offering Scott Brothers a quarter. I express my utmost gratitude for Luke's helpful guidance in the laboratory. The years spent here were made all the better by friendships forged with Jose, Houston Perry, Kevin Gagnon, Kyle Cummins and especially Scott Brothers. I thank Dr. Mike Manson, a dedicated scientist, a great story-teller, and most of all a good friend.

I would like to thank the Dr. Joe Reibenspies and Dr. Nattami Bhuvanesh, and Dr. Kevin Gagnon for help with crystal structures and the X-Ray diffraction laboratory in general. I want to thank Dr. Amanda Young for helping with luminescence measurements. I am especially thankful to Dr. Kim Dunbar, Dr. Andrey Prosvirin, and Toby Woods for their help with the SQUID measurements. Thanks to Bill Merka for constructing and repairing glassware. I thank Sandy Manning for generally keeping everything together. And I thank Brandi Whittington for her patience.

The Advanced Light Source is supported by the Director, Office of Science, Office of Basic Energy Sciences, of the U.S. Department of Energy under Contract No. DE-AC02-05CH11231.

NOMENCLATURE

TACI	1,3,5-triamino-1,3,5-trideoxy-*cis*-inositol
TDCI	1,3,5-tris(dimethylamino)-1,3,5-trideoxy-*cis*-inositol
H_{-3}TDCI	triply deprotonated TDCI
H_{+3}TDCI	triply protonated TDCI
dpm	diplivaloylmethanide
dbm	dibenzoylmethanide
acac	acetylacetonate
H_2tae	tetraacetylethane
hfac	hexafluoroacetylacetonate
Ln_3	$Ln_3(H_{-3}TDCI)$
SMM	Single-molecule magnet
RE	rare earth
Ln	lanthanide

TABLE OF CONTENTS

LIST OF FIGURES

LIST OF TABLES

CHAPTER I

INTRODUCTION

Lanthanide chemistry is of much interest because of a variety of useful properties inherent to lanthanide ions, including interesting magnetic, luminescence, and catalytic properties, among others. Though the physical properties of lanthanide ions are, for the most part, only slightly dependent on their coordination environments, this slight dependence is of crucial importance in tuning these properties. This work fundamentally focuses on the synthesis and characterization of lanthanide coordination compounds, specifically, alkoxide-supported lanthanide clusters. The lanthanide cluster types, $RE_3(H_{-3}TDCI)_2(L)_6$ (TDCI = 1,3,5-tris(dimethylamino)-1,3,5-trideoxy-*cis*-inositol) with a variety of peripheral ligands, L, were synthesized. The Dy clusters exhibit single molecule magnet (SMM) behavior. The luminescence properties of Eu and Tb clusters were determined by spectrofluorimetry. The water ligated Dy_3 and Gd_3 clusters were used as precursors in the synthesis of coordination polymers linked by squarate and benzenedicarboxylate ligands. Presented in this chapter is an overview of SMMs, lanthanide luminescence, and metal coordination polymers.

SINGLE-MOLECULE MAGNETISM (SMM)

Fundamentals

Molecules exhibiting superparamagnetic behavior, including slow magnetic relaxation and magnetic hysteresis, similar to that of bulk magnets, are known as single-molecule magnets (SMM). Unlike bulk magnets, the origin of this behavior is strictly a molecular property—not a consequence of long-range ordering.[1]

Since the discovery of the prototypical SMM, $[Mn_{12}O_{12}(OAc)_{16}(H_2O)_4]$, in 1993, the field of molecular magnetism has been extremely active.[2] For a decade, attention was focused primarily on polynuclear transition-metal based molecules, but discovery of the robust mononuclear single molecule magnet, terbium phthalocyanine $Tb(Pc)_2$ in 2003, has intensified interest in lanthanide-based single molecule magnets.[3] Lanthanide ions, even as mononuclear species, have high spin values and may have large magnetic anisotropies, two basic criteria for single-molecule magnetic behavior. Single ion (and polymetallic) dysprosium-containing SMMS are common for these reasons, as well as significant M_J splittings, and crucially, Kramers' degeneracy.[4,5]

Single-molecule magnet behavior is, fundamentally, the result of a paramagnetic ground state whose easy axis of magnetization lies in a low-energy potential well. In transition metal SMMs, this picture is often described as a double potential well, with $M_S = \pm S$ levels lowest in energy, and lower values of M_S at higher energies. In the absence of a magnetic field, the $M_S = \pm S$ levels are equally populated. When subjected to a magnetic field, the Zeeman interaction splits the maximal M_S levels and aligns the spins with the magnetic field, preferentially populating the

M_S = −S state. When removed from the magnetic field at sufficiently low temperature, the system is trapped in this state because energy is required to climb the potential well and reorient the spins, resulting in a remnant magnetization like that of a tiny, molecule-sized bar magnet. Through one of several mechanisms, the reorientation of spins results in a relaxation of the magnetization. Indeed, one indication of single-molecule magnet behavior is the *slow relaxation of magnetization*. The relaxation rate is most commonly determined by dynamic ac-susceptibility measurements (which will be discussed below), and not by static relaxation as described above, though these experiments are performed on samples with sufficiently slow relaxation.[6,7]

In highly charged (3+) lanthanide ions, 4*f* orbitals are contracted, core-like orbitals. For this and other reasons, the spin-orbit interaction is quite large. In fact, for lanthanide ions, crystal field interactions are subordinate to spin-orbit interactions, in contrast to 1st row transition metals where the opposite is usually true. Since total angular momentum, J $(= L + S)$, is a good quantum number for lanthanide ions, then, the spin-orbit coupled ground electronic levels $^{2S+1}L_J$ are most important. To fully describe the electronic state, the z-component of total angular momentum, M_J, must be specified. There are $(2J+1)$ M_J states (multiplets) for each term, ranging from $M_J = +J$ to $-J$ in integer steps. In a free ion, these states are all degenerate; however, each M_J state has a particular charge density distribution, and as such, crystal field interactions split the degeneracy of the multiplet states.[7] The crystal field is thus able to enhance magnetic anisotropy by stabilizing electronic states the with large values of M_J (or conversely *destabilizing* states with lower values of M_J). Desirable stabilization of high-valued M_J states is of course not guaranteed; it depends upon a the specifics of M_J-state charge distribution and a suitable ligand coordination

environment. The choice of ligands in lanthanide-based SMM is thus extremely important. Although this picture of 4*f* element structure is a good rule of thumb, its predictive power is marginal.

The rather diffuse valence d-orbitals of transition metals participate to an appreciable extent in bonding to ligands, so the geometric and electronic nature of the ligand field is highly correlated to *d*-orbital energies. This allows ligand control of orbital anisotropy; unfortunately because the resident electron's angular momenta are generally only weakly coupled to the orbital angular momenta, ligand control of magnetic anisotropy is difficult. The core-like 4*f* orbitals of lanthanide ions, shielded by 5s and 5p electrons, only weakly interact with ligand fields. The difficulty with control of lanthanide magnetic anisotropy is thus for the opposite reason: the orbital and electronic angular momenta are naturally strongly coupled, but control of the relative energies of *f*-orbitals (or M_J states) is difficult, which in turn complicates predictable control of magnetic anisotropy.

AC magnetic susceptibility[1,5,8]

The most common experimental technique to test for slow relaxation of magnetization, a tell-tale feature of single-molecule magnetism, is ac magnetic susceptometry. Typical magnetic characterization involves determining magnetic susceptibility in a static magnetic field, $\chi_M = \mathbf{M}/\mathbf{H}$, ($\chi_M$ is the molar magnetic susceptibility, **M** is the magnetization, **H** is the static (dc) applied magnetic field). In an ac-susceptibility measurement, a dynamic magnetic field oscillating at variable frequencies is applied to the sample, and both the real (in-phase) χ' and imaginary (out-of-phase) χ'' components of the susceptibility are measured. Both temperature-dependent,

$\chi(T)$, and frequency dependent, $\chi(\omega)$, experiments are routinely conducted.

In a typical temperature-dependent ac-susceptibility measurement, the sample is subjected to an oscillating magnetic field of a single, constant frequency, v (commonly ranging from 1-1500 Hz), and the temperature is swept while measuring the ac-susceptibility. These temperature sweeps are then repeated at several different frequencies, resulting in several curves. A non-zero out-of-phase signal indicates single-molecule magnet behavior in typical molecular magnetic systems. If the temperature at which peaks occur shifts as the applied frequency is changed, a thermally-activated mechanism is indicated.

To extract more information about the dynamic magnetic properties of a molecule such as the mechanism of relaxation and thermal activation barrier, frequency dependent ac-susceptibility, $\chi(\omega)$, measurements are performed. The sample is held at a constant temperature, and the frequency of the applied ac field is varied yielding a single $\chi(\omega)$ curve. The temperature is then changed, and the frequency sweep repeated, yielding several isotherms. It is important to remember that oscillation of the magnetic field is measured in linear frequency, v, and this value must be converted to angular frequency ($\omega = 2\pi v$) before being applied to the following equations, or *vise versa*. A brief discussion of magnetic dispersion relations will help clarify how information such as relaxation times are extracted from these experiments.

The frequency dependent ac susceptibly $\chi(\omega)$ given by Casimir[9] is:

$$\chi(\omega) = \chi_S + \frac{\chi_T - \chi_S}{1 + i\omega\tau} \tag{1.1}$$

where χ_S and χ_T are the adiabatic and isothermal susceptibilities, respectively, and τ is the characteristic relaxation time. This equation is decomposed into its real (χ') and imaginary (χ'') parts as such:

$$\chi' = \chi_S + \frac{\chi_T - \chi_S}{1 + (\omega\tau)^2} \tag{1.2}$$

$$\chi'' = \frac{(\chi_T - \chi_S)\omega\tau}{1 + (\omega\tau)^2} \tag{1.3}$$

These equations draw direct analogy to those of Debye relaxation, which describes the dielectric response of electric dipoles in oscillating ac electric field.

Further discussion of these relations is warranted. In the limit of infinite ac frequency $(\omega \longrightarrow \infty)$, χ' reduces to χ_S. If the magnetic moment were following an extremely fast oscillating magnetic field, there wouldn't be time for the moment to interact with its surroundings, and an adiabatic susceptibility would be expected.In the limit of low frequency $(\omega \longrightarrow 0)$, χ' reduces to the isothermal susceptibility, χ_T, which is equivalent to χ, that of typical static susceptibility. According to equation 1.3, the out of phase susceptibility has quite a different response to limiting frequencies of the applied field. The out of phase susceptibility, χ'', goes to zero as $\omega \longrightarrow \infty$ and as $\omega \longrightarrow 0$. These features are shown in Figure I.1, a plot of χ' and χ'' vs $\omega\tau$. The salient feature of the χ'' plot is the maximum at $\omega\tau = 1$, which implies that a peak should be observed (experimentally) in the out-of-phase-susceptibility when the angular frequency is a reciprocal of the characteristic relaxation time, τ $(\omega^{-1} = \tau)$. Application of these principles is found in Chapter III.

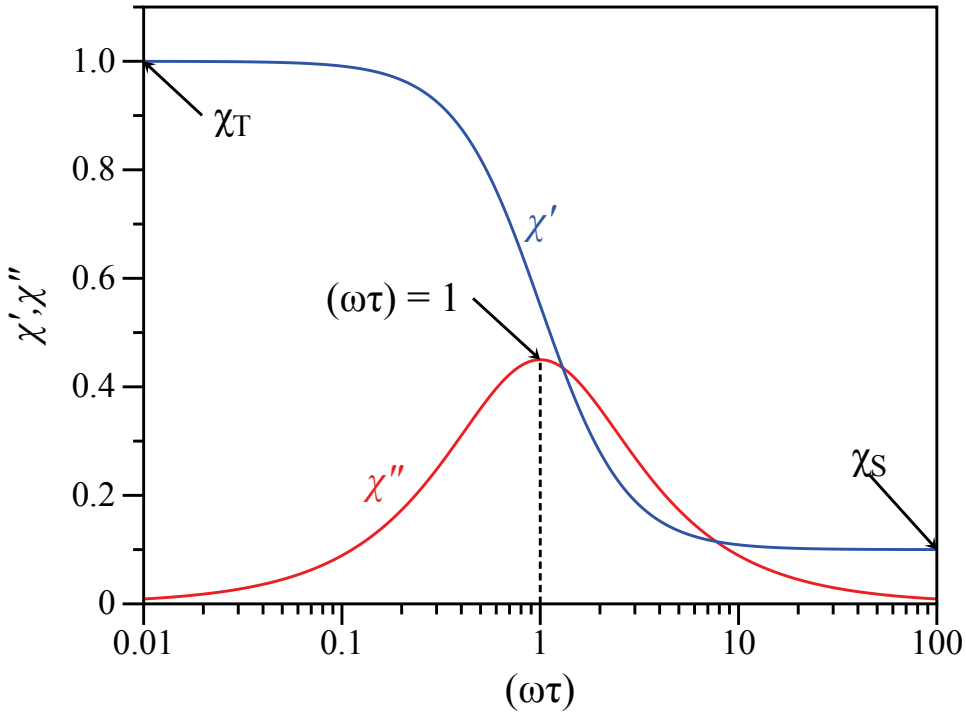

Figure I.1. Idealized ac-susceptibility as a function of ($\omega\tau$). In-phase (χ') and out-of-phase (χ'') susceptibilities are shown, with the limiting values, χ_T and χ_S.[1] Adopted and redrawn from Molecular Nanomagnets (Sessoli, Gatteschi, Villain).

LANTHANIDE LUMINESCENCE

Preliminary results of the luminescence properties of $Ln_3(H_{-3}TDCI)_2(dpm)_3$ (Ln = Eu, Tb; dpm = dipivaloylmethanide) are reported in Chapter III. A brief overview of lanthanide luminescence is given is this section.

Luminescence is the emission of light from a substance which is not the result of heating. In, photoluminescence, the energy source that stimulates this emission is the absorption of light. Lanthanide luminescence is generally characterized by (*i*) very weak absorption due to the

very small molar absorptivity of Ln^{3+} ions (~10 L mol^{-1} cm^{-1}) (ii) relative independence of emission spectra on changing coordination environments and (*iii*) very sharp emission spectra, as opposed to the broad emission spectra seen in fluorescent organic molecules.[10] The sharp emission bands are generally desirable for a wide variety of applications, including bioimaging, security inks, chemical (and other) sensors, and solar energy conversion, among others[11], but solving the problem of weak absorption is one of active research. Weak photoabsorption is usually ameliorated by *sensitizing* the lanthanide ion with organic ligands that act as "antennae".[11-15]

Highly contracted 4*f* orbitals are responsible for these lanthanides' photophysical properties. The relative independence of emission peaks on coordination environment owes to the lack of orbital overlap of 4*f* orbitals with coordinating ligands (Ln^{3+}-ligand bond covalency is 5-7%, at most)[14], though some transition intensities are hypersensitive to crystal field environments.[15] Lanthanide photoaborption and emission is most often due to 4*f*-4*f* electronic transitions (though 4*f*-5*d* transition are observed in some lanthanides ions). That electronic transitions are usually restricted to be within the 4*f* manifold and that these orbitals are only slightly influenced by ligand environments is the reason for sharp emission spectra. Because 4*f*-4*f* transitions are Laporte-forbidden, molar absorptivity is low. The lack vibronic coupling with coordinated ligands makes absent the mechanism for allowedness in electronic transitions (as opposed to transition metals) as well as the broadening of emission and absorption spectra. The lowest energy phototransitions of some lanthanides (e.g., Eu^{3+} and Tb^{3+}) are also spin-forbidden ($^5D_0 \rightarrow {}^4F_J$ for Eu^{3+}). As such, the lifetimes of luminescent excited states can be quite long-lived, from microseconds to milliseconds.[10]

Sensitization of lanthanides to luminesce is usually accomplished by coordinating the ions to organic ligands with high molar absorptivities. If the excited state of the ligand is of the appropriate energy, efficient transfer of this energy can be made to the lanthanide ion. This provides a way around the lower molar absorptivity of the lone Ln^{3+} ion. The mechanism of energy transfer is not universally agreed upon and varies depending on the specific metal complex, but two main mechanisms are accepted for most cases: the Dexter mechanism (a short-range, double-electron transfer process and the Förster mechanism (a longer range dipole-dipole coupling process).[15] Non-radiative quenching is also an issue with lanthanide complexes and is often due to O-H and N-H bond vibrations of ligands. Often β-diketonate ligands are used as sensitizers.[10]

The possibility of interesting luminescence properties in the later-discussed $Ln_3(H_{-3}TDCI)_2(dpm)_3$ clusters is a result of the rigid supporting TDCI ligand, the lack of bound OH or NH groups, and the modularity in peripheral ligand, in this case dpm. Dipivaloylmethanide an be exchanged with other β-diketonate ligands with desirable photoabsorption properties.

LANTHANIDE COORDINATION POLYMERS

Chemists have pushed the boundaries of design in coordination polymers (CPs) and have, through premeditated construction, imparted to such materials the properties of gas sorption, heterogeneous catalytic activity, luminescence, interesting magnetism, and the capacity for chemical sensing, among others. These properties derive from the characteristics of the metal, various attributes inherent to the organic linker, and from the connectivity and architecture of the framework.[16-19] The ability to rationally tune these properties is fundamentally advanced by

an interdisciplinary approach to coordination, solid state, and organic chemistry.

Lanthanide coordination polymers are particularly interesting, in large part because of the intrinsic properties of the lanthanide ions themselves. Trivalent lanthanides are active catalysts as a result of their strong Lewis acidity and exhibit generally sharp luminescence emission and interesting magnetic properties as a result of their partially-filled 4*f*-shells.[20,21,21] However, lanthanides ions exhibit, variable, high coordination numbers and ill-defined coordination geometry, so the purposeful application of synthetic constraints to framework topology is limited. To this end, a lanthanide building-moiety with a well-defined, controllable coordination environment would be valuable in designing CPs with desirable materials properties.

CHAPTER II

SYNTHESIS OF STARTING MATERIALS

INTRODUCTION

This chapter describes the synthesis of starting materials used in this work, including 1,3,5-tris(dimethylamino)-1,3,5-trideoxy-*cis*-inositol (TDCI), β-diketonates, lanthanide salts, and lanthanide bis(trimethylsilyl)amides. The synthesis of lanthanide complexes themselves are described in later chapters.

1,3,5-tris(dimethylamino)-1,3,5-trideoxy-cis-inositol (TDCI)

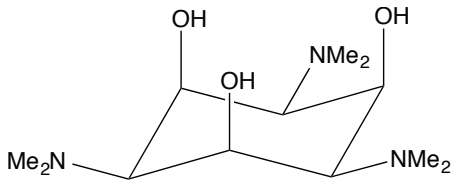

Figure II.1. 1,3,5-tris(dimethylamino)-1,3,5-trideoxy-*cis*-inositol (TDCI)

The rigid, all-*cis* substituted cyclohexanes 1,3,5-triamino-1,3,5-trideoxy-*cis*-inositol (TACI) and its methylated derivative 1,3,5-tris(dimethylamino)-1,3,5-trideoxy-*cis*-inositol (TDCI) (Figure II.1) were originally synthesized in the 1950s; however, the highly explosive precursors and sensitive intermediates used in its synthesis restricted broad availability of this fascinating ligand.[22,23] In the early 1990s, Hegetschweiler and co-workers developed a safe route to synthesizing TDCI using trisodium tris[(p-sulfonatophenyl)azo]phloroglucinol, which avoided shock-sensitive, explosive intermediates such as trinitrosophloroglucinol. This synthet-

ic route also has the benefit of most all reactions being carried out in aqueous solution. The synthetic procedures outlined in the literature are for the most part excellent and would easily suffice as a guide for the preparation of TDCI. For the sake of completeness and to clarify some areas of confusion, the experimental procedures, as performed by msyelf in this laboratory, are described in this chapter.

As a note on nomenclature, the ligands TACI and TDCI are so-named because they can be viewed as derivatives of the carbohydrate inositol, a polyol-substituted cyclohexane. The more standard nomenclature, 1,3,5-triamino-2,4,6-trihydroxycyclohexane and 1,3,5-tris(dimethylamino)-2,4,6-trihydroxycyclohexane, could be used if one so prefers, but here the carbohydrate root was used for reasons of standard practice.

β-diketonate ligands

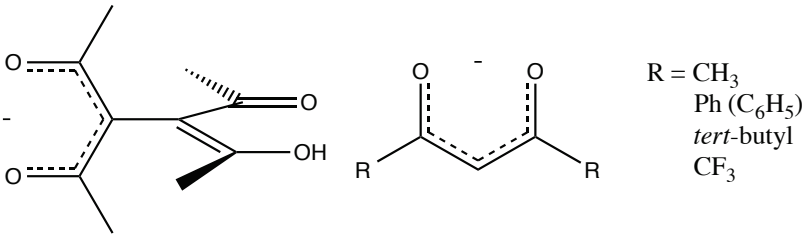

Figure II.2. β-diketonate anions.

Because lanthanide ions are large, hard acids and lack bonding valence electrons, they are oxophilic and prefer anionic ligands. β-diketonate ligands (Figure II.2) are chelating oxo-anions, which helps them fill the many open coordination sites of lanthanide ions. Commercial or easily made β-diketones were used in the synthesis of lanthanide complex described in this work.

Lanthanide tris[bis(trimethylsilyl)]amides

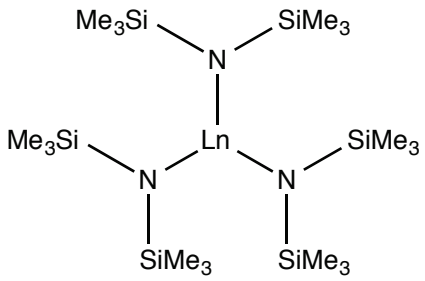

Figure II.3. Lanthanide tris[bis(trimethylsilyl)amide], $(Ln[N(SiMe_3)_2]_3$.

The lanthanide alkoxides in this work (other than $Ln_3(H_{-3}TDCI)_2L_6$ clusters) were synthesized via amide alcoholysis instead of the typical salt metathesis. This is further discussed in Chapter V. Lanthanide tris[bis(trimethylsilyl)]amides ($Ln[N(SiMe_3)_2]_3$, Figure II.3) serve as both a source of lanthanide ion and that of alkoxide ligand when reacted with an alcohol. These unusually low-coordinate lanthanide complexes are fairly easy to synthesize, soluble in low polarity organic solvents, and produce easily separable byproducts in their reaction with alcohols.

Rare earth triflates

Lanthanide trifluormethanesulfonates (triflates) serve as useful lanthanide sources because the preparation of both the hydrous and anhydrous salts is simple and straightforward. Also, the triflate anion has a very low propensity to coordinate, which makes lanthanide triflates ideal starting materials if anion binding is to be avoided. If water is to be avoided, the ease of preparation of the anhydrous salts in comparison to that of the lanthanide chlorides is also to be kept in mind.

EXPERIMENTAL

All reactions were performed in open air with starting materials obtained from commercial sources except for PtO_2 and $(Rh/Pt)O_2$, which were synthesized as discussed in this chapter. Sodium carbonate, sulfanilic acid, sodium nitrite, sodium nitrate, phloroglucinol, concentrated aqueous ammonia, nickel sulfate, sodium bromide, hydrobromic acid, Dowex Marathon 1, Dowex Marathon A, and hydrogen gas were all used as received. A high-pressure Parr reactor with a teflon stir bar was used for hydrogenation.

Synthesis of 1,3,5-tris(dimethylamino)-1,3,5-trideoxy-cis-inositol (TDCI)

Diazotization of sulfanilic acid

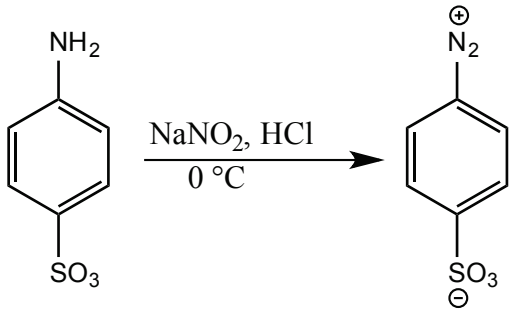

Figure II.4. Diazotization of sulfanilic acid.

In a 500 mL Erlenmeyer flask, 5.3 g of Na_2CO_3 and 17.3 g of sulfanilic acid were dissolved in 230 mL of water with heating. The solution was cooled to <5° C with an ice bath. In a separate 100 mL beaker, 7.4 g of sodium nitrite was dissolved in about 15 mL of water. This mixture was cooled in an ice bath to <5° C. The sodium nitrite was added slowly with stirring to the sulfanilic acid solution. In a separate 500 mL Erlenmeyer, 24.2 mL of conc. aq. HBr (9 M) was

added to 120 g of ice. (Figure II.4) Diazotized sulfanilic acid (p-benzenediazonium sulfonate) was synthesized with sodium carbonate[24] instead of with sodium hydroxide as in the literature preparation outlined by Hegetschweiler et al.[25]

Azo-coupling

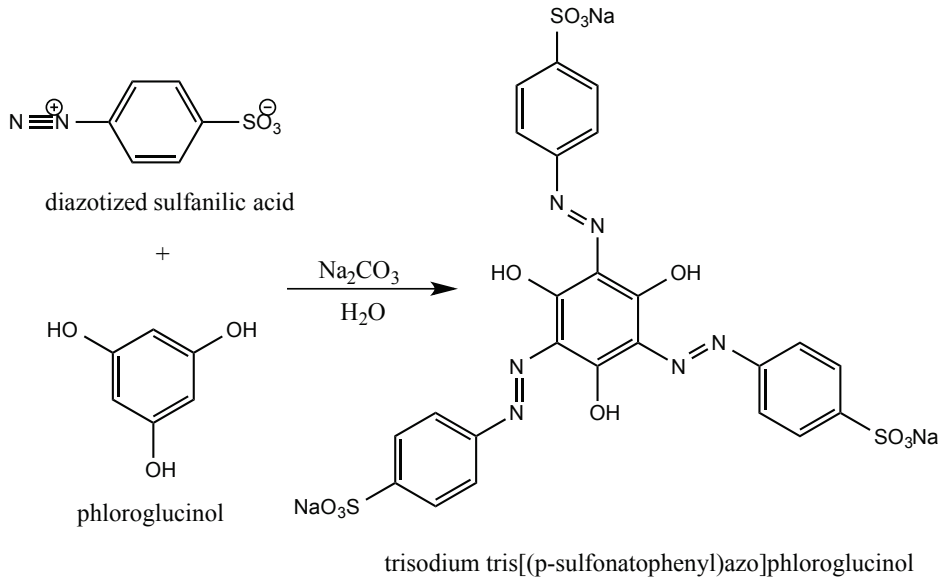

Figure II.5. Azo-coupling of phloroglucinol and p-benzenediazonium sulfonate.

In a 1L round-bottom flask, 41.1 g of Na_2CO_3 and 4.11 g of phloroglucinol were dissolved in 165 mL of water. The phloroglucinol solution was brought to <5 °C with an ice bath. The sodium nitrite/sodium sulfanilate solution was slowly added to the HBr/ice mixture. The diazonium salt precipitated before the addition was complete. The diazotized sulfanilic acid mixture was allowed to stir and stay below 5° C while the phloroglucinol solution was cooled. The diazotized sulfanilic acid mixture was the added slowly to the phloroglucinol solution, making sure the temperature did not exceed 10 °C. In fact, it never exceeded 5 °C. The mixture

was allowed to stir for 2 hours at this same temperature in an ice bath and then for another few hours at room temperature. According to the literature, the product was to be recrystallized from H_2O/acetone, but I found the traditional heat and cool method not to work, so the trisodium tris[(p-sulfonatophenyl)azo]phloroglucinol was precipitated several times from aqueous solution with acetone. (Figure II.5) This method yielded a product of satisfactory purity by ^1H NMR in d_6-DMSO.

Catalytic hydrogenation of trisodium tris[(p-sulfonatophenyl)azo]phloroglucinol

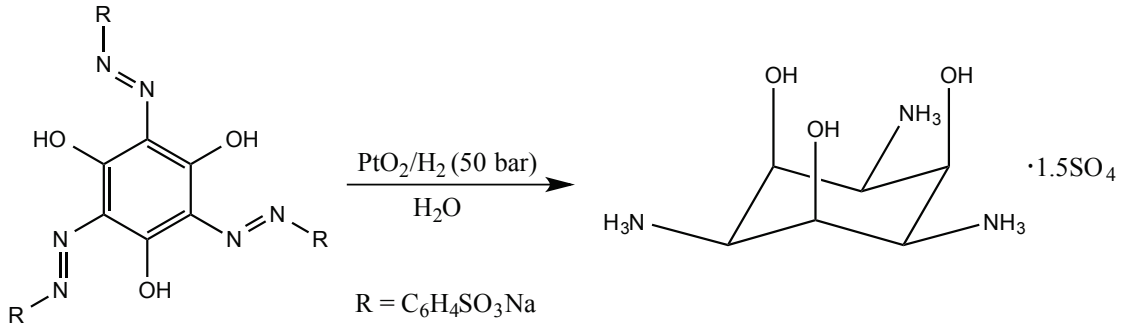

trisodium tris[(p-sulfonatophenyl)azo]phloroglucinol

1,3,5-trimethylammonium-1,3,5-trideoxy-*cis*-inositol sulfate

$(H_{+3}TACl)_2(SO_4)_3$

Figure II.6. Hydrogenation of trisodium tris[(p-sulfonatophenyl)azo]phloroglucinol.

Adam's (or Nishimura) catalyst (1.1 g) and 100 mL of 0.4 M H_2SO_4 were added to a Parr reactor with a glass inset and a Teflon stir bar. (The reactor did NOT have a stirrer, as the stirrers available were all stainless steel, which is not compatible with sulfuric acid. If a HAST B stirrer is available, that can be used.) The catalyst was reduced by hydrogenation (50 bar, 1hr, room temperature, 1150 RPM). After an hour of hydrogenation, 10 g of of trisodium tris[(p-

sulfonatophenyl)azo]phloroglucinol was added and hydrogenation was continued for approx. 13 hours. The black, finally divided catalyst was filtered off with a fine porosity glass frit, and the volume of the colorless supernate was reduced to 100 mL by rotary evaporation. Note that Adam's catalyst, PtO_2, is reduced to platinum black, a pyrophoric solid, during hydrogenation. The catalyst can possibly ignite upon contact with some organic solvents. Methanol (100 mL) was added, and most of the product ($(H_{+3}TACI)_2(SO_4)_3$, 3 g) precipitated out. (Figure II.6) The product was filtered. Addition of more methanol to the filtrate yielded another 0.9 g of crude product. (Additional product remained in solution.)

Purification of $(H_{+3}TACI)_2(SO_4)_3$

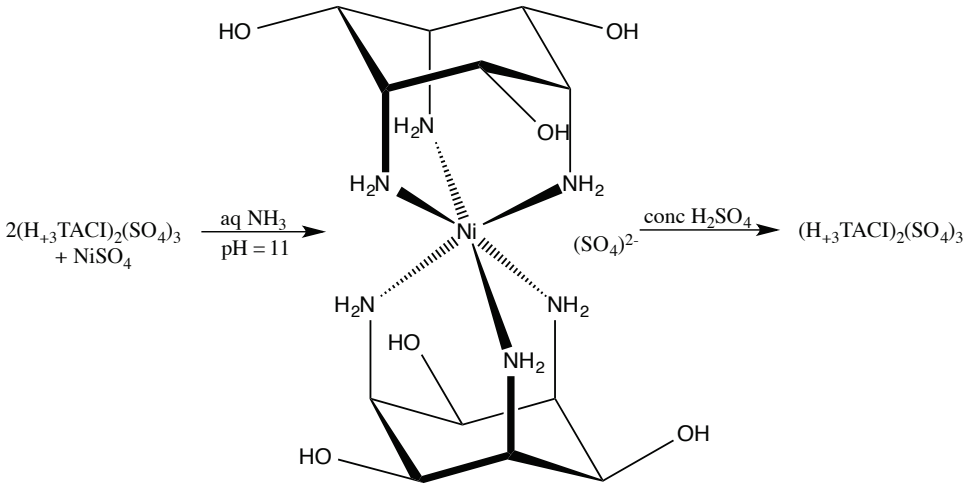

Figure II.7. Purification of $(H_{+3}TACI)_2(SO_4)_3$ by way of nickel complexation.

Crude $H_{+3}TACI$ (3.9 g) was dissolved in 39 mL of water. (This did not produce a suspension, as in the literature, but a solution.) The pH was adjusted to 11 with conc. aq. NH_3. $NiSO_4 \cdot 6H_2O$ (1.3 g) in 19.5 mL of H_2O was added to the TACI solution. A pinkish-purple so-

lution resulted. Within minutes, a pink precipitate of $[Ni(TACI)_2]SO_4$ appeared. The solution/mixture was stored overnight at ~5 °C. The solution was filtered, and the precipitate was recrystallized from boiling water. The recrystallized product (~1.8 g) was isolated by filtration, then dissolved in a minimum amount of water (39 mL) at 80 °C. Concentrated sulfuric acid (1.18 g, 0.64 mL) was carefully added to the hot solution. The color of the solution changed from pink to green. Methanol (40 mL) was added, and the resulting white precipitate was isolated by filtration. Nickel salt were apparently entrained in the solid, giving it a greenish tint. The white solid was recrystallized at least twice more by dissolving the solid in a minimum amount of H_2O and precipitating with methanol. (No heating was involved.) 1.8 g of H_{+3}TACI sulfate was obtained (87% yield). (Figure II.7)The original preparation in the patent involved recrystallizing the crude H_{+3}TACI sulfate six times in this manner. See experimental discussion for further comments.

$(H_{+3}TDCI)_3$ via reductive methylation of $(H_{+3}TACI)_3$

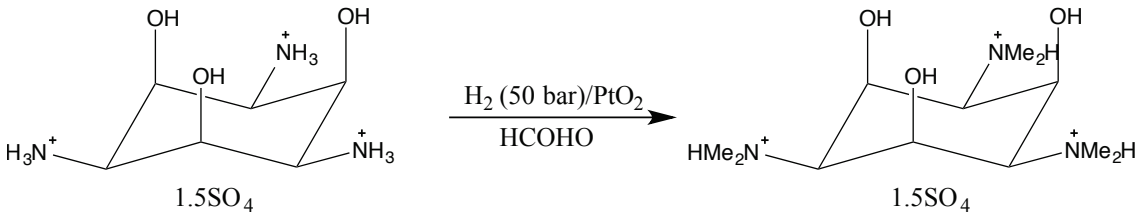

Figure II.8. Reductive methylation of $(H_{+3}TACI)_2(SO_4)_3$.

A stirred mixture of Adam's catalyst, PtO_2, (0.264 g) in 25 mL of water was pre-reduced by hydrogen gas (10 bar, 1 hour) to platinum black in a Parr reactor. Aqueous formaldehyde

(4.8 g) and 1.8 g of H_{+3}TACI sulfate were added to the reaction mixture, and reductive amination was carried out over a period of 48 hours, with stirring. (Figure II.8)The finely divide Pt catalyst was filtered from the solution through a fine porosity glass frit. All volatiles (excess formaldehyde and water) were removed by rotary evaporation to yield a white solid. The crude product was not purified but was subjected to anion exchange to yield either the chloride salt or the free base, as outlined in the next section.

Preparation of $(H_{+3}TDCI)(Cl)_3$ and TDCI

$$(H_{+3}TDCI)_2(SO_4)_3 \xrightarrow{Cl^- exchange} (H_{+3}TDCI)Cl_3$$
$$(H_{+3}TDCI)_2(SO_4)_3 \xrightarrow{OH^- exchange} TDCI$$

Figure II.9. Anion exchange of H_{+3}TDCI sulfate salt.

The crude H_{+3}TDCI sulfate was dissolved in 15 mL of water and subjected to anion exchange (Dowex Marathon A, OH^- form) to yield a solution of the free base. The literature preparation suggest exchanging sulfate for chloride first (Dowex 1, Cl^- form), purifying the H_{+3}TACI chloride salt, then exchanging Cl^- for OH^- to yield the free base. If only the free base is desired, this step is probably not necessary. Both methods were applied over several different preparations of TDCI. (Figure II.9) In any case, the anion exchanged column was washed thoroughly with distilled water to ensure removal of the product. The water of the eluate was removed by rotary evaporation. The crude TDCI free base was recrystallized from boiling hexanes (0.82 g, 89% yield). Consider an alternative to anion exchange involving treatment of $(H_{+3}TACI)_2(SO_4)_3$ sulfate with $Ba(OH)_2$.

Preparation of Nishimura and Adam's catalyst

This preparation of $(Rh/Pt)O_2$ (Nishimura catalyst) is as described in *Handbook of Heterogeneous Catalytic Hydrogenation for Organic Synthesis*.[26] $RhCl_3 \cdot 3H_2O$ (1.075 g) and $H_2PtCl_4 \cdot 6H_2O$ (0.5 g) were dissolved in water in an 80 mL porcelain casserole. Approx. 28.6 g of $NaNO_3$ and a little water was added. The mixture was stirred and heated to dryness. (If heated too quickly, the water with spatter the product out of the casserole.) The mixture was then heated to melt the sodium nitrate with a heating mantle. When this happens nitrogen oxides evolve vigorously. At first the reaction mixture tends to bubble up, so it's advisable to continuously stir. I covered it with a watch glass because of spattering. Gas will continue to evolve for quite some time. The entire casserole and watch glass (at about 350 °C, with tongs) were put into a furnace preheated to 475 °C. for 15 minutes. (5 minutes to get to temperature plus 10 minutes at temperature.) The reaction mixture was allowed to cool to room temperature. Water was added to dissolve away NaCl and excess sodium nitrate. (It takes a while to dissolve, and it's hard to break up without splashing your product all over the place. Two batches of water were used to dissolve everything. The catalyst was filtered off and washed with 200 mL of 0.5% aqueous sodium nitrate. 1.1 g of $(Rh/Pt)O_2$ were recovered, but the theoretical yield was only 0.95 g. The product was not dried over a desiccant as in the Handbook, so water most likely accounts for the extra mass.

Adam's catalyst was prepared *via* ammonium hexachloroplatinate, $(NH_4)_2PtCl_6$, *via* a slightly modified procedure as described in Organic Syntheses.[27] Ammonium hexachloroplatinate (3.0 g) and sodium nitrate (30 g) were heated in a quartz tube approximately 1.5″ in

diameter and 1′ in length, instead of a pyrex or porcelain dish, using an inclined tube furnace. The heating was slow at first, as to avoid spattering, until gas evolution slowed. The furnace temperature was then increased to 520 °C , and the reaction was given 10 minutes to reach this desired temperature, after which heating was continued for 30 minutes at 520 °C. After the requisite heating period, the quartz tube was carefully removed from the hot furnace with tongs and was allowed to cool for a few minutes on a piece of fiberglass insulation, but not long enough for the sodium nitrate to solidify. The molten sodium nitrate and PtO_2 (~450 °C) were poured directly into a large volume of water (500 - 1000 mL) contained in an Erlenmeyer flask of at least twice said volume, with stirring. The sodium nitrate was not allowed to solidify into a solid mass, as in the literature preparation.

The platinum black catalyst can be reused once without a significant lowering of yield for the subsequent hydrogenation. After the catalyst is spent, it can be reworked by dissolving in aqua regia, boiling the solution *just* to dryness, and reacting this chloroplatinic acid product with sodium nitrate as outlined in Organic Syntheses (similar to above mentioned procedure). The resulting chloroplatinic acid can also be converted to ammonium hexachloroplatinate for long term storage and use for other purposes. Chloroplatinic acid (a solid) is extremely hygroscopic and difficult to work with, so ammonium hexachloroplatinate is preferred as the starting material. As a note, a convenient and economical Pt source for this hydrogenation catalyst is a platinum coin of at least 99.9% purity (metals basis). With some patience, the coin can be cut into small pieces with snips (to increase surface area) and dissolved in aqua regia to produce chloroplatinic acid for immediate reaction with sodium nitrate, or it can be converted

to ammonium hexachloroplatinate if so desired. Adam's catalyst prepared from such a source produced perfectly satisfactory results in my experience.

β-diketonate

Acetylacetone (Hacac), dipivaloylmethane (Hdpm), and dibenzoylmethane (Hdbm) were used as received. All β-diketones were added in stoichiometric proportions (the liquid β-diketones (Hacac and Hdpm) were added via syringe) in their respective reactions involving lanthanide H_{-3}TDCI clusters. Triethylamine (in slight stoichiometric excess) was used to deprotonate the β-diketones, and the resulting β-diketonates ($acac^-$, dpm^-, dbm^-) formed the desired lanthanide complexes.

The sodium salts of $acac^-$ (Na(acac))and dpm^- (Na(dpm))were also used as β-diketonate sources in preliminary test reactions. Na(acac) and Na(dpm) and tetracetylethane were synthesized via literature procedures.

Sodium dipivaloylmethane

Dipivaloylmethane was shaken with an ethanolic solution of sodium hydroxide. The precipitate was isolated by filtration.[28]

Sodium acetyacetonate

A solution of 4.0 g (0.1 mol) sodium hydroxide dissolved in 5 mL of water was added to 20 mL of methanol. This solution was added slowly and with stirring to 10 g (0.1 mol) of acetylacetone, resulting in the immediate precipitation of sodium acetylacetonate. The mixture was stored at 5 °C for a few hours, and the precipitate was isolated by filtration on a Büchner funnel . A few rinses with cold methanol removed the majority of colored impurities, but care must be

taken, as the washes dissolve the product and reduce the yield.[29]

Tetraacetylethane (H_2tea)

A scaled down literature procedure was followed.[29] Iodine (2.54 g) dissolved in 30 mL of ether was added to a stirred mixture of hydrated sodium acetylacetonate (2.9g) also in 30 mL of ether. A precipitate formed. The ether was allowed to evaporate, and water was added to the resulting solid. The mixture was filtered, and the solid was washed with several portions of water and recrystallized from boiling methanol.

Lanthanide tris[bis(trimethylsilyl)]amides

All reactions were carried out under inert conditions using a combination of Schlenk techniques and glove box manipulation. THF was distilled from Na/K or a purple Na/benzophenone ketyl, or dried with molecular sieves. Hexane and pentane were dried over Na/benzophenone (with tetraglyme) or dried by a commercial solvent purification column. Sodium bis(trimethylsilyl)amide was obtained from Acros Organics and purified by sublimation under reduced pressure before use.

$$Ln(OTf)_3 + 3\ Na[N(SiMe_3)_2] \xrightarrow{THF} Ln[N(SiMe_3)_2]_3 + 3\ Na(OTf) \qquad (2.1)$$

To a Schlenk flask containing 5 g (27.3 mmol) of purified sodium bis(trimethylsilyl)amide and 9.1 mmol of lanthanide triflate was added 50 mL of dry THF. The mixture was stirred and refluxed for approximately 3 hours. All of the lanthanide triflate had dissolved within the first hour. The solvent was removed under reduced pressure, and solid was extracted with

hexanes or pentane, and the residual solid filtered off. The hydrocarbon solvent was removed under reduced pressure. The white or off-white solid thus obtained was sublimed at ~100 °C at approximately 10^{-4} torr.[30,31] Average yield ranged from 50-60%. Because of the paramagnetic nature of the lanthanide ions, confirmation of purity by NMR was not obtained and were used as-is after purification.

Rare earth triflates

Lanthanide trifluormethanesulfonates (triflates) were synthesized by the addition of 1:1 (v/v) triflic acid in water to a slight stoichiometric excess of lanthanide oxide. The excess lanthanide oxide was filtered off, and the water was removed by rotary evaporation, leaving a white solid of lanthanide triflate hydrate. The anhydrous lanthanide triflate was obtained by heating at 180 °C under reduced pressure (10^{-3} – 10^{-4} torr) for 48 hours and used without further purification.[32-35] Batches of lanthanide triflate used for synthesis in TDCI clusters were stored in a desiccator. Those used for lanthanide amide synthesis were stored in a glove box.

DISCUSSION

Each section in the Experimental section will be briefly discussed, in turn.

1,3,5-tris(dimethylamino)-1,3,5-trideoxy-cis-inositol (TDCI)

Diazotization of sulfanilic acid

Sulfanilic acid, poorly soluble in water, was dissolved with the help of sodium carbonate to yield the sodium salt. Diazotization was carried out at reduced temperature using HBr and sodium nitrite. The reaction is carried out at low temperature to avoid decomposition of the desired diazonium compound, p-benzenediazonium sulfonate. A slight stoichiometric excess of

HBr (2:1) was used to ensure complete conversion to nitrosonium. The zwitterionic p-benzenediazonium sulfonate, poorly soluble in water, precipitates from solution, but subsequent azo-coupling is not affected.

Azo-coupling of phloroglucinol and p-benzenediazonium sulfonate

Azo-coupling of the just-synthesized p-benzenediazonium sulfonate and phloroglucinol was carried out in basic conditions and at reduced temperature, as is typical with these types of couplings.

Catalytic hydrogenation of trisodium tris[(p-sulfonatophenyl)azo]phloroglucinol

In order to achieve the all *cis* configuration of OH/NH_2 groups on the cyclohexane ring of TACI, reductive hydrogenation on a Pt surface is required. The Horiuti-Polanyi mechanism is the commonly accepted one for this process. A variety of heterogeneous catalysts were screened by Hegetschweiler, but Nishimura $(Rh/Pt)O_2$ and Adam's (PtO_2) catalysts were shown to yield the best results in terms of both total yield and regioselectivity. Though Nishimura catalyst was shown to give slightly higher yields, Adam's catalyst was used here because of a practical consideration. Namely, the ease of recycling after the catalyst has been exhausted. Nishimura catalyst reportedly dissolves in aqua regia, and thus should be amenable to recycling, but no such luck was had in this laboratory.

Purification of $(H_{+}3TACI)_2(SO_4)_3$

In the literature preparation, crude H_{+3}TACI sulfate is recrystallized six times by dissolving in a minimum amount of water and precipitating with an equal volume of methanol. Another purification route was suggested. Because of the notable stability of $Ni(TACI)_2(SO_4)$,

the complexation of crude TACI with nickel sulfate is used as a purification method. Reacting crude $(H_{+3}TACI)_2(SO_4)_3$ with nickel sulfate in basic solution (aqueous ammonia, pH 11) leads to slow formation and precipitation of the nickel-TACI complex. Stereoisomerically pure, all-*cis* TACI preferentially binds to nickel, *via* amine N atoms, compared to other stereoisomers and substitutionally incomplete byproducts. Though an elegant method of purification, given the effort involved in the Ni complex preparation and recrystallization, its subsequent decomposition, and the repeated recrystallization of the decomposition product (pure $H+_3TACI$ sulfate) to remove entrained nickel salts, it is not clear that the nickel purification method is as convenient as the original literature preparation suggests.

H_{+3}TDCI sulfate via reductive methylation

Effective conversion of the amino groups of TACI to dimethylamino groups can be achieved by reductive methylation via catalytic hydrogenation. (This reaction is more commonly referred to as a reductive amination. This of course depends on one's point of view. In the current context, it is reasonable to view this reaction as the addition of methyl groups to the amino groups of TACI, as opposed to the addition TACI-amines to formaldehyde!) As with the previous hydrogenation, Adam's catalyst was used for the reaction. Again, finely divided Pt metal (Pt black) is the active catalytic species. The action of excess formaldehyde on sulfate acid salt of TACI under high pressures of H_2 yield the desired product, $(H_{+3}TDCI)_2(SO_4)_3$. The reaction proceeds by way of the reduction of an imine intermediate by hydrogen gas on the Pt surface. Other synthetic routes were attempted in the literature, but this method was deemed necessary for successful conversion to the methylated analogue.

The sulfate salt of $(H_{+3}TDCI)^{3+}$ is nearly insoluble in nonaqueous solvents, which complicates purification and limits the use of the salt in nonaqueous reactions. As such, sulfate was exchanged for chloride or hydroxide to yield either the chloride salt or the free base, respectively. Dowex anion exchange resins of Cl^- and OH^- form were used for this purpose. Anion exchange chromatography can be quite tedious, so a metathesis/acid-base reaction resulting from the treatment of $(H_{+3}TDCI)_2(SO_4)_3$ with $Ba(OH)_2$ would likely be a viable alternative route to the free base.

A summary of the entire reaction scheme for TDCI can be found in Figure II.10.

β-diketonates

The synthesis of β-diketonate-ligated trinuclear lanthanide clusters, $Ln_3(H_{-3}TDCI)_2(\beta\text{-diketonate})_3$ is discussed in Chapter III in detail. Two synthetic routes were explored in the synthesis of these clusters. One route is to deprotonate β-diketones with an alkali-metal hydroxide before reacting with Ln_3 clsuters, introducing β-diketonates as sodium salts (Na(acac), Na(dpm), Na(dbm), (Na(hfac)). A more convenient route, and the typical one taken in this work, is the addition the β-diketone to a solution of Ln_3 clusters in the presence of a slight stoichiometric excess of triethylamine. The *in situ* formation of β-diketonate ligands avoids the extra synthetic effort involved in the preparation of the sodium salt.

Synthesis of 1,3,5-tris(dimethylamino)-1,3,5-trideoxy-*cis*-inositol

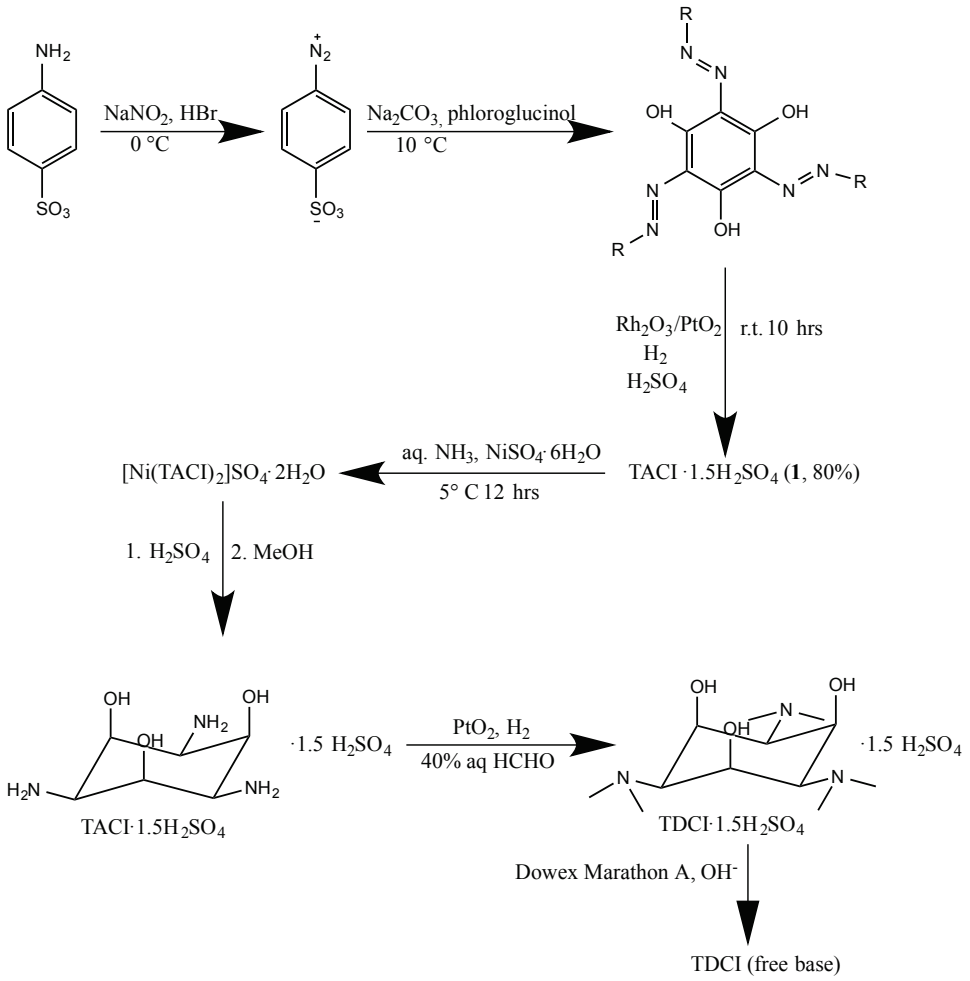

Hegetschweiler, K.; Erni, I.; Schneider, W.; Schmalle, H., *Helv. Chim. Acta* **1990**, *73* (1), 97-105.
Ghisletta, M.; Jalett, H. P.; Gerfin, T.; Gramlich, V.; Hegetschweiler, K., *Helv. Chim. Acta* **1992**, *75* (7), 2233-42.

Figure II.10. Reaction scheme for the synthesis of TDCI.

Tetraacetylethane was synthesized by the action of molecular iodine on sodium acetylacetonate. This oxidation resulted in two acac molecules coupled at their flanked α-carbons, and a sodium iodide byproduct that was easily removed with water.

Lanthanide tris[bis(trimethylsilyl)]amides

The synthesis of $Ln[N(SiMe_3)_2]_3$ is metathesis reaction between $Ln[N(SiMe_3)_2]_3$ and $Ln(OTf)_3$. Synthesis in a low-moderate polarity solvent with high donor strength such as THF somewhat solubilizes the ionic lanthanide triflate compared to that of the a hydrocarbon solvent while still dissolving the sodium amide. The use of only THF likely accelerates the reaction compared to the mixed THF/heptane synthesis used by Belot et al.[30] To ensure complete removal of the sodium triflate byproduct, hexane is used to extract the desired compound and filtered through a fine frit. In the literature, both recrystallization and sublimation are used to purify the product. Here, sublimation alone seemed to produce a satisfactory starting material.

CHAPTER III

SYNTHESIS AND CHARACTERIZATION OF TRINUCLEAR RARE EARTH CLUSTERS SUPPORTED BY TDCI

INTRODUCTION

Among many polynuclear dysprosium magnets, the trimetallic o-vanillin-supported trinuclear cluster, $[Dy_3(\mu_3\text{-}OH)_2(o\text{-vanillin})_3Cl_n(H_2O)_{6-n}]4^{-n}$, is particularly interesting because of its vortex spin structure.[36,37] The dinuclear N_2^{3-} bridged terbium complex $[K(18\text{-crown-}6)(THF)][^{38}{}_2(N_2)]$ exhibits impressive hysteresis up to 14 K.[38,39] The pentanuclear $Dy_5(O)(O\textit{i}\text{-Pr})_{13}$ cluster, was recently shown to be a very robust SMM with a high anisotropy barrier, and interestingly, dilution studies of this compounds and $Dy_4K_2O(O\textit{t}\text{-Bu})_{12}$ have revealed that intramolecular interactions can be quite substantial in polymetallic lanthanide SMM.[40,41]

In the late 1990's, Hegetschweiler et al synthesized trinuclear sandwich-type lanthanide clusters, $Ln_3(TACI)_2L_6$ (L = H_2O, Cl, NO_3) with the versatile supporting ligands TACI (1,3,5-triamino-1,3,5-trideoxy-cis-inositol) and TDCI (1,3,5-tris(dimethylamino)-1,3,5-trideoxy-cis-inositol.[25,42-48] Peripheral ligand substitution studies of these clusters have, to our knowledge, not been reported. Among the vast array of metal complexes formed by TACI , the trinuclear lanthanide clusters supported by TACI are fairly well studied, though those of TDCI much less so. The magnetic and luminescence properties of the cluster-types, however, have scarcely been examined.

This work presents the synthesis and characterization of rare earth trinuclear clusters, $RE_3(H_{-3}TDCI)_2(L)_3$ (RE = Y, Eu, Gd, Tb, Dy, Ho, Er; L= dpm^-, $acac^-$, dbm^-, $hfac^-$, $Htae^-$) and $Dy_3(H_{-3}TDCI)_2(MeOH)_6(OTf)_3$, as well as dilutions studies to probe the effects of intramolecular Ln-Ln interactions. Structures of TDCI and dpm^- are show in Figure III.1.

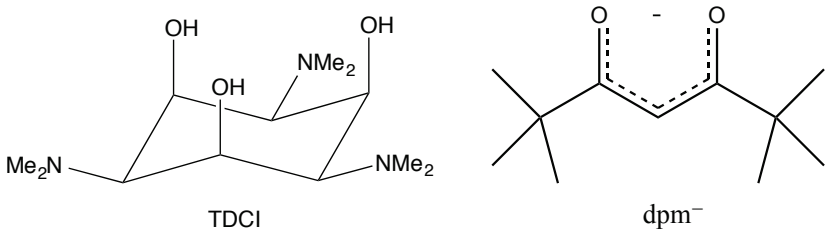

Figure III.1. Skeletal structure for TDCI and dpm^-.

EXPERIMENTAL

All reactions were performed in open air. All materials (rare earth oxides, trifluoromethanesulfonic acid (triflic acid), triethylamine, dipivaloylmethane (Hdpm), and solvents were obtained from commercial sources and used as received. Adam's catalyst was prepared from ammonium hexachloroplatinate.[27] A small portion of 1,3,5-triamino-1,3,5-trideoxy-cis-inositol trihydrochloride ($(H_{+3}TDCI)Cl_3$) was graciously provided by K. Hegetschweiler for preliminary test reactions. All 1,3,5-tris(dimethylamino)-1,3,5-trideoxy-cis-inositol (TDCI) and its hydrochloride salt ($(H_{+3}TDCI)Cl_3$) used in this work was synthesized in this laboratory, via trisodiumtris(p-sulfonatophenylazo)phloroglucinol, according to literature procedures reported by Hegetschweiler and coworkers, with exception of the hydrogenation catalyst used: Adam's catalyst, PtO_2, was used instead of Nishimura catalyst, $(Pt/Rh)O_2$.[25,48]

Synthesis of $RE_3(H_{-3}TDCI)_2(L)_3$·toluene. (RE = Eu, Gd, Dy, Tb, Dy; L = dpm, dbm)

In a typical synthesis, $RE(OTf)_3$ (0.18 mmol) and TDCI·3HCl (0.12 mmol) were dissolved in 10 mL of ethanol or methanol. A slight stoichiometric excess of NEt_3 (0.92 mmol) was added, and the solution was stirred at reflux for 30 minutes. Shortly after the addition of HL (0.18 mmol), a white precipitate formed, and the mixture was stirred under reflux for another hour. Reaction work up was carried out in one of two ways:

(1) Upon cooling, the mixture was centrifuged, the supernate removed, and the precipitate washed three times with ethanol. The product was dissolved in toluene and crystallized by slow evaporation.

(2) The mixture was filtered through a fine glass frit and the product was washed three times with methanol. Hot toluene was poured into the filter funnel, the product dissolved, and the solution was forced through the frit with a positive pressure of nitrogen. Upon evaporation of the filtrate, a white crystalline product was obtained.

For dpm ligated clusters, crystals suitable for X-Ray diffaction were obtained from slow evaporation of a toluene solution. Yield: 70-90%.

Characterization of $RE_3(H_{-3}TDCI)_2(dpm)_3$·toluene:

Elemental analysis (CHN) found (calculated) for

Dy_3dpm: $Dy_3C_{64}H_{113}N_6O_{12}$: C 46.44% (46.67%), H 6.9% (6.76%), N 5.01% (5.11%).

Y_3dpm: $Y_3C_{64}H_{113}N_6O_{12}$: C 53.73% (53.9%); H 7.87% (7.99%); N 5.75% (5.90%).

Eu_3dpm: $Eu_3C_{64}H_{113}N_6O_{12}$: C 47.35% (47.61%); H 6.84% (7.05%); N 5.12% (5.2%).

Gd_3dpm: $Gd_3C_{64}H_{113}N_6O_{12}$: C 46.28% (47.15%); H 6.78% (6.99%); N 4.97% (5.16%).

Tb_3dpm: $Tb_3C_{64}H_{113}N_6O_{12}$: C 45.15% (47.00%); H 6.66% (6.97%); N 5.18% (5.14%).

Ho_3dpm: $Ho_3C_{64}H_{113}N_6O_{12}$: C 46.33% (46.49%); H 6.89% (6.69%); N 5.08% (4.97%).

Er_3dpm: $Er_3C_{64}H_{113}N_6O_{12}$: C 47.35% (46.30%); H 6.84% (6.86%); N 5.12% (5.06%).

Y_3dpm ^{1}H NMR (300 MHz, $CDCl_3$): 5.71 (s, 3H); 4.45 (m, 3H); 2.36 (s, toluene) 2.22 (m, 36H); 1.39 (m, 3H); 1.16 (m, 54H); 1.6 - 2.8 (s, H_2O).

For dbm-ligated clusters, crystals suitable for X-Ray diffaction were obtained from slow diffusion of ethanol into a toluene solution of the product.

Synthesis of $Dy_{0.15}Y_{2.85}(H_{-3}TDCI)_2(dpm)_3$·toluene ($DyY_2$dpm)

A slight stoichiometric excess of NEt_3 (1.97 mmol, 275 μL) was added to a solution of $Dy(OTf)_3$ (19.3 μmol, 11.7 mg) , $Y(OTf)_3$ (366 μmol, 196.3 mg), and TDCI·3HCl (0.257 mmol) in 10 mL of methanol. The solution was stirred at reflux for 30 minutes. Shortly after the addition of Hdpm (0.385 mmol, 80.5 μL), a white precipitate formed, and the mixture was re-fluxed for another hour. Reaction work up was as discussed for the pure trinuclear clusters.

Synthesis of $Dy_3(H_{-3}TDCI)_2(hfac)_3(MeOH)_3$ and $Ln_3(H_{-3}TDCI)_2(acac)_3$ (Ln = Gd, Dy, Tb)

$RE(OTf)_3$ (0.18 mmol) and TDCI·3HCl (0.12 mmol) were dissolved in 10 mL of ethanol or methanol. A slight stoichiometric excess of NEt_3 (0.92 mmol) was added, and the solution was stirred at reflux for 30 minutes. After the addition of HL (0.18 mmol), the solution was allowed to cool. After a few hours, large block shaped crystals formed. A suitable single crystal was characterized by X-Ray crystallography. Yield: 50%.

Synthesis of $Dy_3(H_{-3}TDCI)_2(Htae)_3$

A diffusion of reactants through a three-layer solvent system resulted in the formation of large crystals of $Dy_3(H_{-3}TDCI)_2(Htae)_3$. A bottom layer of two mL of water containing 25 mg of $[Gd_3(H_{-3}TDCI)_2(H_2O)_6](OTf)_3$ (synthesis in Chapter IV) and top layer of two mL of ethanol containing a stoichiometric ratio of 1.5 (with respect to Dy_3H_2O) of tetraactylethane (H_2tae) and a slight excess of triethylamine (NEt_3) was separated by a 1:1 (v:v) solution of water and ethanol. Yield was not determined, as there was very little product..

Regeneration of TDCI·3HCl ligand

To a solid residue containing $Ln_3(H_{-3}TDCI)_2L_6$, either pure or in the presence of $HNEt_3(OTf/Cl)$, was added a two-fold stoichiometric excess of HCl (concentrated aqueous hydrochloric acid). The mixture was heated to boiling until the solid completely dissolved. Upon cooling ethanol was added, and a white solid crystallized out of solution. Crude yield of product is practically quantitative. ^1H NMR is in agreement with that of TDCI·3HCl in the literature.[48] The precipitate was separated by filtration and recrystallized from boiling methanol.

Synthesis of $[Dy_3(H_{-3}TDCI)_2(MeOH)_6](OTf)_3$ (Dy_3MeOH)

$Ln(OTf)_3$ (0.18 mmol, 105 mg) and TDCI (0.12 mmol, 30 mg) were dissolved in 10 mL of methanol. A slight stoichiometric excess of NEt_3 (0.36 mmol, 50 μL) was added, and the solution was stirred and refluxed for 1 hour. Upon cooling clear, colorless crystals were obtained. A single crystal suitable for X-ray diffraction was selected from the mother liquor. Yield: 30%. $Dy_3C_{33}H_{72}O_{21}N_6F_9S_3$: C 22.15% (24.15%); H 4.01% (4.42%); N 5.21% (5.66%).

Elemental Analysis

Carbon, hydrogen, and nitrogen elemental analyses were performed by Robertson Microlit Laboratories using a Perkin-Elmer Model 2400 CHN Analyzer.

Mass Spectrometry

Matrix assisted laser desorption ionization (MALDI) experiments were performed on a Voyager DE-STR mass spectrometer (Applied Biosystems, Foster City, CA) under optimized conditions in positive reflectron mode. Ions were generated by a pulsed nitrogen laser at 337 nm and accelerated through 20 kV. One hundred laser shots were used per spectrum. trans-2-[3-(4-tert-butyl-phenyl)-2-methyl-2-propenylidene]malononitrile (DCTB) was used as matrix at a concentration of 10 mg/ml concentration. The sample solution was mixed with the matrix at a volume ratio of 1:1. About 0.5 μl of this mixture was deposited on a stainless steel sample holder. After air-dried, the sample was analyzed using MALDI TOF MS.

X-Ray Crystallography

Single crystal X-ray diffraction data were collected on a Bruker APEX II diffractometer using Mo-K_α radiation (λ = 0.71073 ang). The samples were dispersed in oil and mounted on a

nylon loop. The cell constants were indexed from reflections obtained from 200 frames with exposure times of 10 seconds per frame. For **RE_3dpm**, (RE = Y, Dy, Tb) a full sphere (1440 or 2400 frames at 6 cm detector distance) was collected with scan widths of 0.5° and 0.3° in omega and exposure times of 10 and 20 seconds per frame for Y and Dy clusters, respectively. For **Dy_3MeOH**, data collection strategies were calculated using COSMO and data were collected from a series of phi and omega scans with scan widths of 0.3° in omega and 10 second exposure times. X-ray diffraction data were collected at 110 K and the space group was uniquely determined to be $P2_1/n$ for all crystals reported herein.

Data reduction and cell refinement for all compounds were performed with SAINT. SADABS was used to obtain absorption-corrected data. The structures were solved by direct methods and refined by full-matrix least squares on F^2 using the Bruker SHELXTL (XS) and XL. Olex2 was used to interface with the refinement software. All non-hydrogen atoms were refined anisotropically. Hydrogen atoms were placed in idealized positions and were set riding on the respective parent atoms. For **Dy_3MeOH**, methoxy hydrogens were found in the difference map, their distances to their respective O atoms were restrained. Elongated anisotropic displacement ellipsoids on the dpm ligand indicated disorder, which was modeled. Restraints and constraints were used to keep the bond distances, angles, and thermal ellipsoids meaningful. Absence of additional symmetry and voids were confirmed using PLATON.

Modeling of disorder for all other dpm- (Ln = Eu, Gd, Ho, Er) and dbm-ligated (Ln = Dy) is not complete, but their structures are not in doubt. For acac-ligated Ln_3 clusters one methanol solvate molecule was masked, as its disorder was severe.

Table III.1. Crystallographic information for MeOH/dpm compounds in Chapter III

Empirical formula	$C_{64}H_{113.87}Dy_3N_6O_{12.20}$	$C_{64}H_{113}Y_3N_6O_{12}$	$C_{33}H_{72}N_6O_{21}F_9S_3Dy_3$
Formula weight	1650.19	1425.36	1643.64
Temperature	110.15 K	110.15 K	110.15 K
Wavelength	0.71073 Å	0.71073 Å	0.71073 Å
Crystal system	Monoclinic	Monoclinic	Monoclinic
Space group	$P2_1/n$	$P2_1/n$	$P2_1/n$
Unit cell dimensions	a = 14.164(5) Å	a = 14.002(8) Å	a = 13.4356(8) Å
	b = 25.847(9) Å	b = 25.894(14) Å	b = 22.1178(13)Å
	c = 20.301(7) Å	c = 20.369(11) Å	c = 18.7424(11)Å
	α= 90°	α= 90°	α= 90°
	β= 106.911(4)°	β= 106.911(4)°	β= 102.706(3)°
	γ = 90°	γ = 90°	γ = 90°
Volume	7111(4) $Å^3$	7082(7) $Å^3$	5433.2(6) $Å^3$
Z	4	4	4
Density (calculated)	1.541 g/cm^3	1.337 g/cm^3	2.009 g/cm^3
Absorption coefficient	3.179 mm^{-1}	2.497 mm^{-1}	4.306 mm^{-1}
F(000)	3342	3008	3228
Crystal size ($mm^{3)}$	0.24 x 0.23 x 0.12	0.1 x 0.083 x 0.07	0.1 x 0.1 x 0.2
Theta range	2.067 to 27.500°	1.306 to 27.606°	1.445 to 27.461°
Reflections collected	82504	81669	96865
Independent reflection	16329 (Rint = 0.0427)	16233 (Rint = 0.0925)	12431 (Rint = 0.0437)
Completeness to θ= 25.242°	99.9%	100%	100%
Absorption correction	Multi-scan	Multi-scan	Multi-scan
Max and min transmission	0.7458 and 0.6347	0.7456 and 0.5948	0.746 and 0.643
Restraints / parameters	16329 / 87 / 763	16333 / 1058 / 993	16333 / 1058 / 993
Goodness-of-fit-F^2	1.032	1.018	1.084
Final R indices (I>2σ(I))	R_1 = 0.0294, wR_2 = 0.0651	R_1 = 0.0515, wR2 = 0.1051	R_1 = 0.0254, wR2 = 0.0545
R indices (all data)	R_1 = 0.0380, wR_2 = 0.0698	R_1 = 0.1001, = wR_2 = 0.1235	R_1 = 0.0344, = wR_2 = 0.0578
Extinction coefficient	n/a	n/a	n/a
Largest diff. peak and hole	1.335 and -1.350 e/$Å^3$	1.740 and -0.839 e/$Å^3$	0.9 and -0.75 e/$Å^3$

Further crystallographic information regarding dpm-ligated and MeOH-ligated compounds can be found in Table III.1 and Table III.2.

Table III.2. Crystallographic information for dpm compounds in Chapter III

Identification code	Eu_3dpm*	Gd_3dpm*	Tb_3dpm	Ho_3dpm*	Er_3dpm*
Empirical formula	$C_{64}H_{113}N_6O_{12}Eu_3$	$C_{64}H_{113}N_6O_6Gd_3$	$C_{64}H_{113}N_6O_{12}Tb_3$	$C_{64}H_{113}N_6O_6Ho_3$	$C_{64}H_{113}N_6O_6Er_3$
Formula weight	1522.34	1528.38	1637.74	1566.29	1573.28
Temperature/K	296.15	296.15	110.15	296.15	296.15
Crystal system	monoclinic	monoclinic	monoclinic	monoclinic	monoclinic
Space group	$P2_1/c$	$P2_1/c$	$P2_1/n$	$P2_1/n$	$P2_1/n$
a/Å	21.022(3)	21.043(3)	14.213(3)	14.1277(15)	14.136(5)
b/Å	25.788(4)	25.897(3)	25.914(5)	25.825(3)	25.778(9)
c/Å	28.027(4)	28.006(4)	20.289(4)	20.306(2)	20.330(7)
α/°	90	90	90	90	90
β/°	109.533(2)	110.034(2)	106.943(2)	106.7930(10)	106.835(4)
γ/°	90	90	90	90	90
Volume/$Å^3$	14319(4)	14339(3)	7149(2)	7092.6(13)	7091(4)
Z	8	8	4	4	4
ρ_{calc} mg/mm^3	1.412	1.416	1.522	1.467	1.474
m/mm^{-1}	2.650	2.790	2.995	3.369	3.573
F(000)	6192.0	6232.0	3323.0	3164.0	3176.0
Crystal size/ mm	.1 × .15 × .1	.1 × .05 × .1	0.2 × 0.15 × 0.14	.15 × .2 × .15	.15 × .15 × .2
Radiation	λ = 0.71073	λ = 0.71073	λ = 0.71073	λ = 0.71073	λ = 0.71073
2Θ range for data collection	2.208 to 55.758°	2.06 to 54.976°	4.342 to 54.97°	2.622 to 55.752°	3.4 to 55.27°
Reflections collected	167772	166604	82494	83085	82567
Independent reflections	33934 R_{int} = 0.0749	32899 R_{int} = 0.0572	16383 R_{int} = 0.0568	16760 R_{int} = 0.0290	16425 R_{int} = 0.056
Data/ restraints/ parameters	33934/12/1585	32899/11/1598	16383/1077/1027	16760/0/811	16425/54/746
Goodness-of-fit on F^2	1.051	1.061	1.040	1.076	1.036
Final R indexes [I>=2σ (I)]	R_1 = 0.0436, wR_2 = 0.0945	R_1 = 0.0441, wR_2 = 0.1179	R1 = 0.0267, wR2 = 0.0644	R1 = 0.0281, wR2 = 0.0723	R1 = 0.0344, wR2 = 0.0794
Final R indexes [all data]	R_1 = 0.0672, wR_2 = 0.1069	R_1 = 0.0645, wR_2 = 0.1372	R1 = 0.0331, wR2 = 0.0682	R1 = 0.0338, wR2 = 0.0792	R1 = 0.0492, wR2 = 0.0881
Largest diff. peak/hole	2.83/-2.82 (e/Å)	2.49/-3.34 (e/Å)	0.97/-1.39 (e/Å)	2.37/-2.07 (e/Å)	2.14/-1.38 (e/Å)

*Structures not finalized.

Table III.3. Crystallographic information for acac compounds in Chapter III

Identification code	Gd_3acac	Tb_3acac	Dy_3acac
Empirical formula	$C_{44}H_{89}N_6O_{17}Gd_3$	$C_{44}H_{89}N_6O_{17}Tb_3$	$C_{43}H_{80}N_7O_{14}Dy_3$
Formula weight	1445.99	1450.99	1572.82
Temperature/K	110	110	110
Crystal system	monoclinic	monoclinic	orthorhombic
Space group	$P2_1/n$	$P2_1/n$	Pnma
a/Å	13.346(4)	13.223(8)	18.104(2)
b/Å	33.182(9)	32.99(2)	20.498(3)
c/Å	13.386(4)	13.279(8)	14.8359(19)
α/°	90	90	90
β/°	103.772(3)	103.982(5)	90
γ/°	90	90	90
Volume/$Å^3$	5758(3)	5621(6)	5505.6(12)
Z	4	4	4
ρ_{calc} mg/mm^3	1.796	1.787	1.898
m/mm^{-1}	3.488	3.800	4.105
F(000)	3112.0	3068.0	3136.0
Crystal size/mm	.1 × .9 × 1.5	.1 × .15 × .1	.1 × .1 × .13
Radiation	λ = 0.71073	λ = 0.71073	λ = 0.71073
2Θ range for data collection	3.872 to 55.366°	3.394 to 54.988°	3.388 to 55°
Independent reflections	67193	64448	61582
Data/restraints/ parameters	13469/0/656	12866/0/631	6484/0/352
Goodness-of-fit on F^2	1.023	1.086	1.190
Final R indexes [I>=2σ (I)]	13469 [R_{int} = 0.0468, R_{sigma} = 0.0353]	12866 [R_{int} = 0.0369, R_{sigma} = 0.0256]	6484 [R_{int} = 0.0274, R_{sigma} = 0.0139]
Final R indexes [all data]	R_1 = 0.0293, wR_2 = 0.0659	R_1 = 0.0410, wR_2 = 0.0984	R_1 = 0.0169, wR_2 = 0.0400
Largest diff. peak/hole	R_1 = 0.0393, wR_2 = 0.0698	R_1 = 0.0459, wR_2 = 0.1004	R_1 = 0.0186, wR_2 = 0.0483

Table III.4. Crystallographic information for compounds in Chapter III

Sample	Dy_3dbm	Dy_3hfac	Gd_3Htae
Empirical formula	$C_{78}H_{95}Dy_3N_6O_{13}$ (0.5 H_2O)	$C_{56}H_{88}N_6O_{15}F_{18}Dy_3$	$C_{57}H_{99}N_6O_{21}Gd_3$
Formula weight	1812.12	1721.45	1676.18
Temperature/K	110	110	110
Crystal system	monoclinic	hexagonal	hexagonal
Space group	$P2_1$	$P6_3/m$	$P6_3/m$
a/Å	14.034(3)	15.5277(15)	19.373(6)
b/Å	27.799(6)	15.5277(15)	19.373(6)
c/Å	19.684(4)	14.0017(19)	10.887(3)
α/°	90	90	90
β/°	91.350(3)	90	90
γ/°	90	120	120
Volume/$Å^3$	7677(3)	2923.7(7)	3539(2)
Z	4	2	3
ρ_{calc} mg/mm^3	1.448	2.175	1.971
m/mm^{-1}	2.946	3.929	4.248
F(000)	3324.0	1892.0	2097.0
Crystal size/mm^3	.1 × .05 × .1	.09 × .1 × .1	.1 × .06 × .1
Radiation	MoKα (λ = 0.71073)	MoKα (λ = 0.71073)	MoKα (λ = 0.71073)
2Θ range for data collection	3.818 to 55.792°	4.2 to 54.952°	4.204 to 54.89°
Reflections collected	92779	32086	36454
Independent reflections	36557 [R_{int} = 0.0347, R_{sigma} = 0.0488]	2327 [R_{int} = 0.1051, R_{sigma} = 0.0380]	2837 [R_{int} = 0.0362, R_{sigma} = 0.0161]
Data/restraints/ parameters	36557/18/1791	2327/3/150	2837/0/156
Goodness-of-fit on F^2	0.566	1.106	1.093
Final R indexes [I>=2σ (I)]	R_1 = 0.0319, wR_2 = 0.0855	R_1 = 0.0280, wR_2 = 0.0727	R_1 = 0.0201, wR_2 = 0.0508
Final R indexes [all data]	R_1 = 0.0365, wR_2 = 0.0917	R_1 = 0.0287, wR_2 = 0.0732	R_1 = 0.0246, wR_2 = 0.0522

Further crystallographic information regarding acac-ligated compounds can be found in Table III.3. For other diketonate-ligated compounds, including tetraacetylethanide, hexafluoroacetylacetonate, and dibenzoylmethanide, can be found in Table III.4.

Luminescence

A PTI QuantaMaster series spectrofluorometer was used to measure the fluorescence intensity of $1x10^{-4}$ M **Tb_3dpm** and **Eu_3dpm** upon excitation at 304-306 nm. A 1 cm path length quartz cuvette was used. Spectra were corrected for lamp emission intensity profile and detector response. The slit width of the source and detector were the same and were adjusted as to maximize the signal but not saturate the photodetector. Felix32 software was used to calculate corrected spectra and to account for intensities and detector efficiencies.

RESULTS AND DISCUSSION

Synthesis

Dy_3MeOH was synthesized in methanol by the reaction of stoichiometric amounts of dysprosium triflate, the free base TDCI (in order to avoid chloride binding), and a slight excess of triethylamine as a proton sink. Either TDCI or TDCI·3HCl can be used as precursors for **RE_3dpm** (or other diketonates) because chloride binding is not a serious concern in the presence of chelating oxo-donors like β-diketonates; though in a typical synthesis, TDCI·3HCl was typically used because of the ease of its preparation compared to the corresponding free base. For the dpm-ligated derivatives, after allowing some time for the formation of the cluster unit as in the procedure described above for Dy_3MeOH, addition of three equivalents of both the Hdpm and triethylamine (in slight excess), resulted in white precipitates of **Dy_3dpm** and **Y_3dpm**. Reactions proceed as in

equations 3.1 and 3.2.

$$3\ Ln(OTf)_3 + 2\ TDCI + 6\ NEt_3 + 6\ MeOH \xrightarrow{MeOH} Ln_3(H_{-3}TDCI)_2(MeOH)_6(OTf)_3 + 6\ HNEt_3(OTf) \quad (3.1)$$

$$3\ Ln(OTf)_3 + 2\ (H_{+3}TDCI)Cl_3 + 3\ HL + 6\ NEt_3 \xrightarrow{MeOH/EtOH} [Ln_3(H_{-3}TDCI)_2(L)_3] + 6\ (HNEt_3)Cl + 9\ (HNEt_3)(OTf) \quad (3.2)$$

L = dpm, acac, dbm, hfac, Htae

The **RE_3dpm** cluster compounds are isolated in good yields of 80-90% and are readily soluble in organic solvents such as hexanes, toluene, and THF.

A dilute mixture of the heterometallic cluster $DyY_2(H_{-3}TDCI)_2(dpm)_3$ in **Y_3dpm** was prepared in a preocedure analgous to that used for the other **RE_3dpm** compounds from a mixture of 95% Y/5% Dy (mole basis). A high dilution factor was used to reduce the statistical likelihood of forming species such as Dy_2Ydpm and Dy_3dpm. In this mixture, the presence of DyY_2dpm and Y_3dpm clusters, as well as the absence of significant quantities of the Dy_2Ydpm and Dy_3dpm, were confirmed by mass spectrometry.

Ln_3acac, **Dy_3hfac, Dy_3dbm**, and **Gd_3Htae** were synthesized in a manner analogous to that of the dpm analogues. The dibenzoylmethane compound had similar solubility properties as the dipivaloylmethane compounds, but its crystallization was not so straightforward. Slow evaporation produce poor quality crystals, but layering with ethanol produced suitable crystals. The **Ln_3acac** and **Dy_3hfac** derivatives were soluble in boiling methanol, and crystallized nicely from the initial reaction solution (in the presence of salt byproducts). **Dy_3acac** was crystallized under different growth conditions. Not out of necessity, but as an attempt at crystal engineering. The compound was dissolved in isopropanol and layered with acetonitrile. The same basic structure emerged, but with different solvate molecules, the compound crystallized in a different space group. **Gd_3Htae** was the unexpected product of an attempted MOF reaction.

X-Ray Crystal Structures

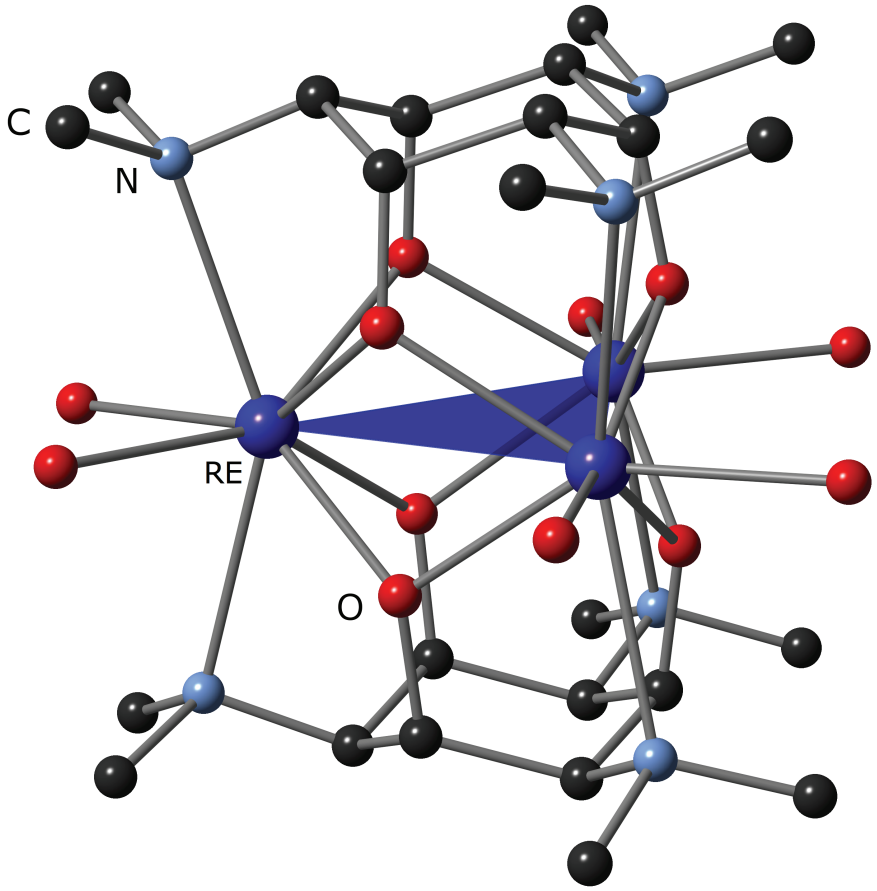

Figure III.2. $RE_3(H_{-3}TDCI)_2(L)_6$ cluster core.

In all structures, the free TDCI ligand adopts a chair cyclohexane ring confromation with hydroxyl substituents in 1,3,5-axial positions and dimethylamino substituents in 2,4,6-equatorial positions. As seen in Figure III.2.

The trinuclear clusters consist of roughly equilateral triangles of lanthanide ions sandwiched between two triply-deprotonated TDCI ligands, with peripheral ligands bound to each vertex in the plane of the triangle. In a trinuclear lanthanide-TDCI cluster, the three axial alkoxo-oxygens of each TDCI bridge two lanthanides, above and below the plane of the triangle, while the dimethylamino groups bind above and below and somewhat exterior to each vertex of the lanthanide triangle. Two triply deprotonated TDCI ligands each carry a −3 charge, while three lanthanides each carry a +3 charge, yielding a cluster core with a net +3 charge. The total charge on a complete cluster depends on the charge of the peripheral ligands. For example, peripheral methanol ligands result in a tricationic cluster with three triflate counteranions; three bidentate, anionic dipivaloylmethanate (dpm) ligands take up the peripheral positions of a charge neutral $RE_3(H_{-3}TDCI)_2(dpm)_3$ cluster.

The isostructural **RE_3dpm** (RE = Tb, Dy, Ho, Er, Y), **Ln_3acac** (Ln= Gd, Tb) compounds and **Dy_3MeOH** crystalize in the $P2_1/n$ space group. **RE_3dpm** (RE = Eu, Gd) compounds are in $P2_1/c$. **Dy_3acac** crystallizes in an orthorhombic space group, **Dy_3dbm** in $P2_1$, and both **Dy_3hfac and Gd_3Htae** in a hexagonal space group, $P6_3/m$.

Each rare earth ion is in an eight-coordinate, distorted bicapped-trigonal-prismatic environment with local pseudo-C_{2v} symmetry (Figure III.3). The interior square face of the prism consists of four μ_2-hydroxo oxygens, two from each TDCI ligand. Two oxygens from peripheral ligands form the top edge of the prism. Two dimethylamino groups, one from each TDCI ligand, cap two of the prism's rectangular faces.

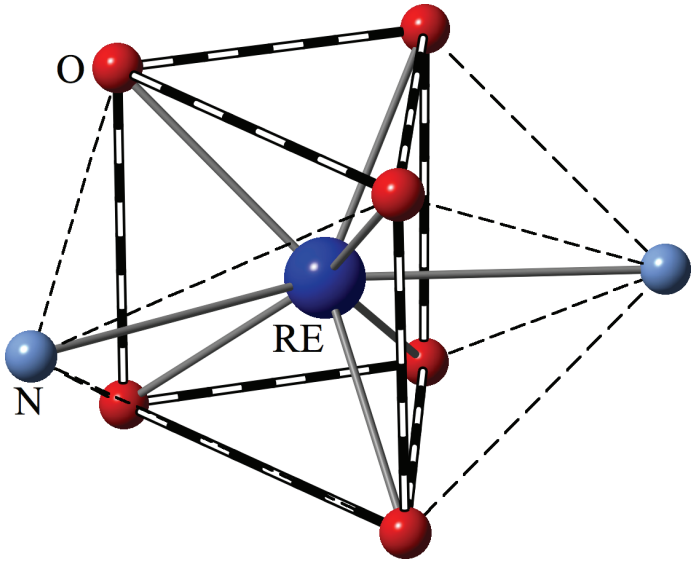

Figure III.3. Rare earth bicapped trigonal prismatic coordination environment.

The Ln-O_{TDCI} distances (2.33 Å) and Ln-O_{dpm} distances (2.35 Å) are comparable. Prism distortion is a result of three factors: (1) longer intra- than inter-ligand O_{TDCI}-O_{TDCI} distances, 2.9 Å vs 2.6 Å, respectively, resulting in a rectangle for the interior face of the prism; (2) longer intraligand O_{TDCI}-O_{TDCI} distances than intraligand O_{dpm}-O_{dpm} distances (2.9 Å vs. 2.8 Å), leading to a shortened exterior edge between triangular faces; (3) peripheral dpm "wag". Wag describes the obtuse angle between the centroid of the rare earth triangle, the rare earth, and the α-C of a dpm. Deviation from ideal D_{3h} symmetry caused by these distortions is in part a result of a toluene molecule of solvation wedged between two of the dpm ligands, as seen in Figure III.4. The wag angles, θ, are 178.8.1° for the dpm opposite the toluene, 169.1°, and 163.3° or 178.8° for the dpm disordered over two positions (Figure III.5). The faces are also asymmetrically capped by N, with the RE-N bond lengths being quite long, at ~2.7 Å.

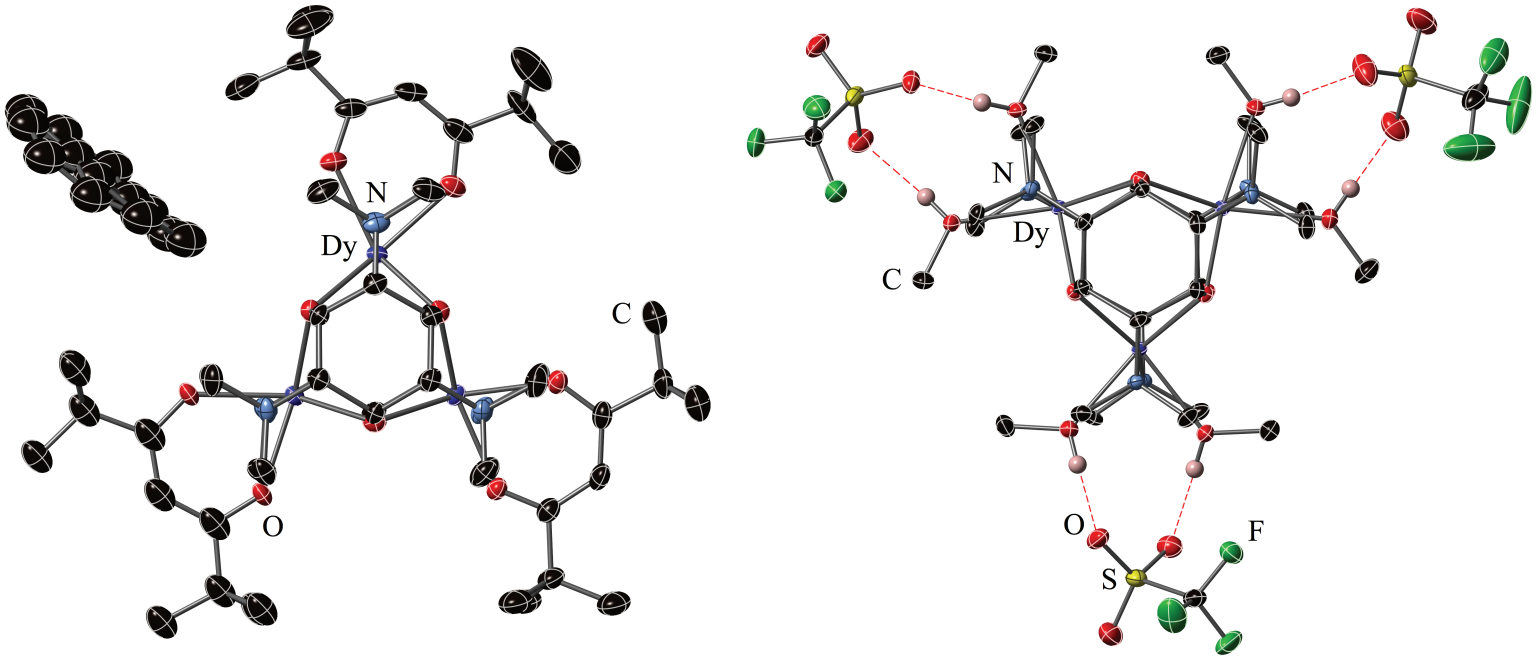

Figure III.4. Top view of **Dy_3dpm** and **Dy_3MeOH**. Thermal ellipsoid plots of $Dy_3(H_{-3}TDCI)_2dpm_3$ (**Dy_3dpm**) with disordered toluene solvate (left) and $Dy_3(H_{-3}TDCI)_2(MeOH)_6](OTf)_3$ (**Dy_3MeOH**) (right). Most hydrogen atoms and disordered dpm positions omitted for clarity. All **RE_3dpm** have similar structures.

The methanol molecules are nearly symmetrically situated in **Dy_3MeOH**, though deviations O-Ln-O bond angles and triflate positioning prohibit ideal *D3h* symmetry.

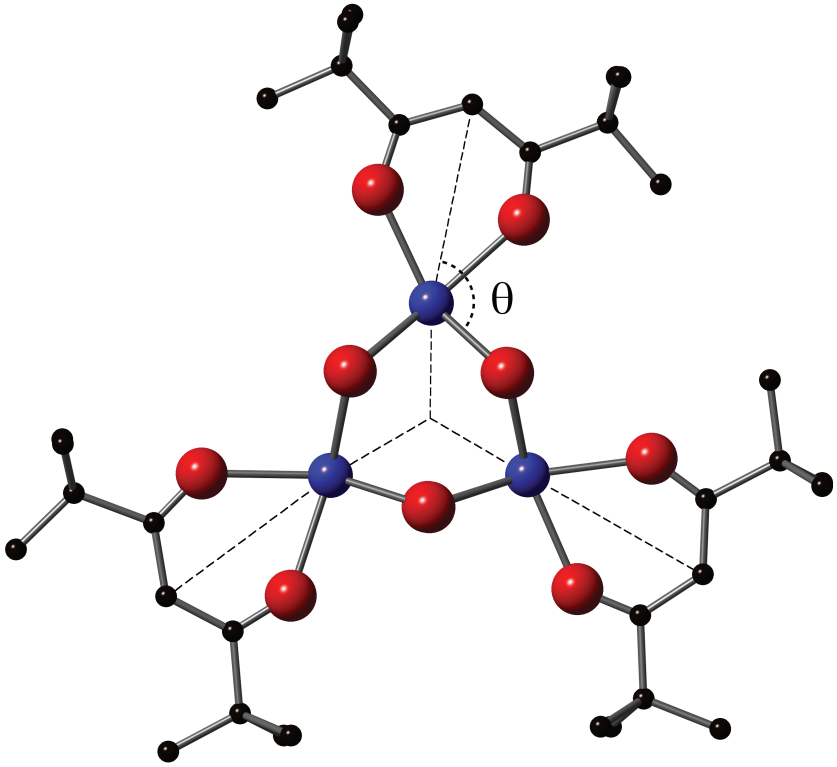

Figure III.5. Depiction of RE_3dpm with disordered dpm and wag angle, θ.

The crystal structures of three other RE_3 clusters ligated by three other β-diketonates are shown on the following three pages. **Tb_3acac** is shown in Figure III.6, **Dy_3hfac** is show in Figure III.7, and **Dy_3dbm** in Figure III.8. The molecular structures are all similar to that of the dpm-ligated clusters.

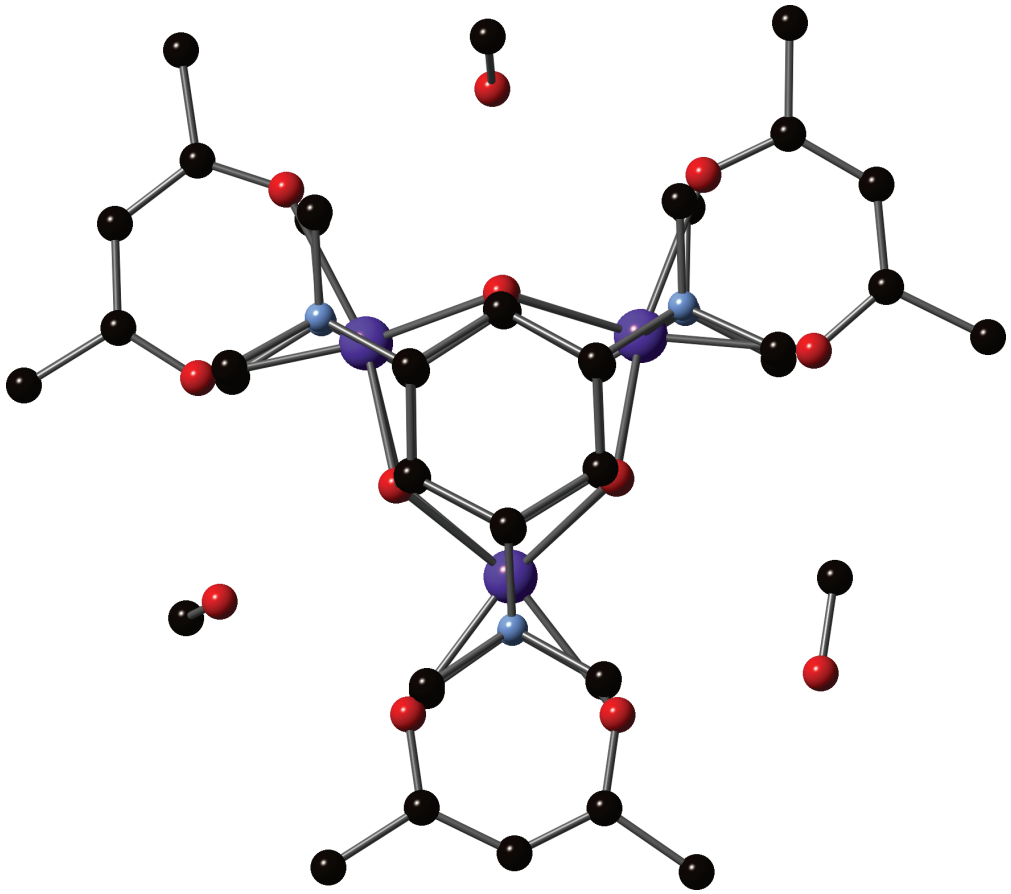

Figure III.6. Crystal structure of **Tb_3acac**. All acac compounds have the same connectivity. Only the solvation is different for the Gd analogue.

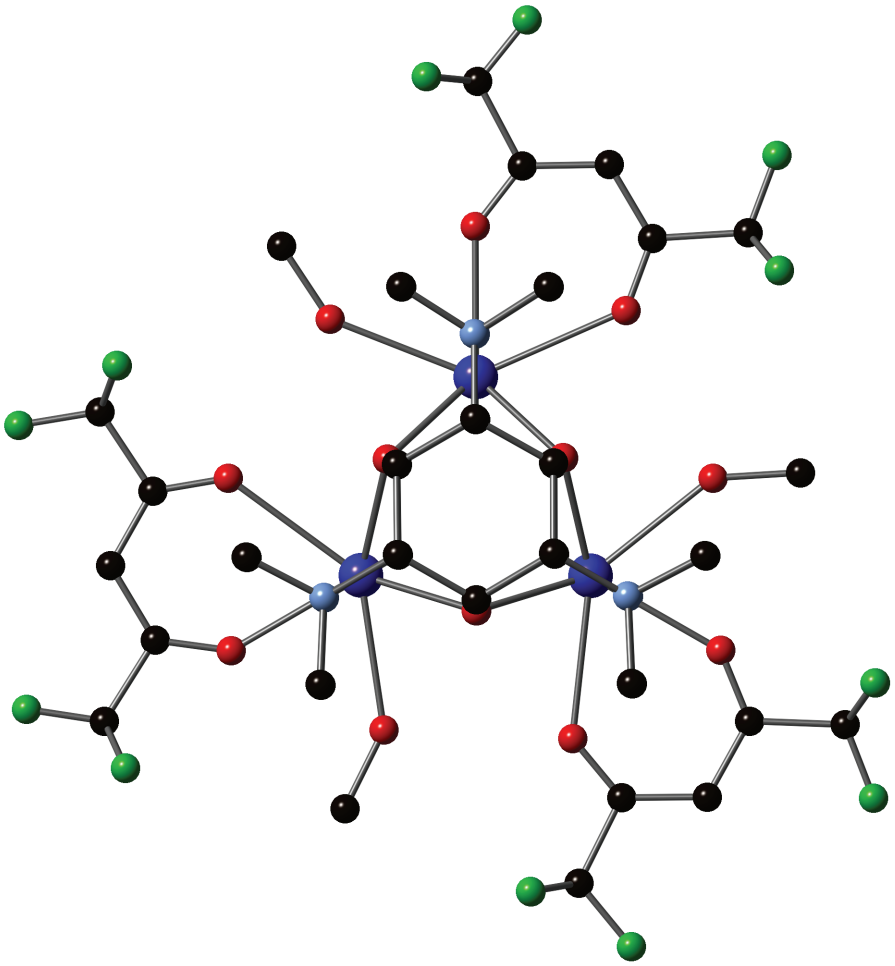

Figure III.7. Crystal structure of **Dy_3hfac**. Notice that Dy is nine coordinate in this structure. Hydrogen atoms omitted for clarity.

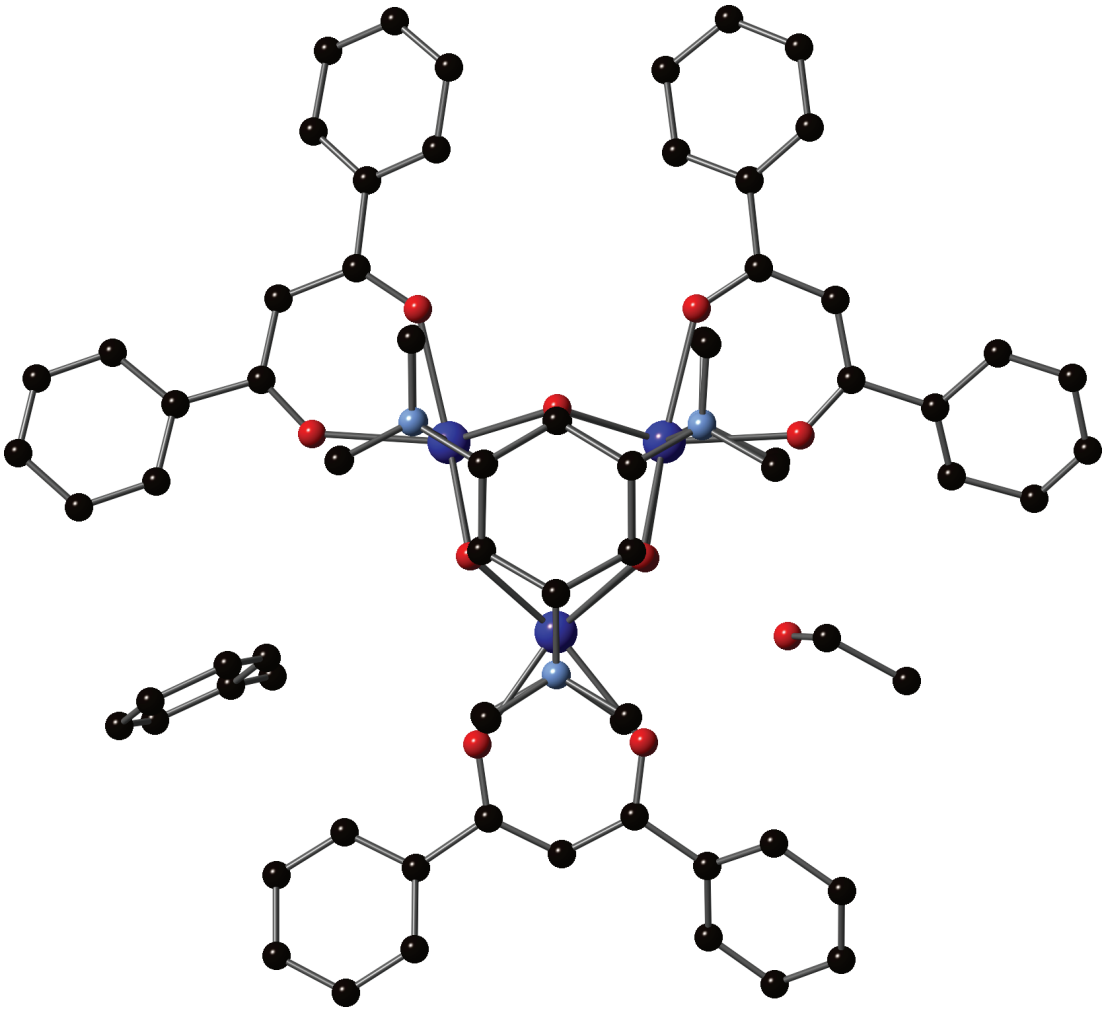

Figure III.8. Crystal structure of **Dy_3dbm**. Toluene and ethanol solvate molecules shown. Hydrogen atoms omitted for clarity.

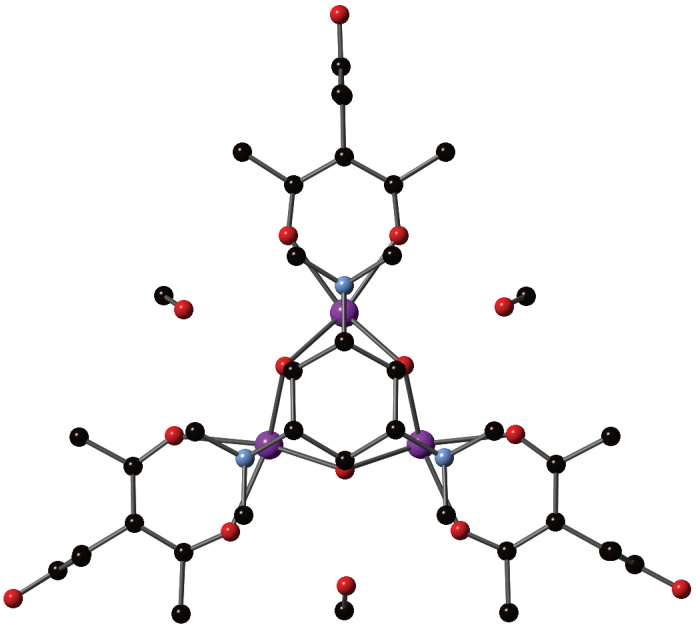

Figure III.9. Crystal structure of Gd_3Htae. Methanol solvates show. Hydrogen atoms omitted.

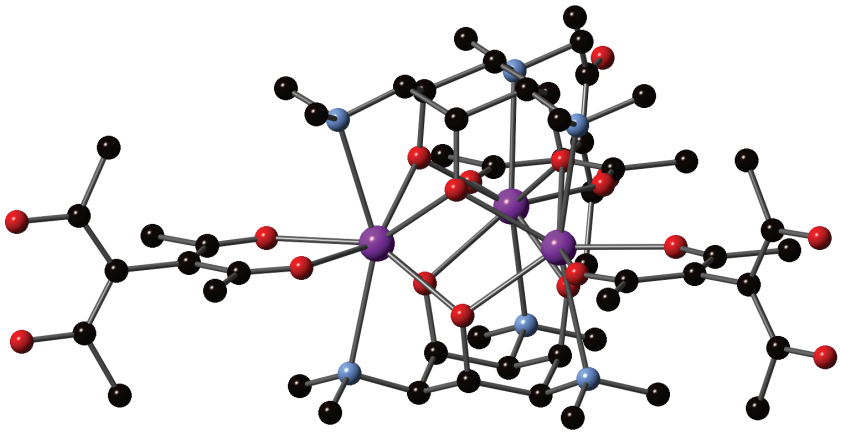

Figure III.10. Tilted view of Gd_3Htae. Uncoordinated ends of Htae are protonated. Hydrogen atom omitted.

The crystal structure of Gd_3Htae, which was obtained in low yield, is seen in a top-down view in Figure III.9 and a tilted view in Figure III.10. The space group was of high symmetry, and the diketonates were arranged quite symmetrically. Note the perpendicular orientation of the outer β-diketone groups.

Mass Spectrometry

MALDI mass spectrometry confirms the presence of **DyY_2dpm** species. Monoisotopic peaks corresponding to $[DyY_2(H_{-3}TDCI)_2(dpm)_2 + H]^{+\cdot}$, m/z 1435, the molecular radical cation $[DyY_2(H_{-3}TDCI)_2(dpm)_3]^{+\cdot}$, m/z 1406.8, and their expected isotope peaks were observed. Similar to these fragmentation patterns were the major peaks corresponding to the $[Y_3dpm]+\cdot$ molecular cation, m/z 1332.5, and $[Y_3dpm – dpm + H]+\cdot$, m/z 1149.4, as expected. Radical cation molecular peaks are expected with the DCTB matrix used in the MALDI experiment.[49] Peaks corresponding to Dy_3 and Dy_2Y were not observed above noise. Theoretical mass spectra generated by Chemcalc.[50,51] The mass spectrum is shown in Figure III.11.

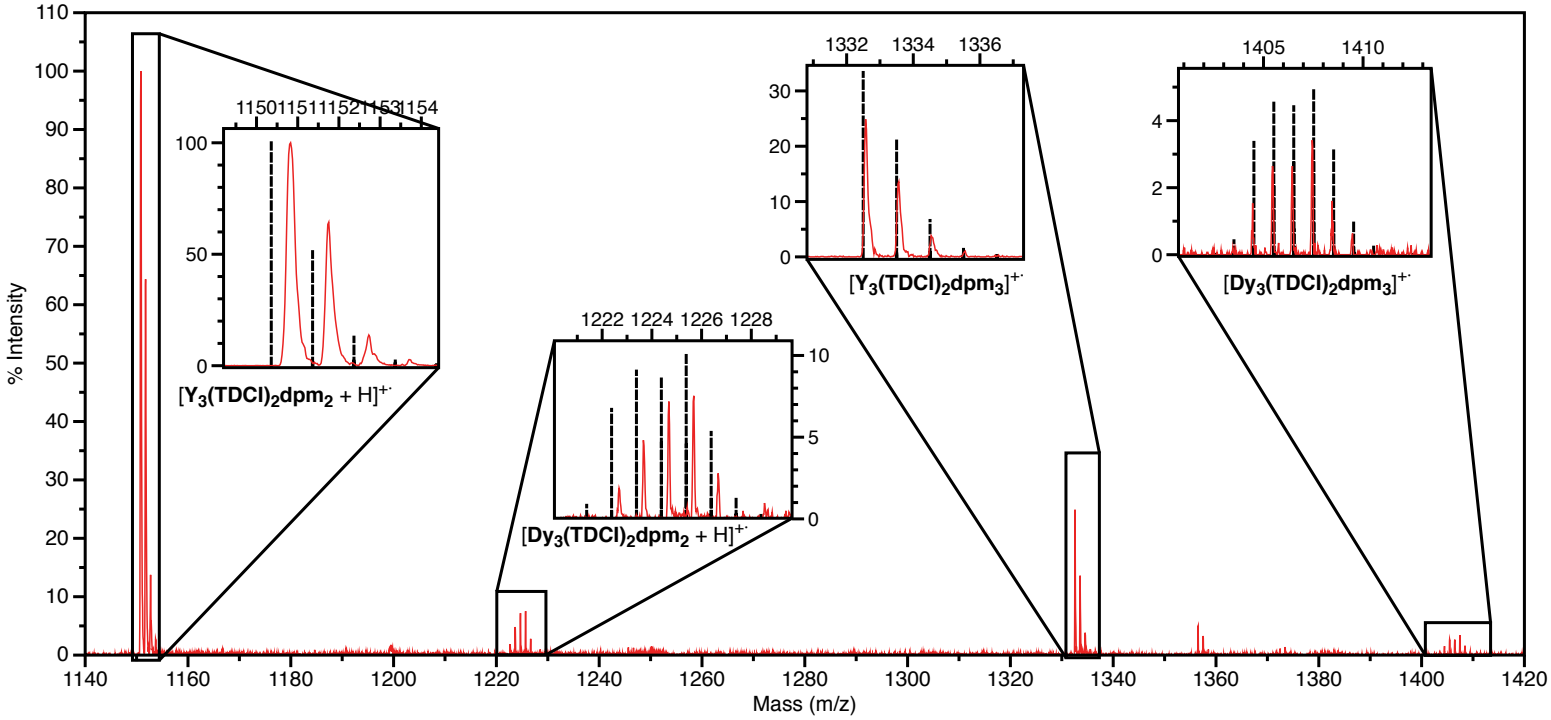

Figure III.11. MALDI Mass spectrum (DCTB matrix) of $Dy_{0.15}Y_{2.85}(TDCI)_2dpm_3$. Sample contains **$Y_3$dpm** and **$DyY_2$dpm**. Theoretical mass spectra generated by chemcalc.org.

NMR

For the diamagnetic **Y_3dpm** cluster, ^{1}H NMR revealed 5 resonances (3 from TDCI, 2 from dpm), of expected intensities, for a D_{3h}-symmetric molecule in solution. A variable resonance due to H_2O is observed in the range of δ =1.6 ppm to 2.7 ppm. Due to hydrogen-bonding interactions between the water and dpm-oxygens, the water peak is observed downfield from free water in $CDCl_3$ (1.56 ppm), and its chemical shift is very dependent on sample concentration (higher sample concentration shifts the resonance downfield) and on the water content of the solvent.

Magnetism

The dc molar susceptibilities, χM, of all compounds were measured in a 1000 Oe field at temperatures ranging from 2-300 K, and χ_MT values are plotted in Figure III.13. The room temperature χT values for **Dy_3dpm** and **Dy_3MeOH** are in good agreement with the expected theoretical values for three uncoupled Dy^{3+} ions, 42.51 emu mol^{-1} K ($^6H_{15/2}$, S = 5/2, L = 5, g = 4/3).[52] Substantial deviation from the Curie-Weiss Law is observed below 50 K for these compounds. Magnetic saturation is not seen even at 70 kOe. Because of the complex electronic structure of Dy^{3+}, no functional fits were attempted for magnetic susceptibility or magnetization measurements.

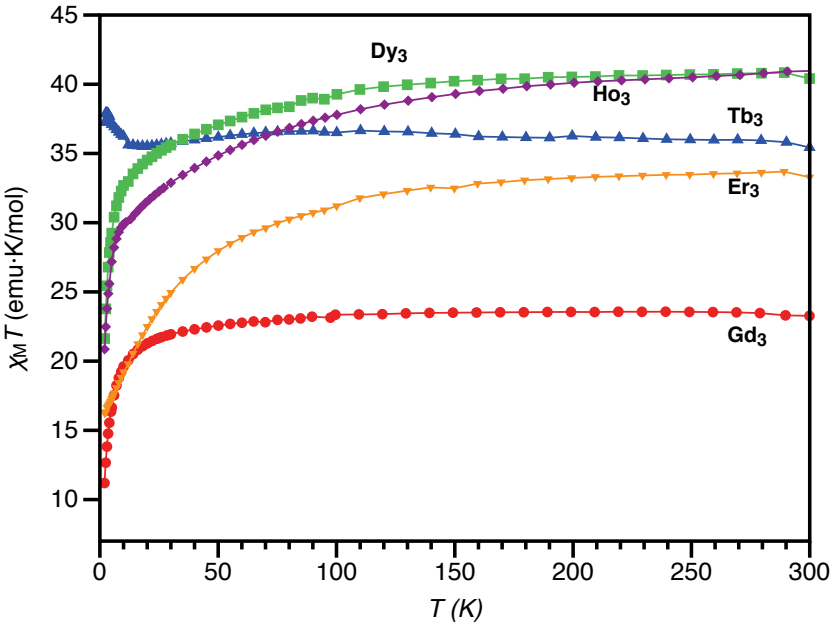

Figure III.12. DC-magnetic magnetic suceptibilities of Ln_3dpm clusters. χ_MT vs T plot from 2 to 300 K.

The dc molar susceptibilities, χ_M, of all compounds were measured in a 1000 Oe field at temperatures ranging from 2-300 K, and χ_MT values are plotted in Figure III.12. The room temperature χ_MT values for **Gd_3dpm** (~22), **Tb_3dpm** (~35), **Dy_3dpm** (~40), **Ho_3dpm** (~40), and **Er_3dpm** (~40) are in good agreement with the expected theoretical values for 3 uncoupled Gd^{3+} ions, 22 ($^8S_{7/2}$, S = 7/2; L = 0, g_J = 2); Tb^{3+} ions, 35 ($^7F_6$, S = 3, *L* = 3, g_J = 3/2); Dy^{3+} ions, 40 ($^6H_{15/2}$, S = 5/2, *L* = 5, g_J = 4/3); Ho^{3+} ions, 40 ($^5I_8$, S = 2, *L* = 6, g_J = 5/4); Er^{3+} ions, ($^4I_{15/2}$, S = 3/2; L = 6, g_J = 6/5).

The dc molar susceptibilities, χ_M, of **Dy_3MeOH** were measured in a 1000 Oe field at temperatures ranging from 2-300 K, and χ_MT values are plotted in Figure III.13.

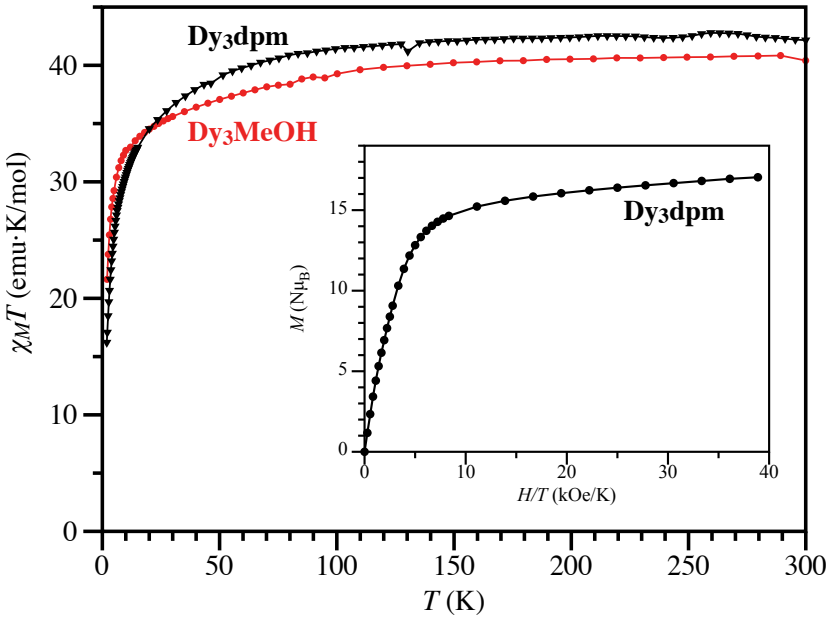

Figure III.13. Temperature dependence of $\chi_M T$ for **Dy_3dpm** and **Dy_3MeOH** (under a 1000 Oe magnetic field). Inset: Plot of *M* vs *H/T* for **Dy_3dpm**. Lines are guides for the eye.

The dynamic magnetic properties of Dy3dpm were revealed by temperature and field dependent ac susceptibility measurements on a polycrystalline sample. As seen in Figure III.14, temperature dependent out-of-phase ac susceptibility (χ'') signals at various ac frequencies are observed at temperatures below 12 K. In general, very broad peaks in χ'' (T) are seen around 2-3 K and shoulders around 7 K. At higher frequencies of the ac magnetic field, the peaks flatten with relatively small changes in peak positions. To probe the effects of close intracluster Dy ion proximity (~3.7 Å), dilutions studies were performed. As with **Dy_3dpm**, temperature and frequency dependent ac-susceptibility measurements were performed on samples of **DyY_2dpm** with total lanthanide composition of 5% Dy/95% Y. This corresponds to approx. one $DyY_2(H_{-3}TDCI)_2(dpm)_3$ cluster for every in seven $Y_3(H_{-3}TDCI)_2(dpm)_3$ clusters, resulting in

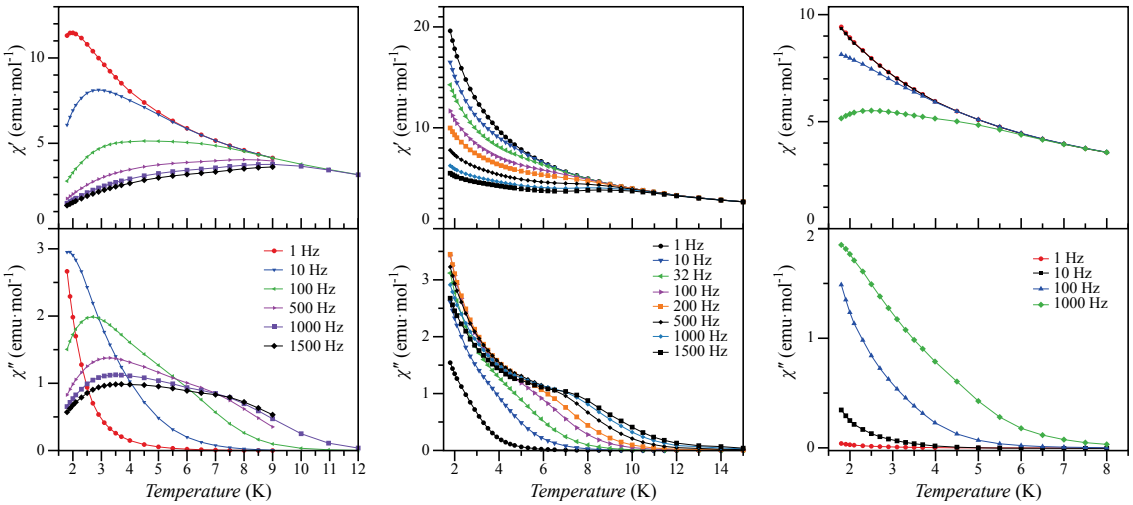

Figure III.14. Temperature dependent in-phase and out-of-phase AC susceptibilities for **Dy_3dpm** (left), **DyY_2dpm** (center), **Dy_3MeOH** (right).

quite isolated Dy centers. Slow magnetic relaxation of Dy^{3+} is indicated from the non-zero signal in the temperature-dependent out-of-phase susceptibility (Figure 4, middle), but defined peaks are absent. This magnetic behavior is in contrast to that of the **Dy_3dpm** sample, which exhibits temperature-dependent peaks in the out-of-phase susceptibility.

Apparently, there is some intra-cluster interaction between the Dy centers in Dy_3 clusters that is responsible for a temperature-dependent relaxation mechanism. Similar behavior is observed with $[Dy_4K_2O(O\textit{t}\text{-Bu})_{12}]$ and its yttrium diluted analogue, though the effects of magnetic concentration on low temperature susceptibility (<10 K) were not discussed.[41] Perhaps neighboring Dy centers supply a sufficient auxiliary magnetic field to partially quench quantum mechanical tunneling of the ground state. Detailed electronic structure and magnetic calculations may yield some insight into these phenomena.

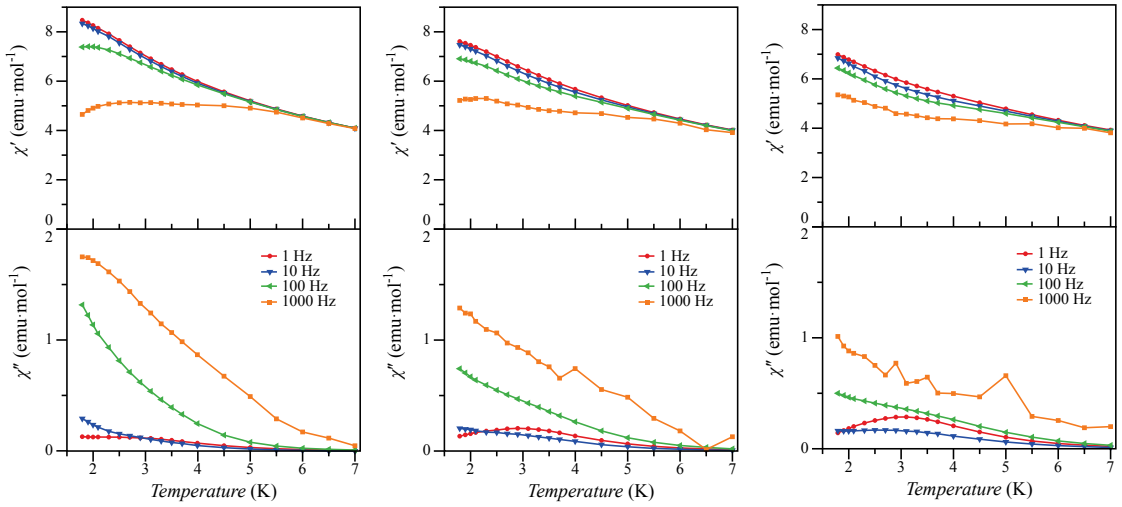

Figure III.15. Temperature-dependent ac susceptibility, $\chi''(T)$, for **Dy_3MeOH** under static 2000 (left), 3000 (center), and 4000 (right) Oe applied fields.

Upon changing peripheral ligands to methanol, the change in dynamic magnetic properties is quite dramatic. As seen in Figure III.14 (right), $\chi''(T)$ is indicative of slow relaxation of magnetization, and with the application of a static magnetic field, no peaks are induced (Figure III.15).

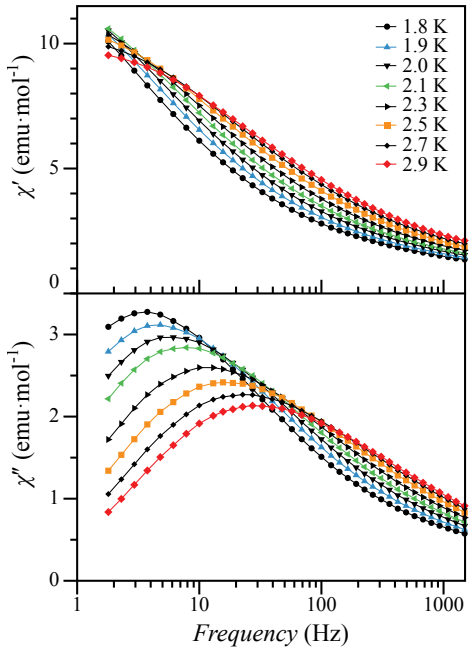

Figure III.16. Frequency-dependent ac susceptibility, $\chi(\nu)$, for **Dy_3dpm**. AC frequencies from 1-1500 Hz, at temperatures ranging from 1.8-2.9 K.

For **Dy_3dpm**, the frequency dependent out-of-phase susceptibility, $\chi''(\nu)$, was measured to determine the characteristic relaxation time and anisotropic energy barrier.[1] As seen in Figure III.16, the peaks in $\chi''(\nu)$ are temperature dependent, broad and quite asymmetrical. Relaxation times were extracted from experimental maxima of $\chi''(\nu)$ plots ($\tau = 1/(2\pi\nu)$) in the temperature range from 1.8 to 2.9 K.[5,8]

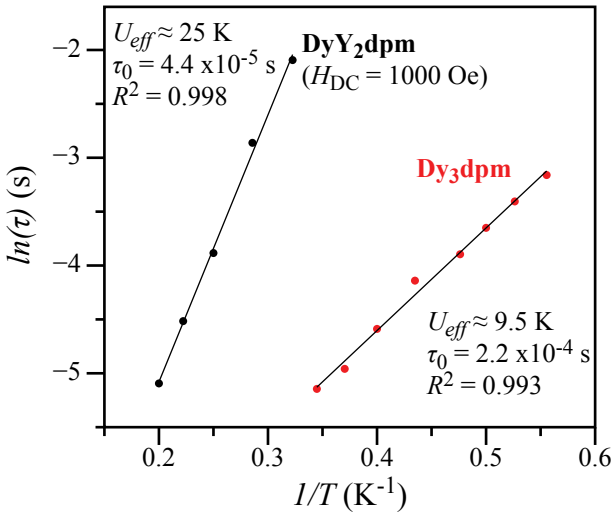

Figure III.17. Arrhenius plot for **Dy_3dpm** and **DyY_2dpm** (1000 Oe) diluted in a **Y_3dpm** matrix. Relaxation times extracted from the maxima of experimental $\chi''(\nu)$ plots.

An Arrhenius plot of relaxation time vs (1/T) yield an anisotropy barrier to relaxation of 9.5 K and a pre-exponential factor of 2.2×10^{-4} (Figure III.17). While the temperature dependence indicates a thermally assisted relaxation mechanism, the flattened semi-circles of the Cole-Cole plots (χ'' vs χ'), (Figure III.18) indicate a distribution of relaxation times. Indeed, fits of the Cole-Cole curves to a generalized Debye model yield a high α value of about 0.5, though the fit was quite poor. This broad distribution of relaxation times is indicative of multiple relaxation pathways or stepwise relaxation pathways with differing rates at each step. Exponential dependence of relaxation time, τ, with 1/T, indicates an Orbach relaxation mechanism; specifically, considering the low anisotropy barrier, thermally assisted quantum tunneling is likely. [53-55] Given the complex electronic structure of Dy^{3+} and that each **Dy_3dpm** molecule contains three symmetry inequivalent dysprosium ions with slightly different coordination environments (see description of structure *vida supra*), a broad distribution of relaxation times is not unexpected.

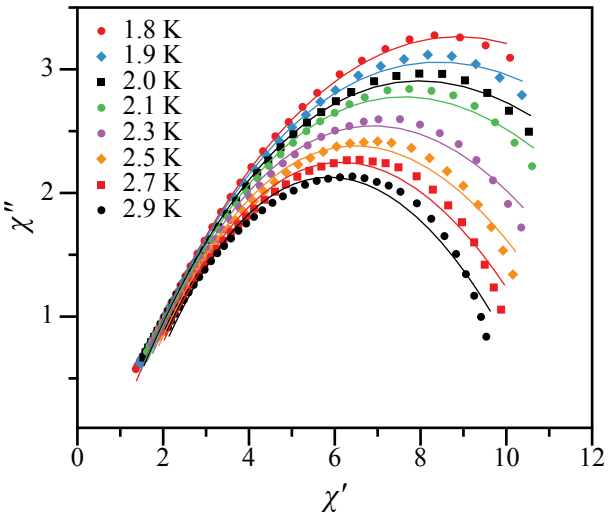

Figure III.18. Cole-Cole plot for **Dy_3dpm** in the temperature range of 1.8-2.9 K. Solid lines are fits to the generalized Debye model with $\alpha = 0.48 \pm 0.07$.

The application of a 1000 Oe static field had little effect on the dynamic magnetic properties of **Dy_3dpm** (Figure III.19).

In an attempt to block quantum tunneling of magnetization in **DyY_2dpm**, ac susceptibility studies were performed in static magnetic fields of 500 and 1000 Oe at temperatures ranging from 1.8 to 5.0 K. As seen in Figure III.20, temperature-dependent peaks were induced by the application of a 1000 Oe static field. A fit of the 1000 Oe frequency dependent data to a generalized Debye model was poor, but suggests an α value of starting at 0.3 at 5.0 K, increasing to ~0.6 at 3.1 K.

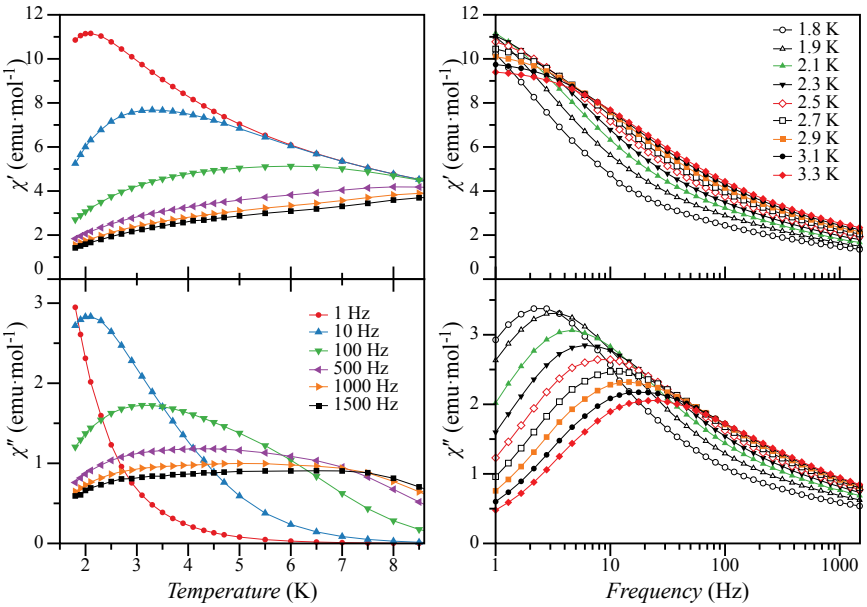

Figure III.19. AC susceptibilities for **Dy_3dpm** under an a static 1000 Oe field. χ(ν) (left) and χ(T) (right), at frequencies from 1-1500 Hz, between temperatures of 1.8-15.0 K.

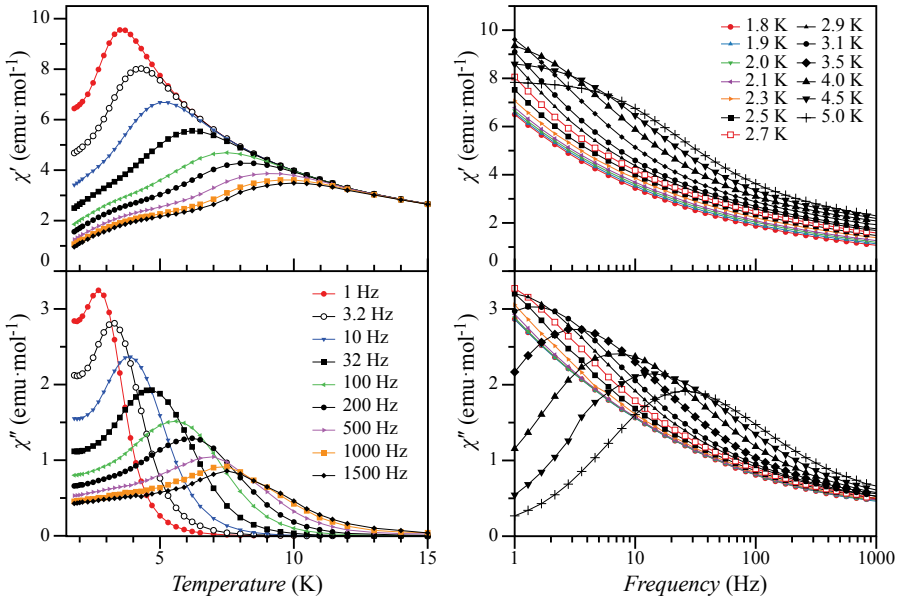

Figure III.20. AC susceptibilities for **DyY_2dpm** under an a static 1000 Oe field. χ(ν) (left) and χ(T) (right), at frequencies from 1-1500 Hz, between temperatures of 1.8-15.0 K.

The broadening of relaxation times suggests that other relaxation mechanisms coming in to play at lower temperatures. Even with the quite temperature-dependent α parameter, extraction of maxima from $\chi''(\nu)$ plots gave τ values that were linear in an Arrhenius plot, yielding activation barriers of around 25 K and a pre-exponential factor of 4.4×10^{-5} (Figure III.17). The applied dc field seems to block quantum tunneling of magnetization in the ground state, leading to a temperature dependent relaxation process. It is of note that the anisotropy barrier is higher compared to its pure Dy analog. As with **Dy_3dpm**, a thermally assisted quantum tunneling mechanism is likely.

Luminescence

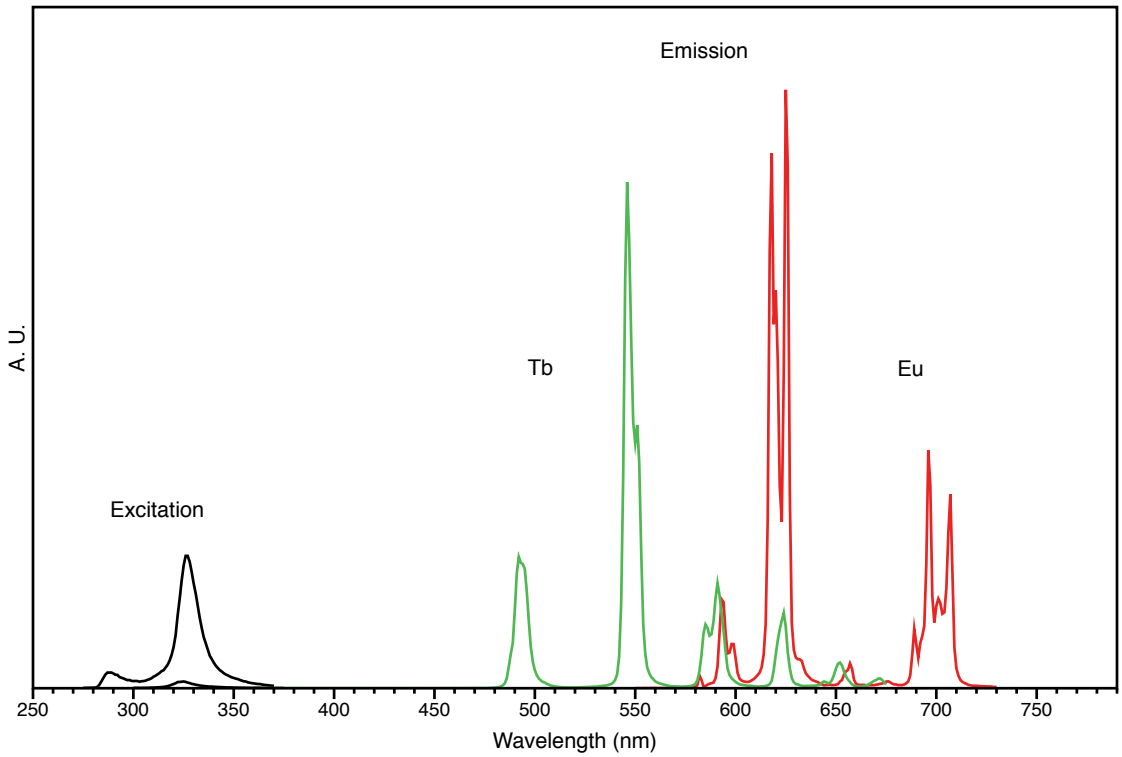

Figure III.21. Luminescence spectra of Eu_3dpm and Tb_3dpm in toluene.

Compared to $Eu_3(TACI)_2^{3+}$ clusters in water, the luminescence displays much finer spectral features.[56] This is likely do the lack of coordinated water and the non-coordinating solvent in which the measurements were taken. The dpm ligands are also acting as sensitizers, though to what extent cannot be determined until quantum yield is determined. The luminescence spectra of the Eu and Tb dpm clusters are shown in Figure III.21.

CONCLUSION

Structural studies of $Ln_3(H_3TDCI)_2(L)_x$ were undertaken, and a variety of resulting compounds were characterized by X-Ray crystallography. It seem β-diketonates are suitable peripheral ligands for these cluster-types.

A trinuclear Dy cluster supported by the TDCI ligand has been synthesized and was shown to exhibit single-molecule magnet behavior. A relatively small change in ligand environment (dipivaloylmethanide to methanol) led to drastic changes in magnetic properties—notably a lack of temperature dependent relaxation. Dilution studies with yttrium revealed that intramolecular interactions in the pure dysprosium cluster induce a temperature-dependent relaxation that is not observed in the yttrium diluted sample containing isolated dysprosium centers. Detailed electronic structure and magnetic calculations are required to possibly further elucidate the underlying causes of this behavior.

The dc and ac magnetic susceptibilities of **Ln_3dpm** (Ln = Gd, Tb, Dy, Ho, and Er) and **Dy_3MeOH** were also measured, with uninteresting results in the ac measurements for all but the Dy compound. Preliminary luminescence measurements of the Eu_3 and Tb_3 dpm-ligated analogues were also performed.

CHAPTER IV

INCORPORATION OF PREBUILT TRINUCLEAR LANTHANIDE CLUSTERS INTO COORDINATION POLYMERS

INTRODUCTION

While we have control of the constituent metals and linkers, the resulting CP geometry, connectivity, and topology is highly variable and depends upon the geometry and bonding properties of the linker units and those of the constituent ions. Control of network architecture has most commonly been achieved through control in the geometry of the linker, *as introduced*, in conjunction with foreknowledge of metal coordination geometry or that of metal clusters formed *in situ*.[57-62] Dinuclear transition-metal paddle-wheels are, by far, the most commonly used preformed polynuclear building units for CPs. At present, examples of incorporation of preformed metal clusters with nuclearities greater than two are exceedingly rare, but the incorporation of hexanuclear $(Re_6Se_8(PEt_3)_4(bipyridine)_2)^{2+}$ clusters and trinuclear $Cr_3(\mu_3\text{-}O)(pyridine\text{-}4\text{-}carboxylate)_6]^+$ clusters into CPs serve as examples. In these cases, the clusters are linked *via* other transition metal centers.[63] A recent report of incorporating the pseudotetrahedral $[\varepsilon\text{-}PMo_{12}O_{36}(OH)_4]^{5+}$ polyoxomolybdate-lanthanide cluster into a 3-D diamondoid network demonstrates direct linker addition at a cluster metal site upon formation of the network.[64]

The water stable trinuclear lanthanide cluster type, $[Ln_3(H_{-3}TACI)_2(L)_6]$ (Ln = lanthanide; L = ligand), supported by 1,3,5-triamino-1,3,5-trideoxy-*cis* inositol (TACI) and its methylated analogue 1,3,5-tris(dimethylamino)-1,3,5-trideoxy-*cis*-inositol (TDCI) have been

known since Hegetschweiler and his coworkers pioneered work with these versatile polydentate ligands.[25,25,42,42,43,48,48] Many of the chemical and physical properties of the H_{-3}TACI-supported cluster are well studied.[44,46,47,65] The H_{-3}TDCI-supported lanthanide clusters have scarcely been examined. The incorporation of these triangular cluster-types into coordination polymers has not been explored.

Herein we describe our successful attempts, of incorporating *preformed* lanthanide clusters, $[Ln_3(H_{-3}TDCI)_2]^{3+}$, into coordination frameworks. We have used these rigid triangular building units in the synthesis of three new 1-D coordination framework materials using squarate and benezenedicarboxylate ligands.

EXPERIMENTAL

Synthesis of lanthanide triflates

See preparation in Chapter II.

Synthesis of $[Ln_3(TDCI)_2(H_2O)_6](OTf)_3$ (Gd_3H_2O, Dy_3H_2O)

In a typical synthesis, $Ln(OTf)_3$ (0.18 mmol) and TDCI (0.12 mmol) were dissolved in 3 mL of water, and the solution was stirred and refluxed for one hour. The volume was reduced to ~1 mL by boiling, and clear, colorless crystals formed upon cooling. Single crystals for X-ray diffraction analysis were obtained from the precipitate. Yield: ~30-38%.

Synthesis of $Ln_3(TDCI)_2(C_4O_4)_{3/2}$ (Dy_3sqr, Gd_3sqr)

In a tall eight mL vial, the following three solutions were layered in the order given from bottom to top: (1) $[Ln_3(TDCI)_2(H_2O)_6](OTf)_3$ (25 mg, 16.3 μmoles) in approximately 2 mL of water. (2) Approximately 4 mL of a 1:1 (v/v) ethanol/water solution. (3) Squaric acid (3 mg,

26.3 μmoles) and triethylamine (5.8 mg, 8 μL, 57.3 μmoles) in approximately 2 mL of ethanol. After a few days, slow diffusion of the reactants resulted in the formation of white crystals of $Ln_3(TDCI)_2(C_4O_4)_{3/2}$ midway up the vial. Singles crystals for X-ray diffraction were obtained in the precipitate.

Synthesis of $Ln_3(TDCI)_2(bdc)_{3/2}$ (Dy_3bdc)

In a tall eight mL vial, the following three solutions were layered from bottom to top in the order given: (1) $[Ln_3(TDCI)_2(H_2O)_6](OTf)_3$ (25 mg, 16.3 μmoles) in approximately 2 mL of water. (2) Approximately 4 mL of a 1:1 (v/v) methanol/water solution. (3) Disodium terephthalate (10.2 mg, 24.0 μmoles) in 2 mL of methanol. After a few days, slow diffusion of the reactants resulted in the formation of white crystals of $Ln_3(TDCI)_2(bdc)_{6/2}$ midway up the vial. Singles crystals for X-ray diffraction were obtained from the precipitate of the dysprosium reaction.

Single Crystal X-ray Diffraction

Single crystal X-ray diffraction data were collected for **Gd_3H_2O** and **Dy_3H_2O** on a Bruker APEX II diffractometer using Mo-Kα radiation (λ = 0.71073 Å). The samples were mounted on MiTeGen kapton pins in a 150(2) K nitrogen cold stream. The cell constants were indexed from reflections obtained from 36 frames with exposure times of 10 seconds per frame. In both cases a full sphere of data (1440 frames at 6 cm detector distance) was collected with scan widths of 0.50° in ω and exposure times of 5 seconds per frame.

The data for the remaining compounds were collected on Beamline 11.3.1 at the Advanced Light Source (ALS), Lawrence Berkeley National Lab (LBNL) using monochromatic synchrotron radiation using silicon(111) to a wavelength of 0.7749 Å. The samples were mounted on MiTeGen kapton mounts in a 100(2) K nitrogen cold stream on the goniometer head of a Bruker D8 diffractometer equipped with an APEX II CCD detector. The cell constants were indexed from reflections obtained from 90 frames with exposure times of 1 second per frame. In all cases a full sphere of data (2400 frames at 5 cm detector distance) was collected with scan widths of 0.30° in ω and exposure times of 1 second per frame.

Data reduction and cell refinement for all compounds were performed with SAINT.[4] SADABS was used to obtain absorption corrected data.[5] The structures were solved by direct methods (SHELXT) and refined by full-matrix least squares on F^2 using SHELXL-2013.[6] All non-hydrogen atoms were refined anisotropically. Hydrogen atoms were placed geometrically on the carbon atoms and refined using a riding model. Any water hydrogen atoms were found in the difference map, their distances to their O atoms were restrained but the coordinates were al-

lowed to refine, also the displacement parameters were ridden on their O atom. Any hydrogen atoms which were not able to be uniquely identified in the difference map were omitted from the refinement. Disordered solvent in several of the structures was removed using the masking algorithm in Olex2.[7] Crystal parameters and information pertaining to data collection and refinement for all structures can be found in Table IV.1.

Table IV.1. Crystallographic information for Chapter IV compounds.

Sample	**Gd_3H_2O**	**Dy_3H_2O**	**Gd_3sqr**	**Dy_3sqr**	**Dy_3bdc**
Chemical formula	$Gd_3N_6O_{12}C_{24}H_{60}$ 3 (CF_3SO_3) · 6.6 (H_2O)	$Dy_3N_6O_{12}C_{24}H_{60}$ 3 (CF_3SO_3) · 6.75 (H_2O)	$Gd_6N_{12}O_{30}C_{60}H_{108}$, C_2H_6O, 6 (H_2O)	$Dy_3N_6O_{15}C_{30}H_{54}$	$Dy_3N_6O_{13}C_{36}H_{54}$, H_2O
Formula mass*	1662.64	1681.09	2575.24	1226.29	1286.38
Crystal system	triclinic	triclinic	monoclinic	monoclinic	monoclinic
Space group	*P*	*P*	$P2_1$	*C2/m*	$P2_1/n$
λ (Å)	0.71073	0.71073	0.7749	0.7749	0.7749
a (Å)	12.813(3)	12.808(3)	10.7339(11)	35.834(6)	13.6621(16)
b (Å)	14.193(3)	14.139(3)	20.860(2)	13.274(2)	19.1740(14)
c (Å)	15.268(3)	15.278(4)	19.245(2)	10.5827(16)	17.370(2)
α (deg.)	93.196(3)	93.147(3)	90	90	90
β (deg.)	95.423(2)	95.561(2)	95.3420(10)	93.093(3)	90.1740(14)
γ (deg.)	96.355(2)	96.425(3)	90	90	90
Z	2	2	2	4	4
V ($Å^3$)	2741.1(10)	2730.3(11)	4290.4(8)	5026.6(14)	4580.8(9)
Temperature (K)	110(2)	110(2)	100(2)	100(2)	100(2)
Unique Reflections (R_{int})	10737 (0.0440)	10707 (0.0545)	24560 (0.0625)	5401 (0.0774)	8397 (0.0743)
Parameters/ Restraints	779/57	779/57	1061/1	283/28	533/3
θ range (deg.)	1.907 - 25.99	1.911 – 25.99	2.691 – 33.071	2.73 – 29.03	2.80 – 27.85
R_1, wR_2 all data	0.0423, 0.01077	0.0447, 0.1179	0.0336, 0.0800	0.0464, 0.1243	0.0498, 0.1348
S (GooF)	1.028	1.024	1.009	1.032	1.056

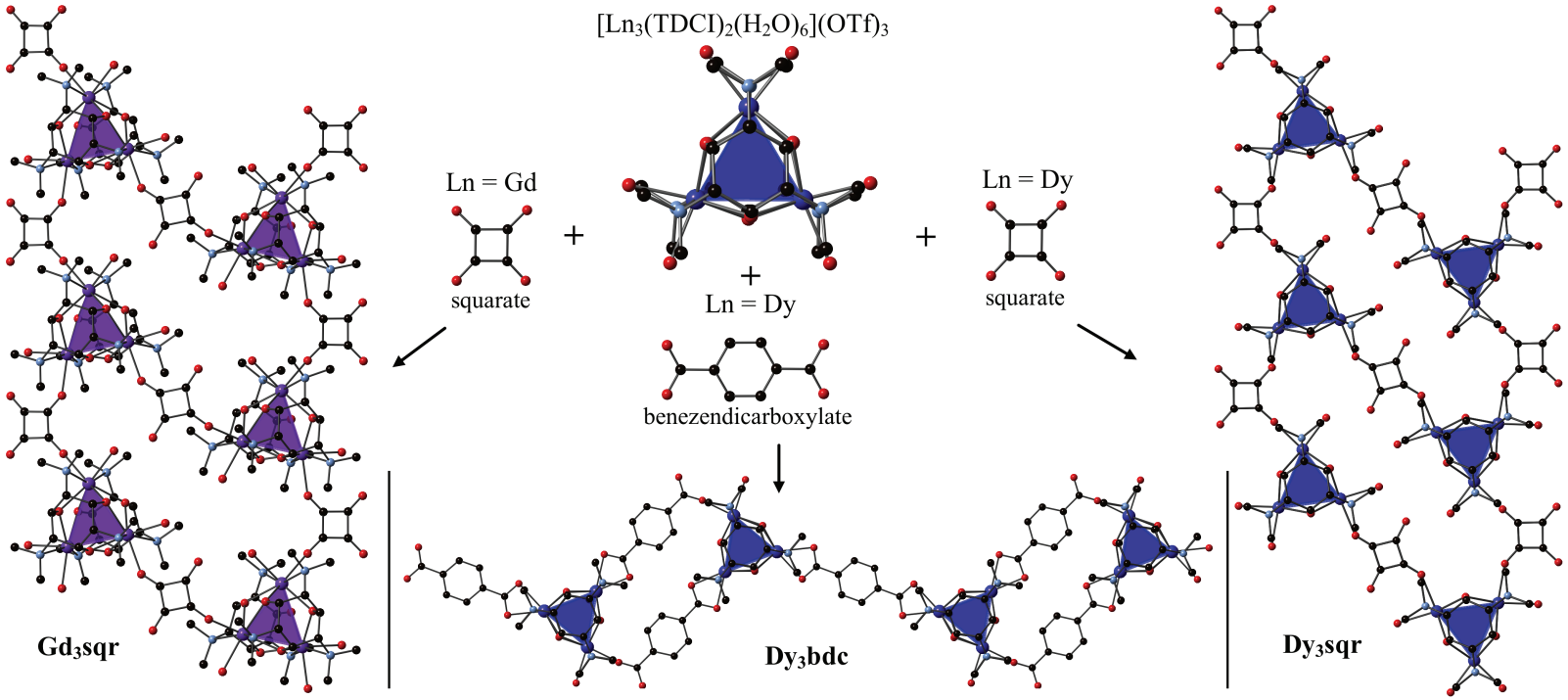

Figure IV.1. Incorporation of $\mathbf{Ln_3H_2O}$ clusters into coordiation networks. Reaction of $[Ln_3(TDCI)_2(H_2O)_6](OTf)_3$ ($\mathbf{Ln_3H_2O}$; Ln = Gd, Dy) with $(HNEt_3)_2(C_4O_4)$ (squarate) and $Na_2(bdc)$ (benzenedicarboxylate) to yield $Ln_3(TDCI)_2(C_4O_4)_{3/2}$ ($\mathbf{Ln_3sqr}$; Ln = Gd, Dy) and $Dy_3(TDCI)_2(bdc)_{3/2}$ ($\mathbf{Dy_3bdc}$). Top-down representations of reactants and products are ball and stick depictions of their respective X-ray crystal structures with hydrogen atoms, solvent molecules, and counterions omitted for clarity. C (black), N (light blue), O (red), Dy (dark blue), Gd (purple).

RESULTS AND DISCUSSION

Synthesis

The previously unreported trinuclear lanthanide cluster starting materials, $[Ln_3(H_{-3}tdci)_2(H_2O)_6](OTf)_3$ (**Gd_3H_2O, Dy_3H_2O**) (Figures 1 and 2 (top)) were synthesized by reacting stoichiometric proportions of TDCI and lanthanide triflate in boiling water. It is interesting to note that these alkoxide clusters were synthesized in *acidic* aqueous conditions without the addition of any base.

Precipitation of $Ln_3(H_{-3}TDCI)_2(C_4O_4)_{3/2}$ (**Dy_3sqr**, **Gd_3sqr**) resulted from the slow diffusion of reactants, **Ln_3H_2O** triangle units and a squarate salt, into a common solvent layer. $Dy_3(H_{-3}TDCI)_2(bdc)_{3/2}$ (**Dy_3bdc**) was precipitated in an analogous manner by the reaction of aqueous **Dy_3H_2O** and disodium benenedicarboxylate. The resulting compounds were characterized by single-crystal X-ray diffraction. Crystallographic information is found in Table IV.1. Figure IV.1 structurally illustrates the results of reactions yielding all reported compounds. As reaction conditions have not been fully optimized, phase purity has not been obtained in these compounds. Current estimates of yield are around 30%. This is a preliminary report of synthesis and structural information.

X-Ray crystal structures

$[Ln_3(H_{-3}TDCI)_2(H_2O)_6](OTf)_3$ starting material

The structure of the cluster core is the same as described in Chapter III. Six water molecules take up peripheral ligand positions, and the cluster has a 3+ charge with triflate counterions. Both starting materials **Gd_3H_2O** and **Dy_3H_2O** are isostructural (Figure IV.2)

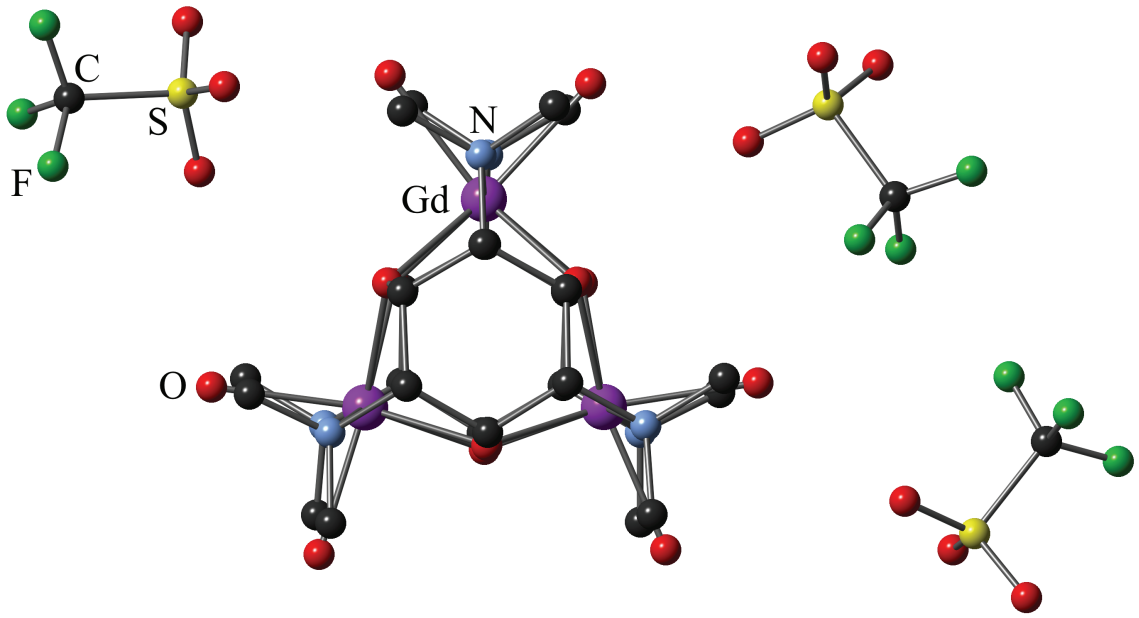

Figure IV.2. X-ray crystal structure of $[Gd_3(TDCI)_2(H2O)_6](OTf)_3$ (**Gd_3H_2O**). Water solvates and hydrogen atoms removed for clarity. **Dy_3H_2O** is isostructural.

The X-ray crystal structures of **Ln_3sqr** and **Dy_3sqr** are depicted Figure IV.1. In both structures, Ln_3 trinuclear clusters are linked via squarate dianions to form canted ladder-type 1-D double chains. Each rail of the "ladder" is a chain of Ln_3 clusters connected *via cis*-squarate oxygen atoms. Squarates bridging *via trans*-oxygen atoms act as rungs of the ladder connecting the two chains (Figure IV.3). The ladders are canted because the rungs are not perpendicular to the rails. Squarate oxygen atoms occupy three of the six open coordination positions of the tri-nuclear Ln_3 clusters, while water molecules take up the remaining three sites. All bond lengths are typical, including Ln-O bonds ranging between ~2.3-2.5 Å. Short $O_{squarate}$-O_{water} (<2.9 Å) distances indicate that the squarates of both **Ln_3sqr** chains are involved in extensive intra-chain hydrogen bonding. Peripheral oxygen atoms (those from water and squarate linkers) form

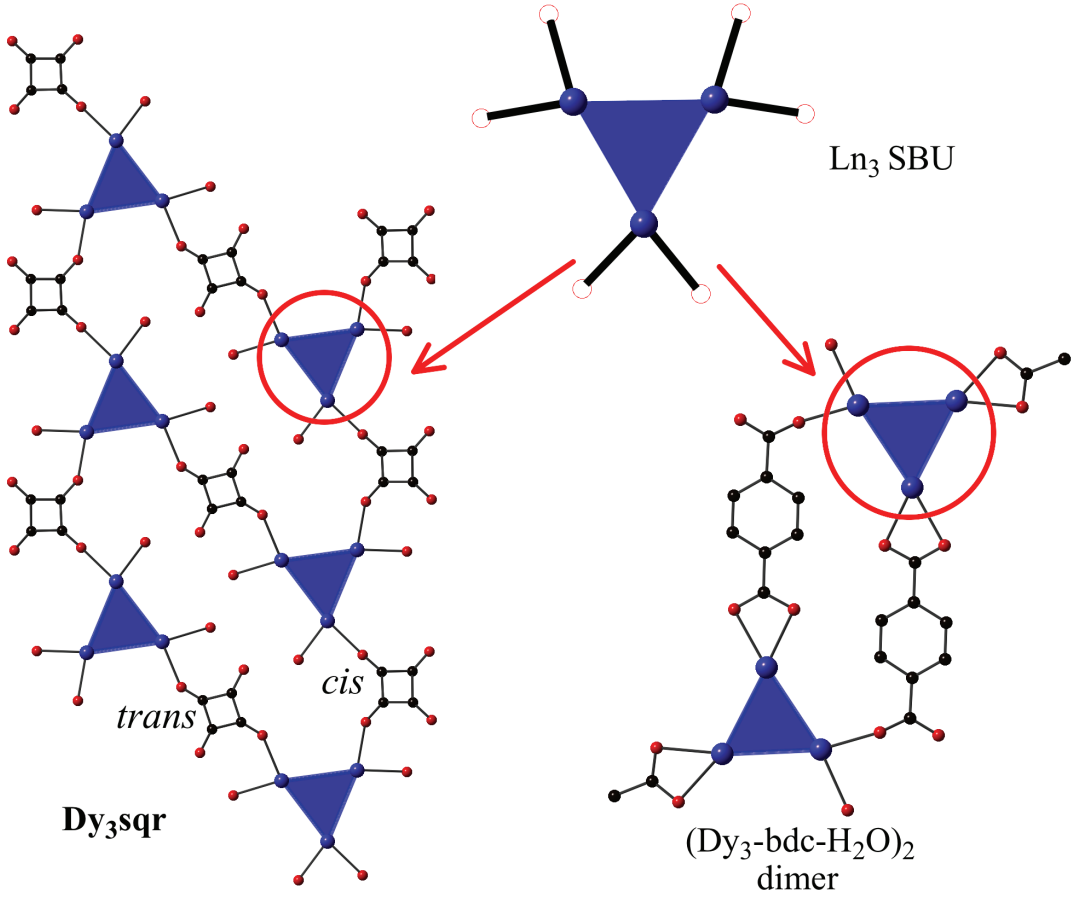

Figure IV.3. SBU schematic diagram. Triangular Ln_3 SBU (top right). Open red circles depict six planar available coordination sites. Incorporation of SBU into **Dy_3bdc** and **Dy_3sqr** with squarate bridging modes indicated (left) and **Dy_3bdc** dimers (lower right).

∠O-Ln-O bond angles ranging between 80-90°. Each double chain is charge neutral, with the Ln_3 cluster building units carrying a +3 charge and three dianionic squarates each bridging two clusters.

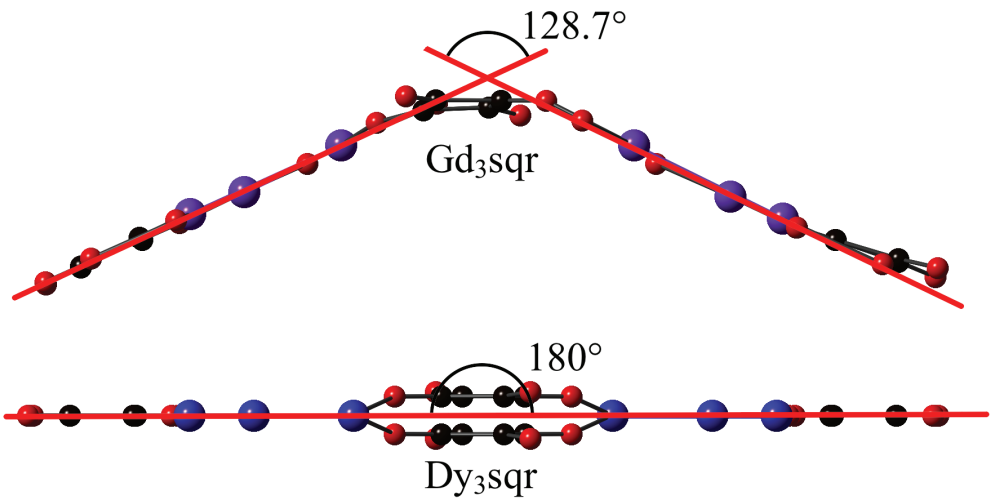

Figure IV.4. Angles between mean Ln_3 planes **Ln_3sqr**. Bent **Gd_3sqr** double chain (top) and coplanar double chain **Dy_3sqr** (bottom). TDCI ligands and solvent molecules omitted for clarity.

$Gd_3(TDCI)_2(C_4O_4)_{3/2}$ (Gd_3sqr)

For **Gd_3sqr**, Gd_3 triangles in both rails are pointing roughly in the direction of chain propagation, along the crystallographic *a*-axis. While Gd atoms within a rail are close to, but not strictly, coplanar, Gd atoms between rails are far from coplanar; the ladder is quite bent with a 128.737(13)° angle between mean Gd_3 planes of the two rails (Figure IV.4). The rails are *syn* with respect to the squarate rungs. Figure IV.5 depicts the crystal packing of the Gd double chains. As view along the chain propagation axis show the the previously mentioned extensive intra-chain hydrogen bonding, as seen in Figrue IV.6.

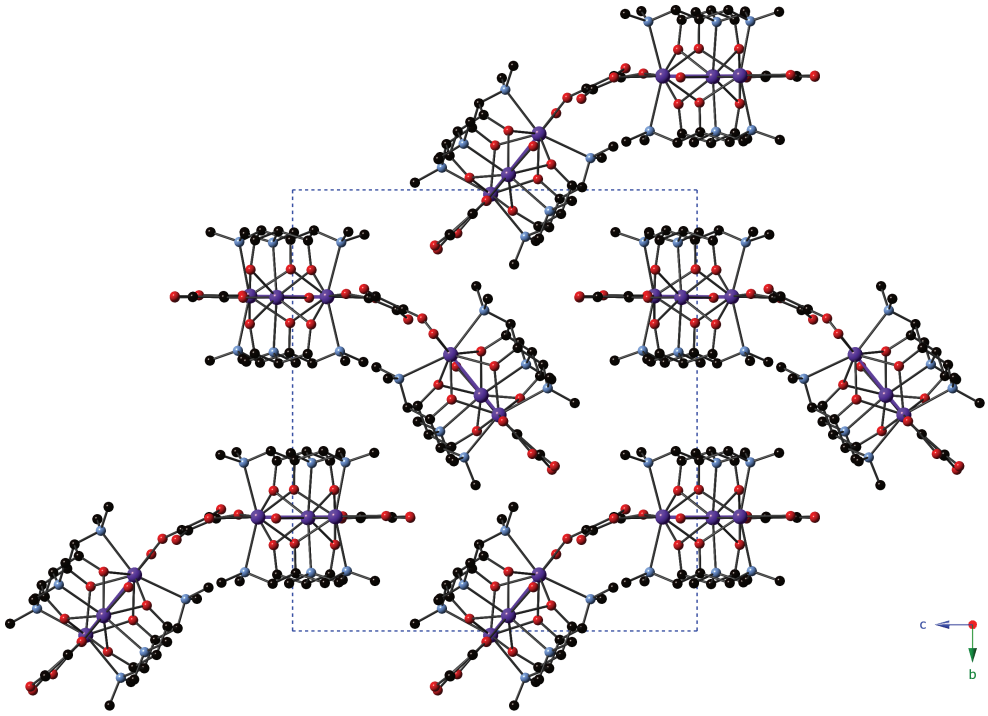

Figure IV.5. View down the crystallographic a-axis of **Gd_3sqr**. The double-chains are bent. Solvent molecules omitted for clarity.

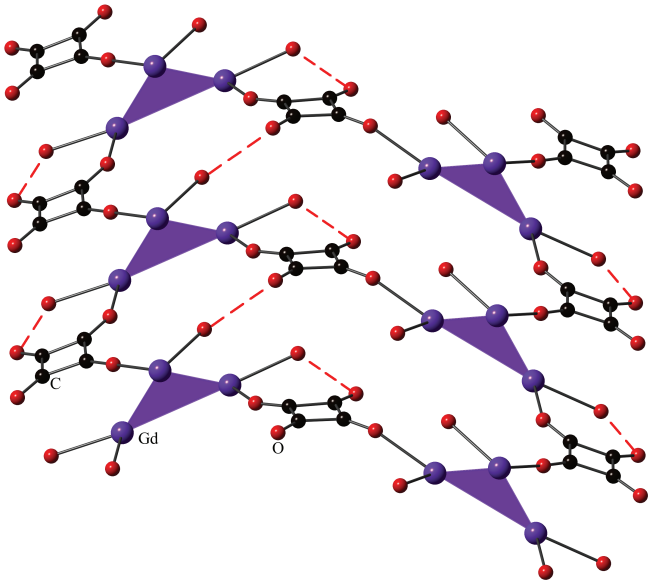

Figure IV.6. H-bonding in **Gd_3sqr**. Tilted view of **Gd_3sqr** along the direction of chain propagation illustrating O-O distances less than 2.9 Å.

$Dy_3(TDCI)_2(C_4O_4)_{3/2}$ (Dy_3sqr)

In the **Dy_3sqr** structure, all Dy atoms in a double chain are coplanar and run along the *c*-axis. This is quite an interesting structural change compared to **Gd_3sqr** considering that the bonding properties of Gd^{3+} and Dy^{3+} are quite similar. The Ln_3 triangles within a rail pointing roughly along one direction, while those in the other rail point in the opposite direction. The double chains pack with four solvent channels surrounding each double chain, on the top, bottom and both sides. Given the hydrophobic nature of the TDCI ligand, it is of note that the packing does not reflect hydrophobic interactions between the supporting ligands. Water and squarate oxygen atoms on the outer edge of each double-chain are involved in hydrogen-bonding networks of solvent molecules (water and ethanol). This hydrogen bonding is the most likely explanation of the solvent channels. Though clear evidence of water and ethanol is seen in the X-ray crystal structure, the solvent molecules could not be satisfactorily refined because of disorder and fractional occupancy and were masked. A view of packing in the **Dy_3sqr** structure can be seen in Figure IV.7. A view of intra-chain hyrogen bonding is seen in Figure IV.8

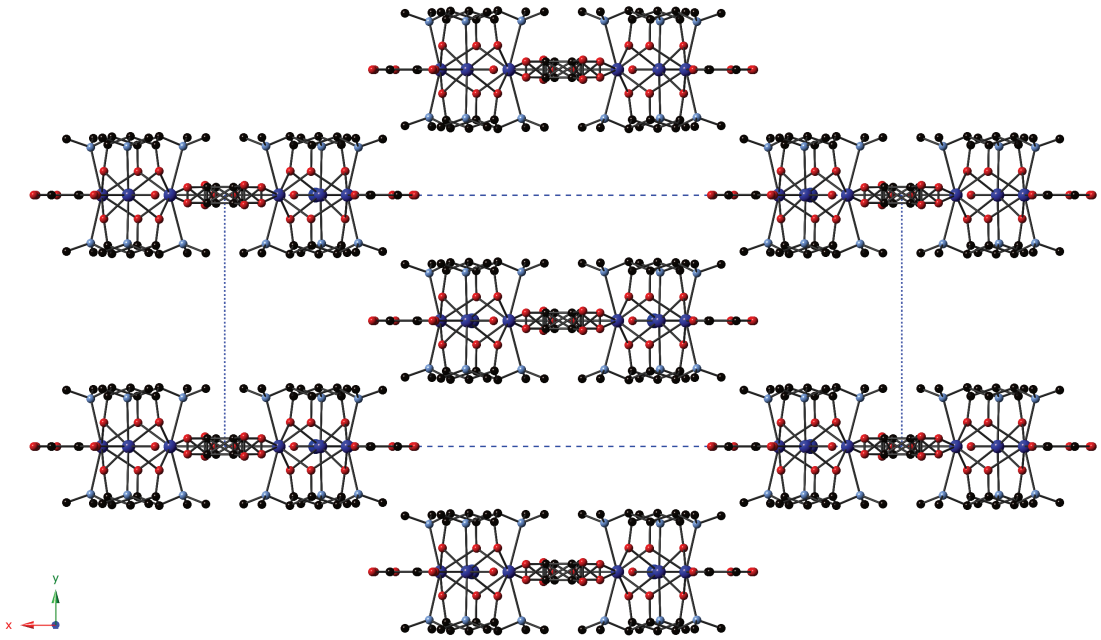

Figure IV.7. View down the crystallographic c-axis for **Dy_3sqr**. The voids above and below the central double-chain are solvent channels. Solvent molecules masked from refinement due to disorder. The squarates linking each double-chain are disordered over two positions.

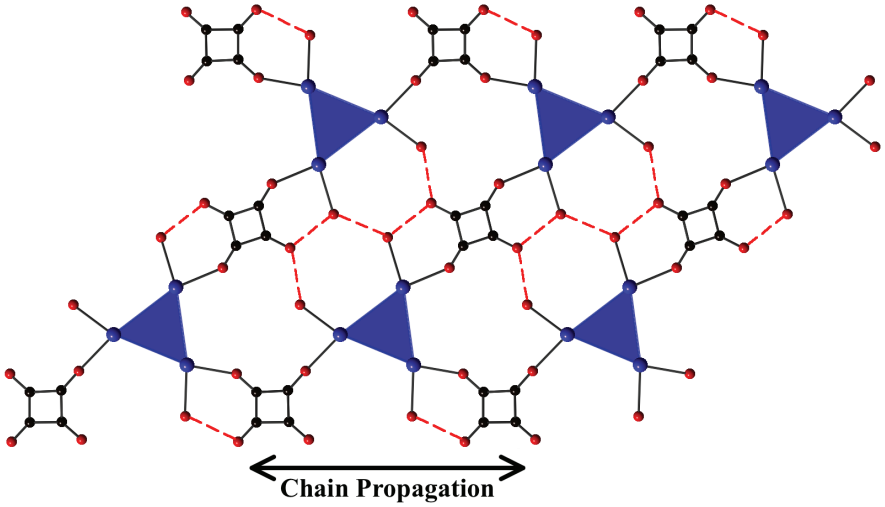

Figure IV.8. Hydrogen bonding in **Dy_3sqr**. Top view of **Dy_3sqr** illustrating O-O distances less than 2.9 Å.

$Dy_3(H_{-3}TDCI)_2(bdc)_{3/2}$ (Dy_3bdc)

Reactions with the benzenedicarboxylate linker were attempted with both **Gd_3H_2O** and **Dy_3H_2O**, but suitable crystals could not be found in the polycrystalline product of the Gd reaction. For the dysprosium clusters, the change in the linking ligand to benzenedicarboxylate (bdc) results in the product, $Dy_3(H_{-3}TDCI)_2(bdc)_{3/2}$ (**Dy_3bdc**) and is again a charge neutral 1-D coordination network. Though the linkages are different than those found in squarate-linked structures, the chains consist of $(Dy_3\text{-bdc-}H_2O)_2$ dimers connected by bdc linkers. Monomer units consist of one Dy_3 cluster bound bidentate to one carboxylate group of a bdc ($\angle$O-Ln-O of ~54.5°). The dimers are bound "head to tail" such that the bdc of one monomer is coordinated to the Dy_3 triangle of the other monomer, monodentate, via its other carboxylate group ($\angle O_{water}$-Ln-O_{bdc} of ~81.9°). The dimers are linked in a chain by bdc ligands with both carboxylate groups bound bidentate to dysprosium ions (Figure IV.1and Figure IV.3). The Dy_3 triangles in these chains are not perfectly coplanar with each other or with the bdc linkers, though the planes in which these atoms lie are roughly parallel. Packing is as seen in Figure IV.9. The packing of the chains is directed by inter-chain hydrogen bonding.

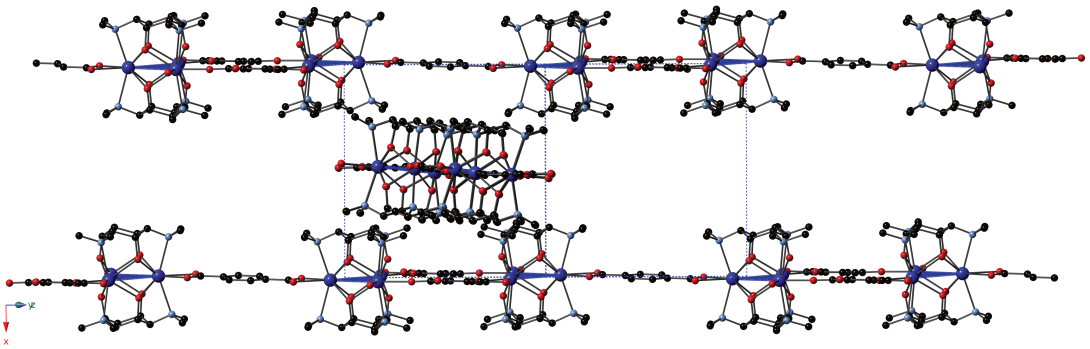

Figure IV.9. Packing of **Dy_3bdc**. View along a chain, roughly down the [0,1,-1] lattice vector, of **Dy_3bdc**. Depiction of Dy_3 triangles emphasizes the cant of the clusters.

Magnetism

The DC magnetic susceptibility of **Dy_3sqr** is seen in Figure IV.10. Though phase purity has not been obtained, preliminary magnetic measurements on a sample obtained by selecting crystals of the Dy product reveal slow magnetic relaxation, indicative of single molecule magnet behavior. (Figure IV.11). An out-of-phase is signal is observed in the ac-susceptibility, though no definite peaks were observed. A slight change is in magnetic response is caused by an applied static 1000 Oe field, but not enough to induce significant peak dependence on temperature. Given the low temperature at which the ac signal is observed, and the lake of temperature-dependence, quantum tunneling of magnetization is the likely mechanism for relaxation.

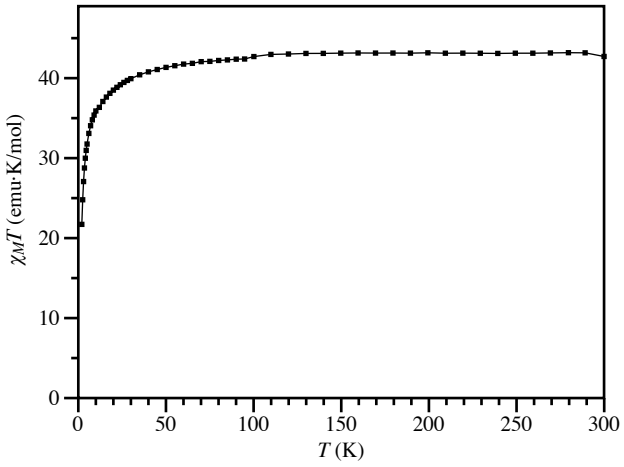

Figure IV.10. DC magnetic susceptibility for **Dy_3sqr**. $\chi_M T$ vs T plot for **Dy_3sqr** at temperatures ranging from 2 K to 300 K. Molar susceptibility values approximate due to phase impurity and desolvation.

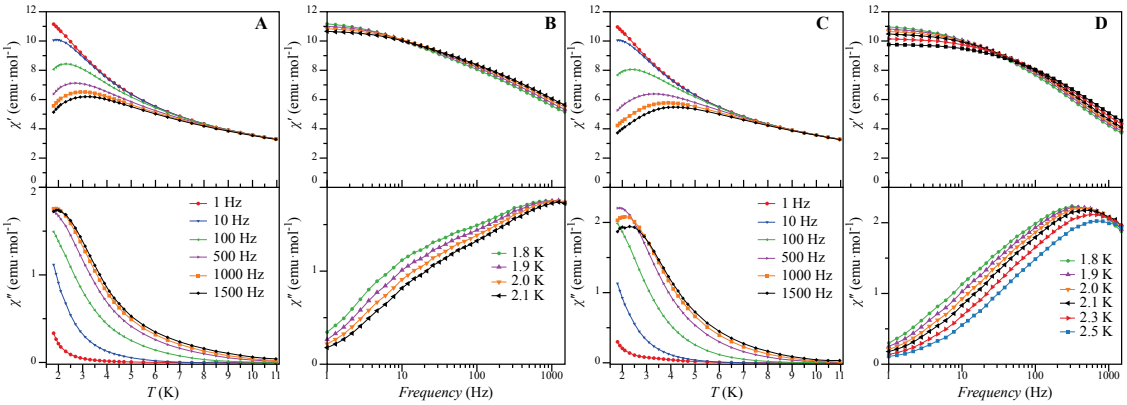

Figure IV.11. AC magnetic susceptibilities of **Dy_3sqr**. (Molar in-phase and out-of-phase.) Temperature and frequency dependent susceptibilities $\chi_M'(T)$ and $\chi_M''(\nu)$ under no applied DC field (A and B) and under 1000 Oe applied DC field (C and D).

CONCLUSION

To our knowledge, this is the first example of a metal-organic coordination network built from organic linkers and a *preexisting* lanthanide-alkoxo polymetallic secondary building unit. The topology of coordination networks composed of these Ln_3 secondary building units is at least partially restricted because of the following geometrical constraints: (1) There are a limited number of available coordination sites per triangular Ln_3 cluster, commonly six--two per lanthanide ion at each vertex of the triangle. (2) The available metal coordination sites all lie in the plane of the Ln_3 triangle. In this case, the resulting structures are 1-D coordination polymers, with out-of-plane framework connections being blocked by the supporting H_{-3}TDCI ligands (Figure 1). The triangular geometry may allow incorporation of these building blocks into 2-D layered networks.

This work demonstrates the synthesis of coordination networks from preformed lanthanide cluster building units $[Ln_3(H_{-3}TDCI)_2]^{3+}$ and organic linking units. Squarate linkers lead to 1-D double chains, while benzenedicarboxylate links $(Dy_3\text{-bdc-}H_2O)_2$ dimers in 1-D chains. Preformed cluster building units with linkage coordination sites, constrained in both number and geometry, restricts the topology of the coordination network. The slow magnetic relaxation of **Dy_3sqr** indicates that materials containing these Ln_3 units can exhibit interesting properties. Synthesis of Eu and Tb analogues may yield compounds with worthwhile luminescence, especially if linked with a suitable antenna linker.[21] Though further study is required to understand the effects of lanthanide identity, linker, solvent, and crystal-growth conditions, incorporation of these clusters into coordination polymers is an important step along the way to

achieving topological control of lanthanide frameworks with desirable properties.

CHAPTER V

HEXANUCLEAR OXO-CENTERED LANTHANIDE CLUSTERS

INTRODUCTION

Lanthanide oxo-alkoxide and oxo-hydroxide clusters, common in solution lanthanide cluster chemistry, serve as prototypes for our synthetic purposes, for example the pentanuclear lanthanide oxo-isopropoxide cluster, $Ln_5(\mu_5\text{-}O)(\mu_3\text{-}OR)_4(\mu_2\text{-}OR)_4(OR)_5$ (OR = isopropoxide)[66-69,69-74] and the hexanuclear lanthanide oxo-hydroxide cluster, $[Ln_6(\mu_6\text{-}O)(\mu_4\text{-}OH)_8L_x]^{n+}$ ($L = H_2O, NO_3^-, ClO_4^-$, DMSO).[75,75-81] Though $Ln_5(\mu_5\text{-}O)(\mu_3\text{-}Oi\text{-}Pr)_{13}$ has recently shown to be a very robust SMM, very magnetic studies have been performed on other oxo-centered lanthanide clusters. This chapter presents preliminary structural results of novel hexanuclear oxo-centered lanthanide clusters whose Dy analogues may prove exhibit interesting magnetic behavior.

Lanthanide alkoxide chemistry

There are four prevalent methods for synthesizing metal alkoxides: metal alcoholysis, alcoholysis, halide metathesis, and amide alcoholysis.[31,82] Metal alcoholysis, which involves directly reducing an alcohol to an alkoxide with lanthanide metal, will not be discussed here because of the cost of this method and due to the limited number of alkoxides which can be formed via this route. Lanthanide metals of sufficient purity are much more expensive than lanthanide oxides, which can be used to synthesize other useful starting materials for alkoxide synthesis. Alcoholysis involves exchanging one alkoxide for another via proton exchange from the desired alco-

hol to the coordinating alkoxide.

A very common route to lanthanide alkoxides is salt metathesis, which consists of reacting an alkali metal alkoxide with an anhydrous lanthanide halide in a suitable aprotic solvent. The products are usually a soluble lanthanide alkoxide and an insoluble alkali metal halide. Although this method was first used when our research in this area started, it was largely abandoned due to complications, namely incorporation of alkali metals or halides into the products.

The amide alcoholysis route in involves a proton exchange between a sterically encumbered, monomeric lanthanide amide precursor, $Ln(N(SiMe_3)_2)_3$ (amide pKa ~26),[83] with an alcohol, HOR (pK_a < 18); the byproduct being an inert, liquid amine with a fairly low boiling point. This route is convenient and without alkali metal or halide contamination, and the only byproduct is bis(trimethylsilyl)amine (hexamethyldisilazane). This route is more solvent restricted than the alkali metal alkoxide route due to the increased basicity of the lanthanide amide.

EXPERIMENTAL

Synthesis

The lanthanide amide starting materials, lanthanide tris[bis(trimethylsilyl)amide] ($Ln[N(SiMe_3)_2]_3$) were synthesized as described in Chapter I. All rections were carried out under inert conditions using Schlenk techniques. Ammonium tetraphenylborate was obtained from Sigma Aldrich. Ethanol was distilled from magnesium turnings. Tetrahydrofuran (THF) was was distilled from Na/K. Dipivaloylmethane (Hdpm) was obtained from a commercial source and stored over molecular sieves.

$Gd_6(\mu_6\text{-}O)(\mu_3\text{-}OH)_8(dpm)_8$ (Gd_6dpm)

To 0.5 g (0.78 mmol) of $Gd[N(SiMe_3)_2]_3$ and 0.042 g (0.26 mmol) of $NH_4(PF_6)$ was dissolved in approximately 8 mL of ethanol. To this solution, dipivaloylmethane (0.78 mmol, 0.143 g, 163 μL) was added. The solution was allowed to slowly evaporate through a rubber septum over the period of a week. Colorless, block-shaped crystals were formed. Approximate yield: 20%.

$Gd_6(\mu_6\text{-}O)(\mu_3\text{-}OH)_6(\mu_3\text{-}O)_2(PhB(OEt)_2)_2(dpm)_6(HOEt)_2$ ($Gd_6dpm(BPh)$)

To 0.5 g (0.78 mmol) of $Gd[N(SiMe_3)_2]_3$ and 0.088 g (0.26 mmol) of $NH_4(BPh_4)$ was added approximately 8 mL of ethanol. A vigorous exothermic reaction occurred upon reaction with the amide, but the $NH_4(BPh_4)$ did not dissolve. To this solution, dipivaloylmethane (0.78 mmol, 0.143 g, 163 μL) was added. The mixture was heated to boiling for 1 hr. The solvent was removed under reduced pressure, after which THF was added and all solids dissolved. The solution was stored at -20 °C for 1 week without crystallization. The solution was then stored at room temperature with a rubber septum capping the Schlenk flask. After a week of slow evaporation of the solvent, colorless block-shaped crystals were formed. Approximate yield: 20%.

$[Dy_6(O)(OCH_2CF_3)_{18}][Na(thf)_6]_2$

$Dy[N(SiMe_3)_2]_3$ (0.256 g, 0.4 mmol) and $Na(N(SiMe_3)_2)$ (0.24 mg, .13 mmol) was dissolved in 10 mL of dry THF. To this solution, a solution of trifluoroethanol (0.1325 g, 1.3 mmol, 100 μL) in 5 mL THF was added slowly, with stirring. The resulting solution was stirred for one hour, and the solvent volume was reduced to 2 mL. The solution was stored at low temperature for a few days. Colorless block-shaped crystals were formed. Approx. yield: 50%.

X-Ray crystallography

Data collection

A Leica MZ 75 microscope was used to identify a suitable colorless block with very well defined faces with dimensions as in from a representative sample of crystals of the same habit. The crystal mounted on a nylon loop was then placed in a cold nitrogen stream (Oxford) maintained at 110 K or 150 K.

A BRUKER APEX 2 X-ray (three-circle) diffractometer was employed for crystal screening, unit cell determination, and data collection. The goniometer was controlled using the APEX2 software suite, v2008-6.0. The sample was optically centered with the aid of a video camera such that no translations were observed as the crystal was rotated through all positions. The detector was set at 6.0 cm from the crystal sample (APEX2, 512 × 512 pixel). The X-ray radiation employed was generated from a Mo sealed X-ray tube (K_α = 0.70173Å with a potential of 40 kV and a current of 40 mA) fitted with a graphite monochromator in the parallel mode (175 mm collimator with 0.5 mm pinholes).

Sixty data frames were taken at widths of 0.5°. These reflections were used in the autoindexing procedure to determine the unit cell. A suitable cell was found and refined by nonlinear least squares and Bravais lattice procedures. The unit cell was verified by examination of the *h k l* overlays on several frames of data by comparing with the orientation matrices. No supercell or erroneous reflections were observed.

A full sphere (2400 frames at 6 cm detector distance) was collected with scan widths of 0.5° or 0.3° in omega and exposure times of 10 s or 20 s depending on the compound.

Data Reduction, Structure Solution, and Refinement

Integrated intensity information for each reflection was obtained by reduction of the data frames with the program APEX2.[2] The integration method employed a three dimensional profiling algorithm and all data were corrected for Lorentz and polarization factors, as well as for crystal decay effects. Finally the data was merged and scaled to produce a suitable data set. The absorption correction program SADABS was employed to correct the data for absorption effects.[3]

Systematic reflection conditions and statistical tests of the data suggested the space group seen in (Table V.1). A solution was obtained readily using SHELXTL (XS).[4] Hydrogen atoms were placed in idealized positions and were set riding on the respective parent atoms. A molecule of toluene was found solvated and disordered between two positions; the disorder was successfully modeled. All non-hydrogen atoms were refined with anisotropic thermal parameters. The organic ligands and the tert-butyl groups indicated disorder, which was modeled. Restraints and constraints were used to keep the bond distances, angles, and thermal ellipsoids meaningful. Absence of additional symmetry and voids were confirmed using PLATON.[#] The structure was refined (weighted least squares refinement on F^2) to convergence.

The structure for is incomplete for $Gd_6(\mu_6\text{-}O)(\mu_3\text{-}OH)_8(dpm)_8$. However, the refinement indicates the connectivity of the molecule and its identity as an oxo-centered hexanuclear cluster is clear.

Table V.1. Crystallographic detail for Chapter V compounds.

Empirical formula	$C_{84}H_{132}O_{31}F_{54}Na_2Dy_6$	$C_{90}H_{162}B_2O_{27}Gd_6$	$C_{88}H_{160}O_{25}Gd_6$
Formula weight	3684.87	2641.37	2561.71
Temperature	150.15 K	110.15 K	110.15 K
Wavelength	0.71073 Å	0.71073 Å	0.71073 Å
Crystal system	trigonal	triclinic	tetragonal
Space group	P-3	P-1	I4/m
a	17.579(3)	15.1661(2) Å	19.0889 (11)Å
b	17.579(3)	15.2490(2) Å	19.0889 (11) Å
c	12.764(2)	15.4108(2) Å	17.1552(11) Å
α	90°	67.597(1)°	90°
β	90 °	69.875(1)°	90°
γ	°	62.524(1)°	90°
Volume	3416.0(12) $Å^3$	2861.22(7) $Å^3$	6251(8) $Å^3$
Z	1	1	4
Density (calculated)	1.791 g/cm^3	1.532 g/cm^3	2.511 g/cm^3
Absorption coefficient	3.179 mm^{-1}	6.947 mm^{-1}	6.372 mm^{-1}
F(000)	1788	2182	4616
Crystal size ($mm^{3)}$	0.24 x 0.23 x 0.12	0.2 x 0.15 x 0.2	0.1 x 0.1 x 0.15
Theta range	2.082 to 25.99°	1.46 to 27.598°	1.509 to 30.855°
Reflections collected	42903	66900	48383
Independent reflection	4490 (R_{int} = 0.04767)	13255 (R_{int} = 0.0209)	5032 (R_{int} = 0.0323)
Completeness	100%	99%	100%
Absorption correction	Multi-scan	Multi-scan	Multi-scan
Restraints / parameters	4490/54/345	13255/3/619	5032/0/195
Goodness-of-fit-F^2	1.086	1.040	0.976
Final R indices (I>2σ(I))	R_1 = 0.0348, wR_2 = 0.0928	R_1 = 0.0255, wR2 = 0.0655	R_1 = 0.0612, wR2 = 0.1890
R indices (all data)	R_1 = 0.0434, wR_2 = 0.0967	R_1 = 0.293, wR_2 = 0.0672	R_1 = 0.0673, wR_2 = 0.1958
Largest diff. peak/hole	1.335 and -1.350 $e/Å^3$	2.04 and -0.67 $e/Å^3$	4.41 and -2.14 $e/Å^3$

RESULTS AND DISCUSSION

Synthesis

An attempt was made to synthesize the hexanuclear lanthanide dpm species under similar conditions described by Cot et al, namely in refluxing ethanol. (A mixture of isopropanol and ethanol was used in the literature preparation, however.).[84,85] An ethanolic solution of either ammonium hexafluorophosphate and ammonium tetraphenylborate with a stoichoimetric amount of water and Hdpm was added to gadolinium tris(bis(trimethylsilyl)amide) and refluxed for about an hour.

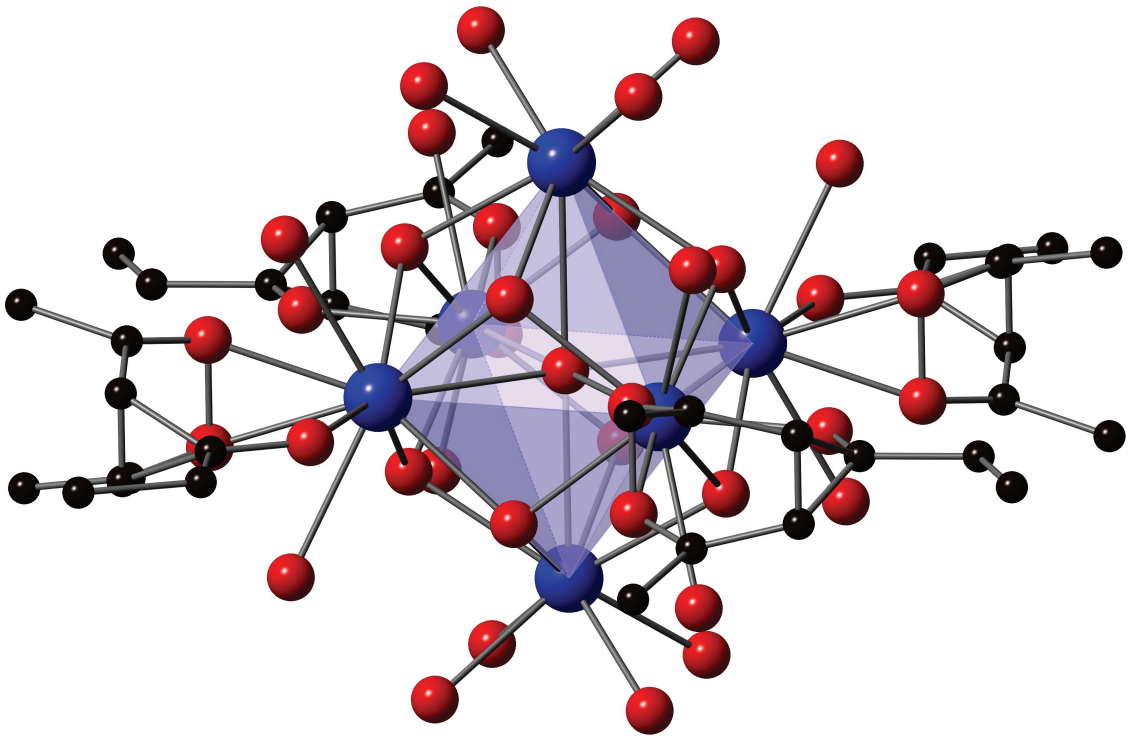

Figure V.1. Crystal structure of $Gd_6(\mu_6\text{-}O)(\mu_3\text{-}OH)_8(dpm)_8$. Disordered apical dpm ligands and hydrogen atoms omitted for clarity.

$Gd_6(\mu_6\text{-}O)(\mu_3\text{-}OH)_8(dpm)_8$

The reaction with hexafluorophosphate produced a crystalline material. Seemingly nice quality crystals were obtained, but attempts to collect X-ray data have so far failed. Crystals degrade rather quickly due to either chemical decomposition or desolvation. After the reaction tube sat for several days, it was noticed that nice quality, differently shaped crystals had formed. X-ray data was collected, and the product was determined to be $Gd_6(\mu_6\text{-}O)(\mu_3\text{-}OH)_8(dpm)_8$ (Figure V.1), although the structure solution is not complete.

The structure consists of a typical hexanuclear lanthanide oxo-hydroxide cluster with hydroxides capping the eight faces of an lanthanide octahedron and one dpm ligand terminating each of four "equatorial" gadolinium ions in a plane and two dpm ligands on each of the "apical" gadolinium ions, trans to one another. This product, in particular the μ_6-oxygen, was likely produced by atmospheric water slowly diffusing into the reaction mixture.

$$6\ Gd[N(SiMe_3)_2]_3 + 9\ H_2O + 8\ Hdpm \xrightarrow{EtOH/THF} Gd_6(O)(OH)_8dpm_8 + 18\ HN(SiMe_3)_2 \qquad (5.1)$$

$Gd_6(\mu_6\text{-}O)(\mu_3\text{-}OH)_6(\mu_3\text{-}O)_2(PhB(OEt)_2)_2(dpm)_6(HOEt)_2$

For the reaction with tetraphenylborate as the counterion, somewhat unexpected results were obtained. Similar reaction conditions were initially attempted, but ammonium tetraphenylborate is not soluble in ethanol, so the gadolinium bis(trimethylsilyl)amide was added to the ethanol mixture, and the solvent evaporated and THF was added. All solids quick-

ly dissolved, after which the solution was reconcentrated by removing excess solvent. After an unsuccessful attempt to grow crystals at -20°C for a week, the reaction was set aside at room temperature. After several days, X-ray quality crystals were obtained. The product was determined to be a cluster $Gd_6(\mu_6\text{-}O)(\mu_3\text{-}OH)_6(\mu_3\text{-}O)_2(PhB(OEt)_2)_2(dpm)_6(HOEt)_2$ (Figure V.2).

$$6\ Gd[N(SiMe_3)_2]_3 + 9\ H_2O + 6\ Hdpm + 2\ NH_4BPh_4 \xrightarrow{EtOH/THF} Gd_6(O)(OH)_8dpm_6(PhB(OEt)_2)_2 + 18HN(SiMe_3)_2 \quad (5.2)$$

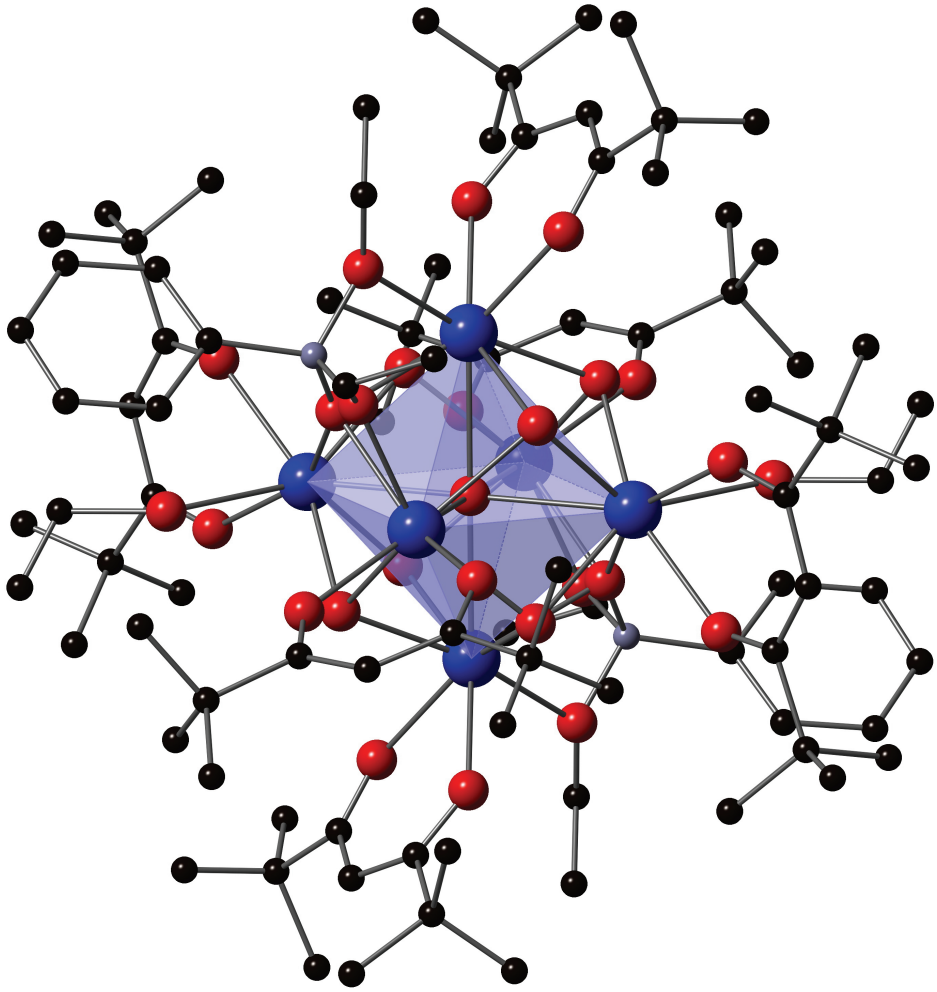

Figure V.2. $Gd_6(\mu_6\text{-}O)(\mu_3\text{-}OH)_6(\mu_3\text{-}O)_2(PhB(OEt)_2)_2(dpm)_6(HOEt)_2$. Ball and stick representation of the crystal structure. Hydrogen atoms omitted for clarity.

The structure consists of a hexanuclear arrangement of gadolinium ions around a central oxo ligand. Six of the octahedral faces are capped by hydroxo ligands, and two *trans* faces are capped by oxo ligands. There are six dpm ligands, one on each of the six vertices of the octahedron. The two trans oxo ligands are each donating into the boron of the two diethyl phenylboronates, while the two ester oxygens are each coordinating to one gadolinium. One ethanol molecule is coordinated to each of the two gadoliniums not coordinated by ester oxygens. The structure is as seen in Figure V.3. This suprising structure is a result of tetraphenylborate anion decomposing in refluxing basic ethanolic solution, although the mechanism of decomposition isn't completely understood. It is presumed that the μ_6-oxo and μ_3-OH groups were introduced as the result of adventitious water as well.

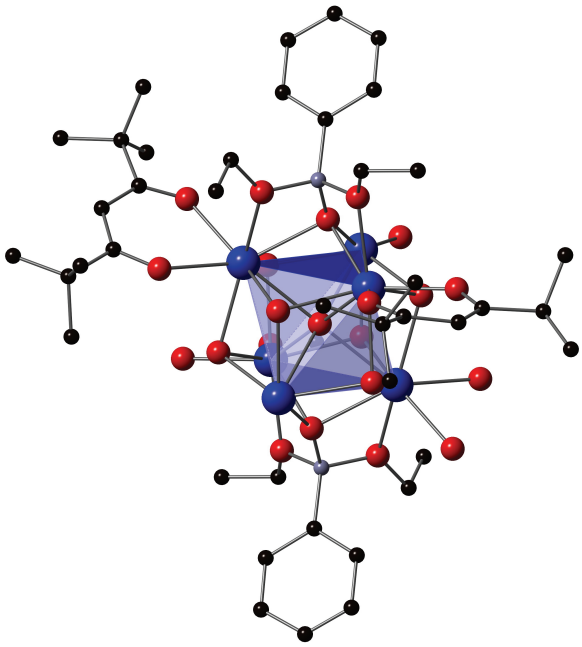

Figure V.3. View of borate substituents of Gd_6 cluster.

$[Dy_6(O)(OCH_2CF_3)_{18}][Na(thf)_6]_2$

The previously reported oxo-centered hexanuclear rare earth alkoxide cluster anions $[RE_6(\mu_6\text{-}O)(\mu_2\text{-}OCH_2CF_3)_{12}(OCH_2CF_3)_6][Na(thf)_6]_2$ (RE = Y, Er) serve as a promising structure-type for magnetic studies.[86,87] To pursue a magnetic investigation, the Dy analog was synthesized, $[Dy_6(\mu_6\text{-}O)(\mu_2\text{-}OCH_2CF_3)_{12}(OCH_2CF_3)_6][Na(thf)_6]_2$ via an alternate synthetic route to that used in the literature. The literature preparation involves elimination of alkali metal-halide via salt metathesis.[86] A THF solution of sodium trifluoroethoxide (produced by the action of sodium metal on trifluoroethanol) was added to a suspension of rare earth halide in THF. Sodium chloride was removed by filtration or centrifugation, and the RE_6 product was crystallized from the supernate. To avoid the mechanical separation of byproducts, the amide alcoholysis route was used. A The reaction of $Dy[N(SiMe_3)_2]_3$ and trifluoroethanol in THF produced crystals of the desired product, $[Dy_6(O)(OCH_2CF_3)_{18}][Na(thf)_6]_2$.

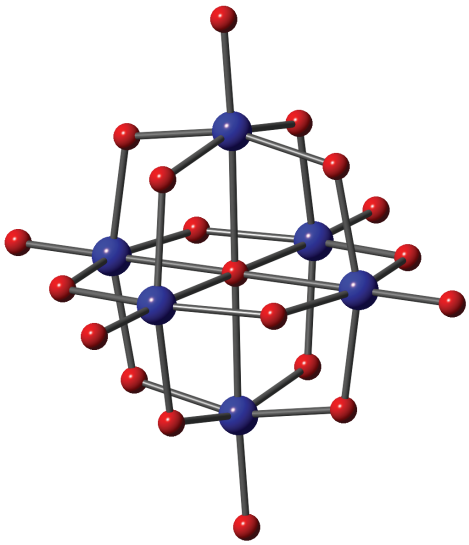

Figure V.4. Cluster core of $[Dy_6(O)(OCH_2CF_3)_{18}][Na(thf)_6]_2$. The coordiation environment of each Dy ion is a distorted octahedron.

The **Dy**$_6$ cluster core is shown in Figure V.4, and that of the entire **Dy**$_6$ dianion is shown in Figure V.5.

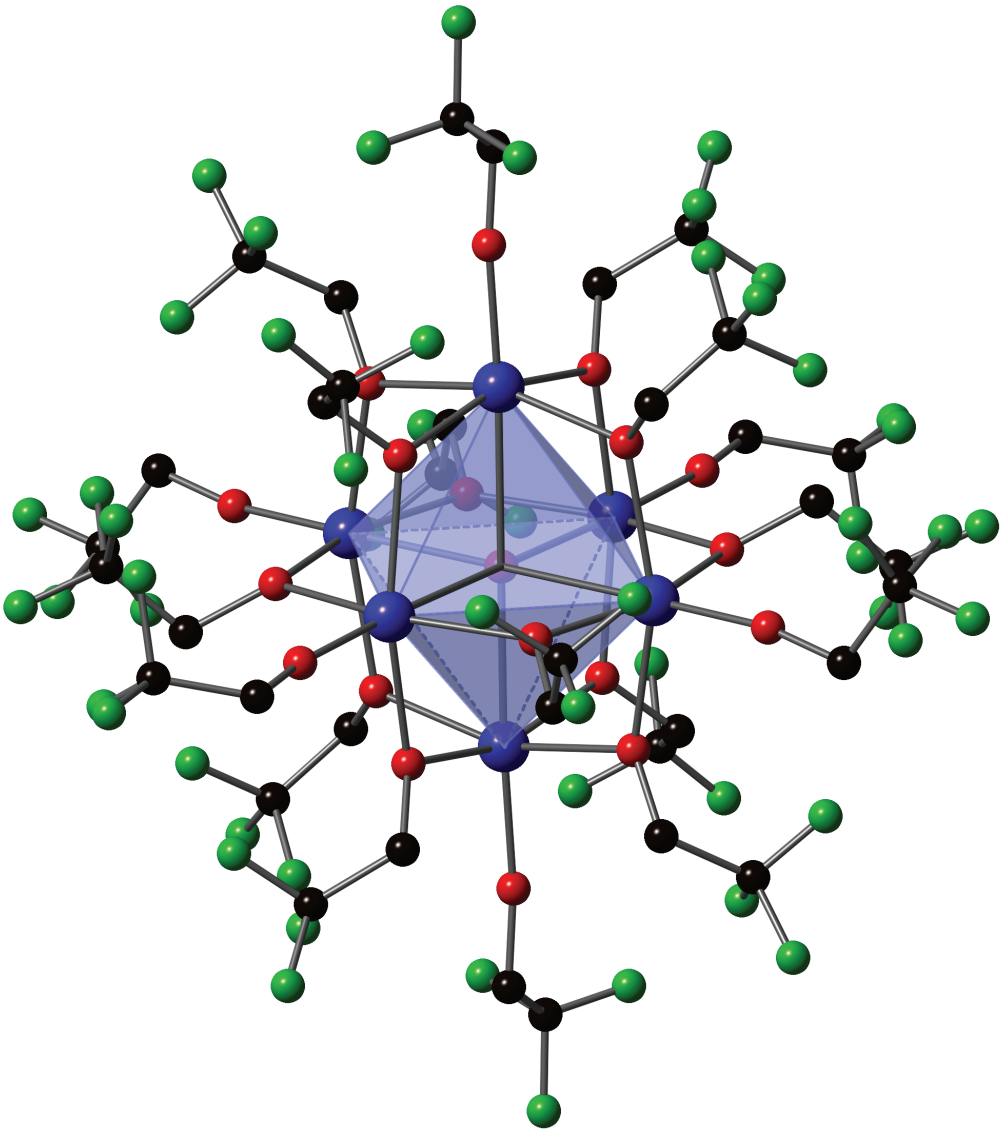

Figure V.5. Crystal structure of $[Dy_6(O)(OCH_2CF_3)_{18}][Na(thf)_6]_2$. THF coordinated sodium counter cations omitted for clarity.

$$6\ Dy[N(SiMe_3)_2]_3 + 2\ NaN(SiMe_3)_2 + 20\ HOCH_2CF_3 \xrightarrow{THF} [Gd_6(O)(OCH_2CF_3)_{18}][Na(THF)_6]_2 + 18HN(SiMe_3)_2 + O(CH_2CF_3)_2 \quad (5.3)$$

CONCLUSION

Novel hexanuclear lanthanide oxo-hydroxo and oxo-alkoxo cluster were synthesized via amide alcoholysis and characterized by single-crystal X-Ray crystallography. A new route to the hexametallic dysprosium trifluoroethoxide dianion was used. Further study is needed to determine the magnetic properties of these compounds.

CHAPTER VI

CONCLUSIONS

The synthesis and characterization of alkoxide-supported polynuclear lanthanide clusters were explored in this work. Two different classes of clusters were synthesized: TDCI-supported trinuclear clusters and oxo-centered hexanuclear clusters.

TDCI (1,3,5-tris(dimethylamino)-1,3,5-trideoxy-*cis*-inositol was used as a support for a triangular lanthanide arrangement yielding $Ln_3(H_{-3}TDCI)_2$ cluster types, leaving six open coordination sites in the plane of the triangle. With the supporting ligand blocking coordination sites above and below the plane of the triangle, ligand replacement reactions that take place only at the periphery (vertices) of the triangle are possible. There being two open coordination sites available per (hard) lanthanide ion, makes bidentate oxo-donating β-diketonates ideal participants in these coordination reactions. Indeed, quite a rich family of $Ln_3(H_{-3}TDCI)_2(L)_3$ clusters with rare earths ions ranging from Y to the Eu, Gd, Dy, Tb, Ho, and Er and a variety of peripheral ligands including dipivaloylmethane, dibenzoylmethane, acetylacetone, and hexafluoroacetylacetone were produced. Other, neutral ligands such as methanol, water, and DMSO also readily coordinate to these clusters. Because of these structural properties, the Ln_3 clusters are also amenable to incorporation into coordination polymers, with various oxo ligands including benzenedicarboxylate and squarate acting as linkers.

It should be noted that although these are technically alkoxide complexes, the Ln_3TDCI clusters are formed in water with no additional base or in various other solvents with

the addition of the mild base, triethylamine. Though the synthesis of the TDCI ligand is quite involved, the lanthanide coordiation reactions are surprisingly convenient, and yields are generally high. The clusters prove to be robust enough to maintain their form upon incorporation into a coordination network, in part thanks to the mild conditions under which these reactions take place. It is indeed exceedingly rare for a metal-cluster to remain intact in their introduction into organic-linked networks.

Not only are these triangular cluster types rich in their coordination chemistry, but also in their physical properties. The Dy_3 analogues ligated by dpm proved to be single-molecule magnets with apparent intra-cluster magnetic effects, likely due to close Ln-Ln proximity. Other Dy_3 clusters ligated by methanol and included in the squarate-linked coordination network showed slow relaxation of magnetization. Initial luminescence measurements of the Eu and Tb-clusters indicate possibly robust emission properties.

The other class of molecules produced in this work, the hexanuclear lanthanide-oxo clusters are also interesting in their own right. Through the use of a relatively convenient lanthanide tris(bis(trimethylsilyamide)) starting material, a variety of these clusters are available. Two general types of hexanuclear cluster cores were made: face-capped and edge-bridged octahedral clusters. Preparation of these clusters is not as convenient as that of the TDCI-supported ones, but it is fairly quick and isolation tends to be with complication.

Looking to the future, there is much more work to be done with respect to both the TDCI clusters and the hexanuclear ones. There are still many more β-diketones available to tune the magnetic and luminescence properties. It has been shown that a change in electon-

withdrawing characteristics an enhance anisotripic energy barriers in SMMs.[88] These clusters are ideal for such studies because a single ligand can be replaced while keeping the rest of the coordiation geometry unchanged. Also, the coordination environment available of peripheral ligand substitution is open enough to accommodate many types ligands. With the proper choice of antennae ligands, enhancement of luminescence properties may also be attained.

Though the oxo-centered clusters were characterized by X-Ray crystallography, their magnetic properties have not been measured. Much more work is needed to further explore these compounds. Because of the symmetrical, coordination environment of lanthanides in these oxo-clusters, interesting magnetism is no unexpected. Indeed, it expected that the Dy hexanuclear clusters might show much promise as robust SMMs, like those of other oxo-centered lanthanide alkoxide clusters.[41]

REFERENCES

1. Dante Gatteschi, R. S., and Jacques Villain. *Molecular Nanomagnets*; Oxford University Press: Oxford, U.K., 2006;

2. Sessoli, R.; Tsai, H. L.; Schake, A. R.; Wang, S.; Vincent, J. B.; Folting, K.; Gatteschi, D.; Christou, G.; Hendrickson, D. N. *J. Am. Chem. Soc.* **1993**, *115*, 1804-1816.

3. Ishikawa, N.; Sugita, M.; Ishikawa, T.; Koshihara, S.-; Kaizu, Y. *J. Am. Chem. Soc.* **2003**, *125*, 8694-8695.

4. Woodruff, D. N.; Winpenny, R. E. P.; Layfield, R. A. *Chem. Rev.* **2013**, *113*, 5110-5148.

5. Sessoli, R.; Powell, A. K. *Coord. Chem. Rev.* **2009**, *253*, 2328-2341.

6. Christou, G.; Gatteschi, D.; Hendrickson, D., N.; Sessoli, R. *MRS Bull.* **2000**, *25*, 66-71.

7. Rinehart, J. D.; Long, J. R. *Chem. Sci.* **2011**, *2*, 2078-2085.

8. Guo, Y.-N.; Xu, G.-F.; Guo, Y.; Tang, J. *Dalton Trans.* **2011**, *40*, 9953-9963.

9. Casimir, H. B. G.; du, P., F.K. *Physica* **1938**, *5*, 507-511.

10. Binnemans, K. *Chemical Reviews Chem. Rev.* **2009**, *109*, 4283-4374.

11. Bunzli, J.-C. G.; Eliseeva, S. V. *Chemical Science Chem. Sci.* **2013**, *4*, 1939-1949.

12. Moore, E. G.; Samuel, A. P. S.; Raymond, K. N. *Acc. Chem. Res.* **2009**, *42*, 542-552.

13. Bünzli, J.-C. G.; Comby, S.; Chauvin, A.-S.; Vandevyver, C. D. B. *Journal of Rare Earths* **2007**, *25*, 257-274.

14. Werts, M., H.V. *Sci Prog Science progress* **2005**, *88*, 101-131.

15. Bunzli, J.-C., G.; Eliseeva, S., V. *Springer Ser. Fluoresc. Springer Series on Fluorescence* **2011**, *7*, 1-46.

16. Rosi, N. L.; Eddaoudi, M.; Kim, J.; O'Keeffe, M.; Yaghi, O. M. *CrystEngComm* **2002**, *4*, 401-404.

17. Furukawa, H.; Cordova, K. E.; O'Keeffe, M.; Yaghi, O. M. *Science (Washington, DC, U. S.)* **2013**, *341*, 974.

18. Kreno, L. E.; Leong, K.; Farha, O. K.; Allendorf, M.; Van, D. R. P.; Hupp, J. T. *Chem. Rev. (Washington, DC, U. S.)* **2012**, *112*, 1105-1125.

19. Janiak, C.; Vieth, J. K. *New J. Chem.* **2010**, *34*, 2366-2388.

20. Huang, Y.-G.; Jiang, F.-L.; Hong, M.-C. *Coord. Chem. Rev.* **2009**, *253*, 2814-2834.

21. Rocha, J.; Carlos, L. D.; Paz, F. A. A.; Ananias, D. *Chem. Soc. Rev.* **2011**, *40*, 926-940.

22. Lichtenthaler, F. W.; Leinert, H. *Chem. Ber.* **1966**, *99*, 903-907.

23. Quadbeck, G.; Rohm, E. *Chem. Ber. Chemische Berichte* **1956**, *89*, 1645-1648.

24. Harvison, P., J.; Forte, A., J.; Nelson, S., D. *J. Med. Chem. Journal of Medicinal Chemistry* **1986**, *29*, 1737-1743.

25. Ghisletta, M.; Jalett, H. P.; Gerfin, T.; Gramlich, V.; Hegetschweiler, K. *Helv. Chim. Acta* **1992**, *75*, 2233-2242.

26. Nishimura, S. *Handbook of Heterogeneous Catalytic Hydrogenation for Organic Synthesis*; John Wiley & Sons: New York, 2001; pp 40-41.

27. Adams, R.; Voorhees, V.; Shriner, R. L. *Organic Syntheses*; Wiley & Sons: New York, 1941; pp 463.

28. Hammond, G. S.; Nonhebel, D. C.; Wu, C.-H. S. *Inorg. Chem.* **1963**, *2*, 73-76.

29. Charles, Robert G. *Organic Syntheses*; Wiley & Sons: New York, 1963; Collect. Vol. IV, pp 869.

30. Schuetz, S. A.; Day, V. W.; Sommer, R. D.; Rheingold, A. L.; Belot, J. A. *Inorganic Chemistry Inorg. Chem.* **2001**, *40*, 5292-5295.

31. Hitchcock, P. B.; Hulkes, A. G.; Lappert, M. F.; Li, Z. *Dalton Trans.* **2004**, 129-136.

32. Kobayashi, S.; Hachiya, I. *J. Org. Chem.* **1994**, *59*, 3590-3596.

33. Di, B., Plinio; Choppin, G. R.; Portanova, R.; Zanonato, P. L. *Inorg. Chim. Acta* **1993**, *207*, 85-91.

34. Hamidi, M. E. M.; Pascal, J.-L. *Polyhedron* **1994**, *13*, 1787-1792.

35. Seminara, A.; Rizzarelli, E. *Inorg. Chim. Acta* **1980**, *40*, 249-256.

36. Tang, J.; Hewitt, I.; Madhu, N. T.; Chastanet, G.; Wernsdorfer, W.; Anson, C. E.; Benelli, C.; Sessoli, R.; Powell, A. K. *Angew. Chem. Int. Ed.* **2006**, *45*, 1729-1733.

37. Luzon, J.; Bernot, K.; Hewitt, I. J.; Anson, C. E.; Powell, A. K.; Sessoli, R. *Phys. Rev. Lett.* **2008**, *100*, 247205.

38. Rinehart, J. D.; Fang, M.; Evans, W. J.; Long, J. R. *Nat. Chem.* **2011**, *3*, 538-542.

39. Rinehart, J. D.; Fang, M.; Evans, W. J.; Long, J. R. *J. Am. Chem. Soc.* **2011**, *133*, 14236-14239.

40. Blagg, R. J.; Muryn, C. A.; McInnes, E. J. L.; Tuna, F.; Winpenny, R. E. P. *Angew. Chem. Int. Ed.* **2011**, *50*, 6530-6533.

41. Blagg, R. J.; Ungur, L.; Tuna, F.; Speak, J.; Comar, P.; Collison, D.; Wernsdorfer, W.; McInnes, E. J. L.; Chibotaru, L. F.; Winpenny, R. E. P. *Nat Chem* **2013**, *5*, 673-678.

42. Hedinger, R.; Ghisletta, M.; Hegetschweiler, K.; Toth, E.; Merbach, A. E.; Sessoli, R.; Gatteschi, D.; Gramlich, V. *Inorg. Chem.* **1998**, *37*, 6698-6705.

43. Hegetschweiler, K. *Chem. Soc. Rev.* **1999**, *28*, 239-249.

44. Chapon, D.; Husson, C.; Delangle, P.; Lebrun, C.; Vottero, P. J. A. *J. Alloys Compd.* **2001**, *323-324*, 128-132.

45. Chapon, D.; Delangle, P.; Lebrun, C. *J. Chem. Soc., Dalton Trans.* **2002**, 68-74.

46. Chapon, D.; Morel, J.-P.; Delangle, P.; Gateau, C.; Pecaut, J. *Dalton Trans.* **2003**, 2745-2749.

47. Delagrange, S.; Gateau, C.; Chapon, D.; Lebrun, C.; Delangle, P.; Vottero, P. *Eur. J. Inorg. Chem.* **2002**, 2991-2998.

48. Hegetschweiler, K.; Erni, I.; Schneider, W.; Schmalle, H. *Helv. Chim. Acta* **1990**, *73*, 97-105.

49. McCarley, T. D.; McCarley, R. L.; Limbach, P. A. *Anal. Chem.* **1998**, *70*, 4376-4379.

50. Patiny, L.; Borel, A. *Journal of Chemical Information and Modeling* **2013**, *53*, 1223-1228.

51. Patiny, L. B., A. **2013**,

52. Benelli, C.; Gatteschi, D. *Chem. Rev.* **2002**, *102*, 2369-2388.

53. Orbach, R. *Proc. R. Soc. London, Ser. A* **1961**, *264*, 458-484.

54. Orbach, R. *Proc. Phys. Soc., London* **1961**, *77*, 821-826.

55. Finn, C. B. P.; Orbach, R.; Wolf, W. P. *Proc. Phys. Soc., London* **1961**, *77*, 261-268.

56. Taylor, D. P.; Choppin, G. R. *Inorg. Chim. Acta* **2005**, *358*, 459-466.

57. Zhao, D.; Timmons, D. J.; Yuan, D.; Zhou, H.-C. *Acc. Chem. Res.* **2011**, *44*, 123-133.

58. Eddaoudi, M.; Moler, D. B.; Li, H.; Chen, B.; Reineke, T. M.; O'Keeffe, M.; Yaghi, O. M. *Acc. Chem. Res.* **2001**, *34*, 319-330.

59. O'Keeffe, M.; Yaghi, O. M. *Chem. Rev. (Washington, DC, U. S.)* **2012**, *112*, 675-702.

60. Koberl, M.; Cokoja, M.; Herrmann, W. A.; Kuhn, F. E. *Dalton Trans.* **2011**, *40*, 6834-6859.

61. Cotton, F. A.; Murillo, C. A.; Walton, R. A.; Editors. *Multiple Bonds Between Metal Atoms, Third Edition*; Springer: 2005; pp 818 pp.

62. Li, J.-R.; Yakovenko, A. A.; Lu, W.; Timmons, D. J.; Zhuang, W.; Yuan, D.; Zhou, H.-C. *J. Am. Chem. Soc.* **2010**, *132*, 17599-17610.

63. Selby, H. D.; Orto, P.; Zheng, Z. *Polyhedron* **2003**, *22*, 2999-3008.

64. Mandic, S.; Healey, M. R.; Gotthardt, J. M.; Alley, K. G.; Gable, R. W.; Ritchie, C.; Boskovic, C. *Eur. J. Inorg. Chem.* **2013**, *2013*, 1631-1634.

65. Ouali, N.; Rivera, J.-P.; Chapon, D.; Delangle, P.; Piguet, C. *Inorg. Chem.* **2004**, *43*, 1517-1529.

66. Kritikos, M.; Moustiakimov, M.; Wijk, M.; Westin, G. *J. Chem. Soc., Dalton Trans.* **2001**, 1931-1938.